Seismicity of the East African Rift System determined from the Kaptagat array

Leslie R. A. Arnold

Seismicity of the East African Rift System determined from the Kaptagat array

by

Leslie R. A. Arnold

A thesis submitted for the degree of
Master of Science
in the
University of Durham

Van Mildert College

February 1978

Acknowledgements

I would like to thank Professor M.H.P. Bott for the opportunity to work in the Department of Geological Sciences, and the Natural Environment Research Council who sponsored my studentship.

I should also like to thank Dr. R.E. Long for his guidance and patience throughout my research and for invaluable criticism of this work.

Of my many colleagues in the department I would like to thank Dr. R.W. Backhouse, Dr. C.H. Boynton and Dr. P. Forth who helped me during this study. Special thanks are due to Dr. P.K.H. Maguire for help on difficult problems.

I would also like to thank my wife, Valerie, who typed this thesis and Mr. G. Dresser for photographing the diagrams.

ABSTRACT

The seismicity of East Africa has been investigated using the Durham University seismometer array at Kaptagat. Events recorded by this station originate from five main seismic regions. Three of the five regions, the Kavirondo Rift, the Sirla Fault and the area from Entebbe to the Ruwenzori Mountains, form east-west bands of activity. The activity in the remaining regions, the Western Rift, in particular the Ruwenzori Mountains, and the Gregory Rift shows a north-south distribution. Earthquakes from the Western Rift are associated with the boundary faults. In the Kavirondo Rift the events are associated with the eastern end of the graben and have been used to infer an easterly extension of the faults. Within the central Gregory Rift the shocks are associated with the axis of the rift. Where the Gregory Rift passes into the North Tanzania Divergence and the Turkwel Depression the events are distributed across the width of the Rift.

From the slope, b, of the cummulative frequency-magnitude curve it is suggested that the Western Rift can be divided into a northern and southern section. The former section is the younger and is tectonically similar to the Kavirondo graben. The Eyasi and Gregory Rifts have shown the same value for 'b' and seem to be tectonically similar. However, they differ in the upper cutoff limit on the magnitude of the earthquakes.

The pattern of seismicity in the Gregory Rift and the travel time, compared to normal shield structure, across the rift have been interpreted to give a model for the crustal structure within the rift. The model consists of a continuous velocity increase with depth interrupted by a drop in velocity. The anomalous material which the model represents also has a low Q value of approximately 100.

C O N T E N T S

CHAPTER 1

THE AFRICAN RIFT SYSTEM

1:1 The broad pattern of faulting.

A belt of anastomosing faults runs southward from the junction of the Gulf of Aden and the Red Sea for 4000 Km (McConnell, 1972). This belt of faults is known as the East African Rift System. At the northern end of the system, in the centre of the Arabian Ethiopia dome, a triple junction is formed in the Afar triangle where the Red Sea, the Gulf of Aden and the East African Rift meet. From this junction the faulting runs across the dome, through the Rudolf graben and into the Gregory and Eyasi Rifts. The last two rifts form the eastern margin of the Pre-Cambrian Tanganyika shield and are collectively known as the Eastern Rift. A maximum distance of 1000 Km to the west, the Western Rift valley forms the western margin to the shield. This rift valley encloses the lakes Albert (Mobutu Sese Seko), George, Edward (Idi Amin Dada), Kivu, Tanganyika and Rukwa. Neogene-age faulting in the Lake Malawi area may represent a tenuous connection between the Eastern and Western Rifts. More definite evidence of a junction is hidden by the Pleistocene-Holcene age volcanics of the Rungwe Mountains (McConnell, 1972).

Dixey (1946) defines a Southern Rift which runs southward from Lake Malawi for 1280 Km. At the end of the Southern Rift the faulting bifurcates, the two arms encircling the Rhodesian Shield. Around the Rhodesian Shield the rifting is represented by troughs of Karoo sediments formed by faulting during the Karoo and Cretaceous periods (Vail, 1967). South of these troughs the line of tectonic features is represented by igneous complexes such as the Bushveld and the Great Dyke (McConnell, 1967).

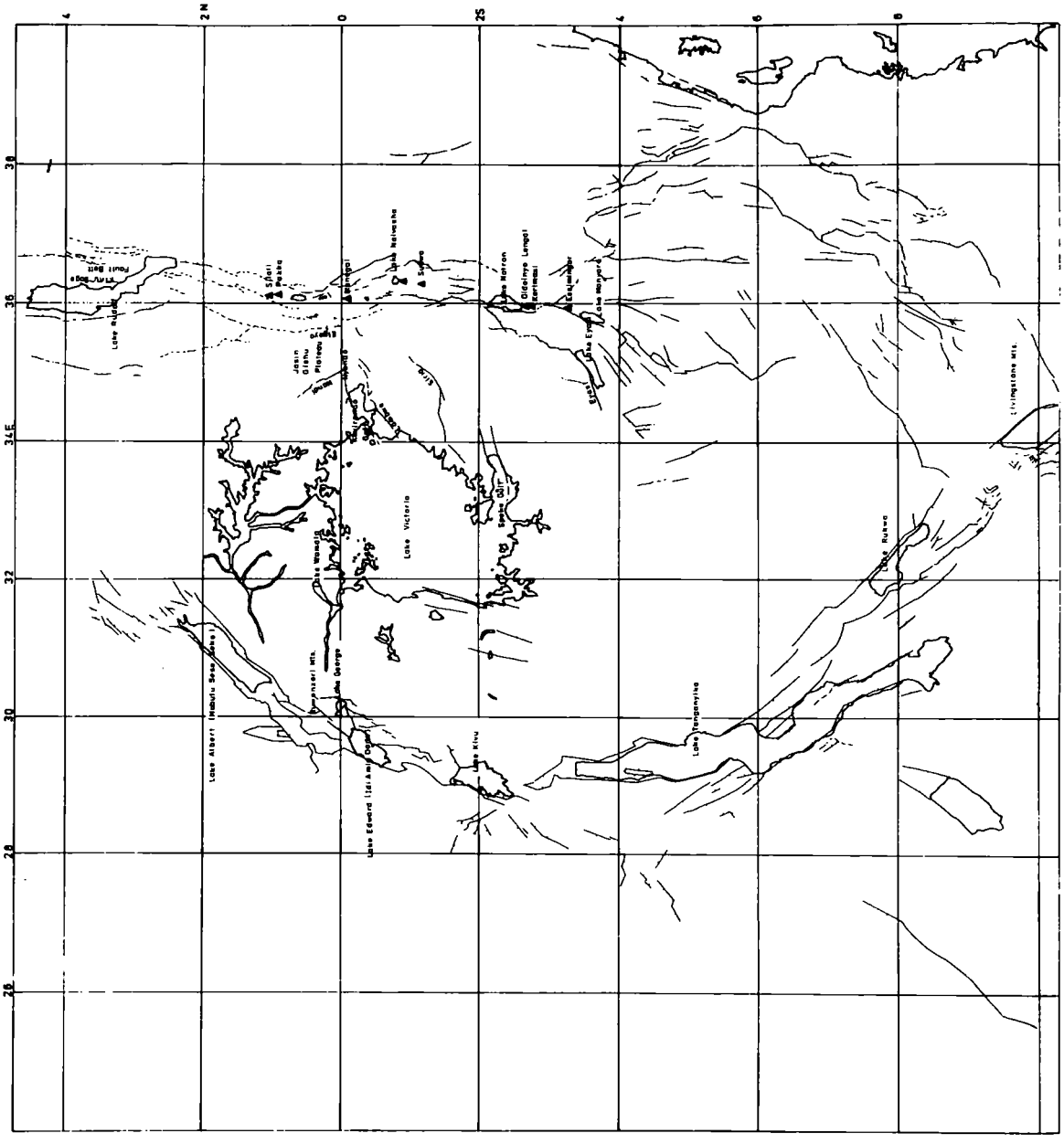

Geography of East Africa

Fig 1:1

Unlike the oceanic rift valleys, the Continental rift, which runs from Malawi to Ethiopia is not a continuous physical feature (Le Bas, 1971). From the pattern of faulting McConnell (1972) has suggested that the distribution of the faults is controlled by the Pre-Cambrian orogenic belts within the continent. This may not be completely true of the whole rift system as Mohr (1974a) has suggested that satellite photographs show that the NNE trending Gregory Rift in north central Kenya is not aligned with N-NNW trending Pre-Cambrian structures. On the other arc of the rift system, the Lake Tanganyika Rift, often regarded as an example par excellence of a rift determined by older structures, persists in its curving arc despite linear Ubendian trends. The relationship between the faulting and the Pre-Cambrian orogenic belts would suggest that the geology has influenced, but does not completely control, the distribution of the faults.

1:2 The Western Rift.

The Western Rift, as defined by Dixey (1946), is restricted to a series of north-south trending features enclosing the lakes Albert, Edward, Kivu and Tanganyika. This belt of faulting extends from the Rungwe Mountains to north of Lake Albert where the faulting abuts against the Madi Series of Sudan and the Aswa shear belt of northern Uganda. Throughout its length, the Western Rift is confined to Pre-Cambrian orogenic belts. Where these belts depart from a north-south trend the faulting becomes en echelon reflecting the older grain but still maintaining an overall north-south direction (McConnell, 1967).

The Lake Tanganyika graben, which lies within the NW-SE trending Ubendian belt, was probably initiated in the Late Palaeozoic (McConnell, 1967). Then, during the Jurassic, elongated basins with

partly faulted margins were formed and filled with Karoo sediments. Further downfaulting or folding protected these sediments from the following planation which formed the Post Jurassic - Pre-Cretaceous erosion level. Movement of the faults occurred again during the Upper Pliocene and caused the uplift of the Livingstone Mountains much further south (Quenell, 1956). The north-eastern margin of the Tanganyika Rift is formed by two uplifted blocks. These blocks are terminated by a downfaulted belt which forms the Rukwa valley to the south of Lake Tanganyika (Sutton and Watson, 1959).

The Ubendian, with which the Tanganyika Rift is associated, is dated as 2.15 - 1.65 10^3 my., (M^{c}Connell, 1967). This prominent orogenic belt is a metamorphic complex of ortho- and paragneisses. Across the gneissic complex shear zones run in a NW-SE direction parallel to the regional strike. Evidence of Pre-Cambrian faulting is present in the form of two sets of nearly vertical mylonite bands running NW-SE and N, NE-S, SW. These mylonites are thought to have been formed at depth by transcurrent faulting which generated the heat necessary for the mineral assemblage within the zones. Cataclastic rocks and elongated anatectic granites, totally different to those within the mylonite belts, are also associated with the faults that form the present rift (Sutton and Watson, 1959).

North of Lake Tanganyika the geology changes as the Pre-Cambrian basement disappears beneath a volcanic field of alkali basalts, basanites, trachytes and trachyandesites. Sandwiched between this volcanic field and the Birunga-Bufumbria lave fields further north is Lake Kivu. The Birunga-Bufumbria field was formed by eight volcanoes which align in an east-west direction perpendicular to the line of faulting (Holmes, 1965).

The faulting that lies on either side of Lake Edward follows the line of the Ubendian orogenic belt. On the eastern flank where the faulting dies out the persistance in the line of weakness is illustrated by downwarping and volcanics (Reece, 1961). Further north into west central Uganda the rift turns from the Ubendian trend to follow the strike of the Toro system of Uganda, (King, 1970). The Toro system is of Ubendian age but has had Karagwe-Ankolean structures, 1.29 - 0.85 10^3 my. Image (McConnell, 1967), impressed upon it. These structures are mainly NNW-SSE folds with minor NE striking cross folds and similarly aligned small scale thrusting.

Rurther north the 50 x 120 Km Pre-Cambrian block of the Ruwenzori Mountains perturbs the persistant rifting. This block is bounded to the west by westward hading faults, dipping at 10 - 30 degrees, and the Semliki Rift (Davies, 1951). To the east the block is bounded by an upwarp and the Pre-Cambrian Wasa fault. The Wasa fault is probably a Pre-Cambrian dextral transcurrent shear of 8 Km which has been exploited by Tertiary movement, (McConnell, 1972). The northern nose of the Ruwenzori is composed of basement gneiss over and against which is thrust the Ubendian front to give east-west synclines of schists and quartzites. Dixey, (1946), has suggested that the Ruwenzori is the remnant of a much larger block formed during the Jurassic since when it has suffered erosion with minor uplift. However, recent movement of the Ruwenzori is indicated by grid faulting in the Albert Graben (Bishop and Trendall, 1946) and adjustment of the faults to the west, (Wohlenberg, 1966). Holmes (1965) suggests, from the present height of the Miocene planation levels in the Ruwenzori area, that 3 Km of uplift has occurred since the Miocene. If this is correct, Dixey's

suggestion must be wrong.

Beyond the Ruwenzori lies the Albertine Rift. Near Murchison Falls, the floor of the Albertine Rift is 2250 feet O.D. and falls steadily southwestwards to drop to -6000 feet O.D. in 100 miles (Bishop and Trendall, 1967). Faulting in the Albert graben is simple but there is evidence of two periods of movement. Sandstones in river valleys in the southeast of the area suggest that subsidence occurred in the south first and that downward movement stopped temporarily after 500 feet (Davies, 1951). The greater part of the movement is of Pleistocene age but drilling has revealed older faulting. These older faults are overlain by Plio-Pleistocene sediments (King, 1970, and Davies, 1951). Faulting does not extend much further north but ends where it encounters the Madi and Aswa zones. The Aswa zone is a 6 mile wide strongly foliated basement gently folded about steeply plunging NW axes; (Hepworth and Macdonald, 1966).

The overall impression of the Western Rift is that the faulting becomes younger toward the north. Miyamura (1962) has suggested that as the tectonic features become older the seismicity changes. As the faulting in the Lake Tanganyika area is probably the oldest in the Western Rift, and well established, the seismicity may be different compared to the Albert Rift. The scarcity of faulting to the north of the Albert Rift may be due to the Madi Series and the Aswa shear zone. If these two features are resisting the northward extension of faulting, the northern end of the Albert Rift may be an area of stress accumulation.

1:3 The Eastern Rift.

The arrangement of the faults in the Eastern Rift zone is different to that within the arc of the Western Rift. Even within

the Eastern Rift the style of the faulting changes considerably. In the region known as the North Tanzania divergence, north of the Rungwe Mountains, the faulting forms a basin and range structure (Quenell, 1956). This structure is the result of a series of blocks, faulted and upthrown on the eastern side and tilted toward the northwest. From west to east across the area these blocks are known as the Mbulu, Konda, and Letatema structural blocks. The faults within the North Tanzania divergence are not all of the same age. Faults in the centre of the area are of Lower Pliocene to Pleistocene age and away from the centre of the zone the faulting generally becomes progressively older (Girdler et al., 1969).

As the faulting is followed northward across the Kanya dome the structure formed by the faults changes from a basin and range province to the graben of the Gregory Rift. The size of the doming is reflected in the height of the valley floor which is at 2000 m O.D. on the crest of the dome and drops to 650 m O.D. at the southern extremity of the rift valley (Baker et al., 1972). The sides of the rift valley are the product of a series of faults each of which shows considerable variation in amplitude. In the southern part of the rift the western margin is formed by the Nguruman fault which has a maximum throw of 5000+ feet. As the Nguruman fault is followed northwards the amplitude of the throw decreases until the fault passes into an eroded downwarp. North of this downwarp faulting once again develops. This pattern of fault-downwarp-fault is found along the length of the rift valley. The variation in the throw of the faults is well illustrated by the Elgeyo fault which develops a throw of 5000 feet in a few miles (King, 1970). A similar pattern of faults and downwarps is found on the eastern margin of the rift valley. The pattern on

the eastern margin is assymetrical to the distribution of faults and downwarps on the western edge of the rift valley, with a fault opposite a downwarp and vice versa (King, 1970).

The faulting in the Gregory Rift can be divided into three episodes which are of Lower Pliocene, Upper Pliocene and Pleistocene age. During the first episode faulting was restricted to the western margin of the rift valley to give an assymetric trough formed from eastward tilted blocks (Baker and Wohlenberg, 1971). Not all of the western margin of the future rift valley was affected by this faulting. The Nakuru section in line with the Kavirondo Gulf was probably an upstanding area during this period (McCall, 1967). But where the faulting did take place it produced large scale scarps as in the Lake Hannington area where throws of 4000 feet have been measured. In the second episode of faulting the rift valley was developed with faults formed on both sides of the rift and the valley floor at a lower level than the flanks of the rift. Again the form of the faulting is not constant, some sections of the sides of the valley being produced by step faults whilst other sectors are formed from single large continuous faults (McCall, 1967). The faults formed during this period are fairly widely spaced. The final episode of faulting produced a series of grid faults with throws rarely more than 150 m (Baker et al., 1972) but as much as 300 m in the Nakuru area (McCall, 1967).

To the west of the Gregory Rift valley the faulting can be divided into two groups, an important group of faults trending in a general east-west direction and minor faulting in a north-south direction. The dominance of the east-west trend is illustrated in satellite photographs which show that the ENE-WSW lineaments are frequent to the south and southeast of Lake Victoria but scarce to the north of Lake Victoria (Mohr, 1974b). In this study three east-

west structures were found to be the site of earthquake activity. These structures were the Kavirondo Rift, the Siria fault and the Ngorikia fault. The northern margin of the Kavirondo graben is formed by the Nyando fault which decreases in throw westward to pass into a monocline. On the other side of the Kavirondo graben, the southern margin is formed by the Sondu fault which grades eastward into a flexure. The pattern of faulting is similar to the Gregory Rift in that a flexure lies opposite a fault on the other side of the rift. Any junction with the Gregory Rift is hidden by the Uasin Gishu phonolite lavas. Further south the Siria and Ngorika faults run in a NE-SW direction and have downthrow to the east of 800-900 feet and 700 feet respectively. These normal faults each lie in a mylonite zone which is the location of a healed thrust plane. This thrusting was probably of Pre-Cambrian age as it truncates the post-Kavirondian, pre-Bukoban Kilgoris granite (Williams, 1964). Of the north-south features west of the Gregory Rift the Nandi fault is probably the most important. This is a recent normal fault that has exploited a mylonite zone formed by a Pre-Cambrian thrust (Jennings, 1964). In the Eldoret and Kapsabet areas near the Kaptagat array, the north-south faulting is a mixture of healed Pre-Cambrian thrusts of varying extent and minor normal recent faults (Sanders, 1963 and Jennings, 1964).

As the Gregory Rift is traced northwards the fault belt widens and passes into the Turkana depression. This region of faulting is almost a mirror image of the North Tanzania divergence which suggests a symmetry of faulting about the Kenya Dome. In the Turkana depression the small Suguta graben, south of Lake Rudolf, and the Baringo trough are the northward extension of the Gregory Rift. The Suguta graben is approximately 20 Km wide and is bounded by escarpements rarely more than 400 m in height (Dodson, 1963).

To the west of the Suguta-Baringo graben the Uganda and Turkwel escarpements form the western border of a triangular lowland (Baker et al., 1972). These escarpements are probably the oldest faults in the Gregory Rift and may degrade into monoclinal flexures in the north (Walsh and Dodson, 1969). The Suguta graben does not persist for long but degenerates, as it encounters a region of shallow uplift, into a zone of Pleistocene faulting known as the Kinu Singo fault belt. Within the Kinu Singo fault belt the faults are all normal and have a small throw (Baker et al., 1972). The triangular shape of the Turkana depression forms a lowland feature between the Kenya and Ethiopia domes and serves as a northern boundary to the Gregory Rift.

Three questions are posed by the pattern of faulting in and near the Eastern Rift. The first question is: are the east-west structures outside of the rift active and in any way related to the main rifts? Secondly, as the structure of the Turkana and Tanzania areas is different from the structure of the Gregory Rift, there may be a difference in the seismicity between the two structural regimes. The third question concerns the Kavirondo Graben and any possible connection with the Gregory Rift. As Kaptagat lies close to both the Kavirondo and Gregory rifts, it is in an ideal position to outline any connection, under the Uasin Gishu lavas, between the two rifts. This connection, to be observable, must be made by currently active faults.

1:4 Volcanism in the East African Rift.

The extruded igneous rocks in East Africa are associated with faulting and in particular with the Eastern Rift. In the Eastern Rift the volcanism and faulting are closely linked as the volcanic activity developed at the same time as the faulting (King, 1970).

Within the Eastern Rift zone the first magmas to be erupted during the Tertiary-Quarternary period came from two lines of volcanoes. One line of volcanoes lies along the line of the Kavirondo Graben and the other in Eastern Uganda (Logatchev et al., 1972). The lower to middle Miocene volcanoes Elgon, Kordam, Napak, Kisingri and Tinderet erupted alkaline rocks such as melanephlenite. Carbonatites may be associated with these alkali rocks, as th the case of Napak, the eroded base of which shows a core of carbonatite (King, 1970). To the north and northeast of the above central volcanoes, fissure eruptions created a Basalt series in the northern area of the incipient rift (Baker et al., 1971). The difference in volcanism of the two areas immediately suggests a structural difference between the two areas.

Later, in the Upper Miocene, the centre of eruption changed to the Kenya Dome area of the future rift. During this period large quantities of phonolite was extruded from long fissure vents (Logatchev et al., 1972 and Baker and Wohlenberg, 1971). The phonolite is of uniform mineralogical composition (Williams, 1972) which suggests that the source was either large or continually replenished.

After the first phase of faulting in the lower Pliocene the form of the volcanic eruption changed from fissures to central volcanoes. During this episode 19 volcanoes were active along the rift valley with subsidiary fissures, close to and in the rift valley, issuing phonolite lavas (Logatchev et al., 1972). Rhyolites, ignimbrites and trachyte occurs in the downfaulted axial part of the Kenya Dome (Williams, 1972). The main eruptions initially started with minor phonolitic and trachyte magmas in the central sector followed by voluminous basalt lavas in the Aberdare Mountain

range. Williams (1972) found that the alkali to silica ratio in these and subsequent lavas is lower than the ratio in the earlier volcanics. This suggests a change in the status of the source.

In the Upper Pliocene and Lower Pleistocene basalts were emplaced along the whole of the Gregory Rift. In the north and central rift sectors these basalts were erupted from fissures but in the south from shield volcanoes. Carbonatite magmatism took place 130 Km south of the main area and autonomous centres of melting were initiated east of the rift (Logatchev et al., 1972). These centres east of the rift gave rise to basalts, nephelinites and trachybasalts with lavas becoming more alkaline in later flows. The middle and upper Pleistocene saw the completion of the rift trough and effusion of trachyte and phonolitic trachytes through out the length of the Gregory Rift.

In the Western Rift the volcanic suite of rocks is not so well developed. The northernmost activity in the Western Rift occurs afound the Ruwenzori block where the volcanic field consists of a great number of ring craters. Lava flows from these craters are rare and the main erupted material is rounded blocks of foundation rocks, pyroclasts and rock powder. The lavas range from carbonatites to potash rich ultrabasic lavas (Holmes, 1965). Further south the eight volcanoes of the Birunga-Bufumbria volcanic field produced potassium rich lavas ranging from nephelinites to trachytes. Of the eight volcanoes in the field the two westernmost vents are still active. To the south of Lake Kivu there is a volcanic field composed of silica saturated tholeitte lavas (Baker and Wohlenberg, 1971). The volcanoes within this tholeitte field were active from the Lower Pliocene to middle Pleistocene. As the volcanic activity is traced southwards from the Ruwenzori Mountains it becomes progressively older. This is the reverse of the trend displayed

by the volcanic activity in the Eastern Rift.

The volcanic suite found within the East African Rift may be due to either an upwelling geothermal current (Baker et al., 1972) or the depression of the phase transformation boundaries (Harris, 1969) or both. Carbonatite rocks within the rift zone are enriched with rare elements. This suggests that the Carbonatite probably resulted from volatile enrichment of a stagnant magma deep in the upper mantle. The primary magma may have had a high CO_2 content which combined with the calcium to produce the Carbonatite. Removal of the calcium from the fluid would result in the production of nepheline and aegirine instead of albite and augite. The elimination of the silica phases may have taken place as the 'carbonatite magmas' rose to the surface (O'Hara, 1965). In North Tanzania the Lashine lavas contain xenoliths of Garnet Lherzolite. These xenoliths, which probably correspond to the mantle at depths of 90-100 Km, are relatively uncorroded suggesting that the magma ascended quickly. The magmas, in which these xenoliths were suspended, probably represent the lower melting temperature components of mantle peridotite (Dawson et al., 1970). Further north in the Gregory Rift, the lavas of the Sialí volcano may be differential products of a basaltic magma confined to cupolas high in the crust (M^{c}Call and Hornung, 1972). Chemical relationships within the Sialí lavas suggests that the magma within the cupolas was initially of upper mantle origin.

The East African Rift system has frequently been compared with oceanic rift systems and the difference in the volcanic suites is an important aspect of this comparison. Oceanic ridges are characterized by basaltic and tholeiitic lavas, transform faults and a high heat flow. The Ethiopian Rift, which is the section of the continental rift nearest to an oceanic ridge, is characterized

by large volumes of Tertiary basalts. These basalts are intermediate between tholeiites and alkal basalts and have a tholeiitic chemistry but an alkali mineralogy (Baker et al., 1972). Further south in the Kenya Dome the most striking feature is the abundance of phonolites. The petro-chemistry of the Kenya and Ethiopian Domes shows that the rocks in Kenya are richer in CaO-MgO-FeO than the extrusive rocks in Ethiopia. Because of the high percentage of calcium, magnesium and iron oxides it is thought that the Kenya basalts have addeeper origin than the Ethiopian basalts. This suggests a trend along the rift with the source of the magma becoming progressively deeper towards the south. A second pattern is superimposed across the rift with basalts tending to be more tholeiitic in the rift than on the plateau (Baker et al., 1972). Reay and Harris, (1964), have suggested that for a silica saturated tholeiitic liquid to be in equilibrium with a parent ultramafic liquid, the confining pressure must be in the range 0-10 Kbar. The confining pressure for an alkali basalt liquid, to be in equilibrium with an ultramafic parent, must be in the range 20-30 Kbar (Kushiro, 1965, and Green and Ringwood, 1967). This suggests a shallow origin for the tholeiitic oceanic lavas and a deeper origin for the alkali basalt series of the continental rifts. The gradual increase in the depth of origin of the lava toward the southern part of the rift is indicated by the nephelinite-carbonatite-kimberlite provinces of the continental rift. Le Bas (1971) has suggested that these alkali lavas may be the result of degassing of the deep upper mantle. Le Bas also invokes expansion of the top of the upper mantle to give the doming of the crust and the peralkaline volcanoes.

Two questions are posed by the distribution of the various types of magma. The distribution of lavas within the Gregory Rift

and adjacent areas would suggest that the depth of origin of the magmas increases as the distance to the centre of the dome increases. Within the Gregory Rift the volcanoes may be fed from local crustal reservoirs. The mantle dome and crustal cupolas, from which the magmas originate, may affect the strength of the crust and the stress distribution. These effects may be reflected in the seismicity and the magnitude of the earthquakes.

1:5 Geophysical studies.

Geophysical investigations can be divided into studies concerned with structures within the rift and studies associated with the structure outside of the rift.

Gravity surveys conducted by Bullard (1936) revealed a negative Bouguer anomaly associated with the East African plateau. Bullard suggested that the anomaly is the result of a mass deficiency within the mantle and that the plateau is in isostatic equilibrium. Fairhead and Girdler (1969), from more recents surveys have found that the anomaly, which has a maximum amplitude of 1500 g.u (1g.u = 0.1 mgal), has gradients of approximately 3 g.u. Km^{-1}. Small gradients, as found by Fairhead and Girdler, suggest that the anomaly is produced by a deep body of small density contrast. Seismic studies have produced a number of models, Fig (1:3), for the crust of the plateau. Maguire (1974) generated a model for the crust south and west of Kaptagat from the apparent velocity of signals across the Kaptagat array. This model is similar to that derived from earthquake data by Rykounov et al., (1972) for the crust at the southern end of the Gregory Rift. The similarity of the two models would suggest that the crust is continuous between the two areas. When the two models for the

crust near the Gregory Rift are compared with models for the shield crust of South Africa (Gane et al., 1956, Hales and Sachs, 1959, Willmore et al., 1952) the two groups of models are found to be similar. This suggests that the crust of the East African plateau is of the same structure as the crust of the South African shield. Further confirmation of the similarity between the crust of the East African plateau and the South African shield is displayed in surface wave studies. Using multimode surface wave dispersion techniques, Block et al., (1969), have demonstrated that crust and mantle under South Africa is similar to the Cansd model, of Brune and Dorman, 1963), for the Canadian shield. Gumper and Pomeroy, (1970), using surface wave velocities have derived a model, the Afric model, for the crust and mantle under the whole of Africa. The Afric model is similar to the Cansd model which supports the assumption that normal African crust is of shield type structure. The structure of the East African plateau has been investigated by Sundarlingham (1971) who has shown from the dispersion of Rayleigh waves between Bulawayo-Nairobi, Addis Ababa-Nairobi and Addis Ababa-Lwiro that the crust of the East African plateau is similar to the crust of the Afric model. This close similarity is evident from the merging at short periods, of the dispersion curves for the East African plateau given by Sundarlingham and the dispersion curve generated by the Afric model. However, at long periods the two dispersion curves diverge. The dispersion curves of Sundarlingham reveal a significant reduction, at long periods, in the phase velocity; this suggests a low velocity upper mantle anomaly (Long et al., 1972). This low velocity anomaly is probably coincident with the anomaly indicated by the gravity surveys.

In the Gregory Rift gravity surveys have revealed a negative Bouguer anomaly of amplitude 1000 g.u and 500 Km wide. This

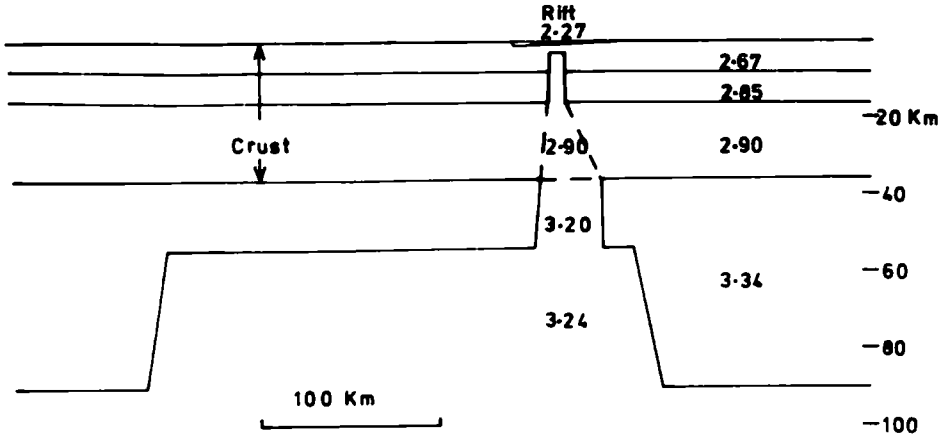

Darracott et alia 1972

Latitude 1·8°S

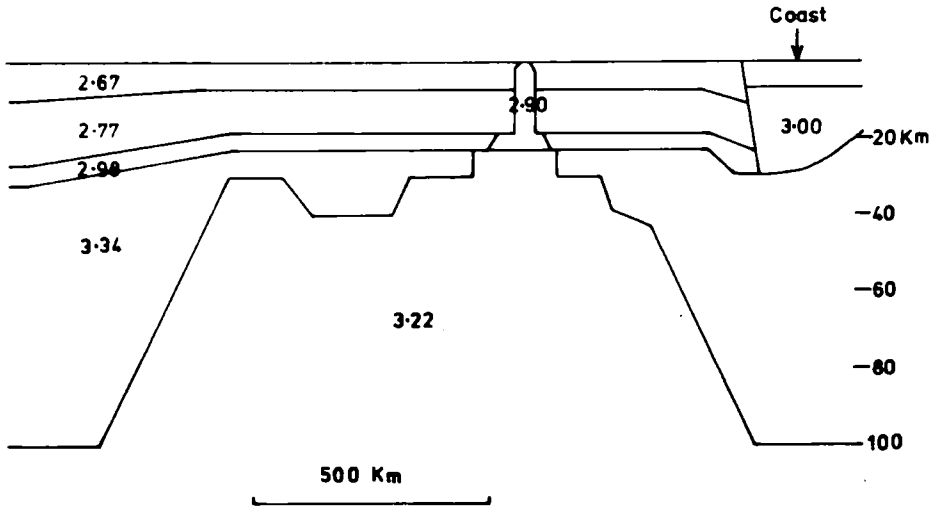

Fairhead and Girdler 1972

Latitude 0·0

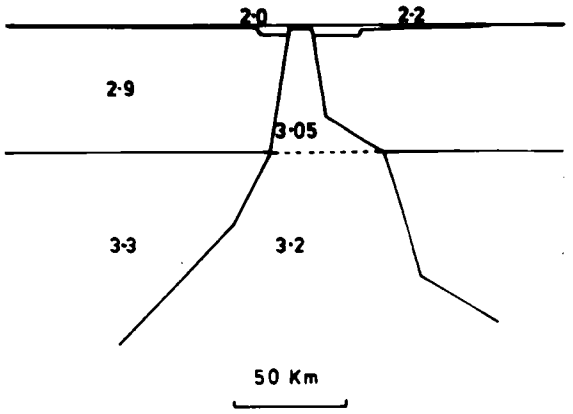

Baker and Wohlenberg 1971

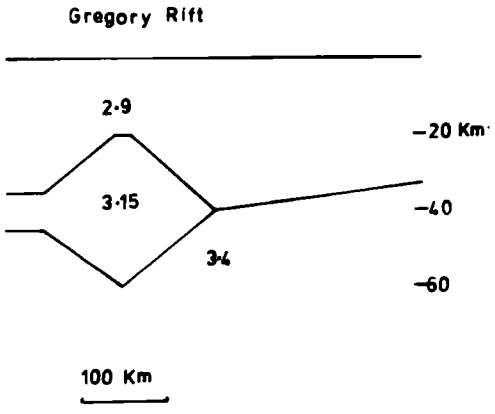

Khan and Mansfield 1971

Gravity Models for East Africa

Fig 1:2

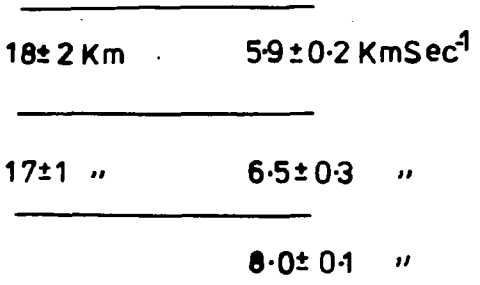

Maguire 1974
Western Flanks of
the Kenya Dome

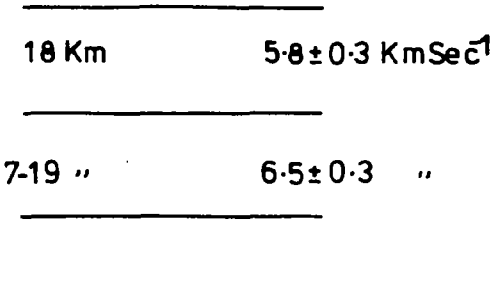

Rykounov et al 1972
Northern Eyasi Rift

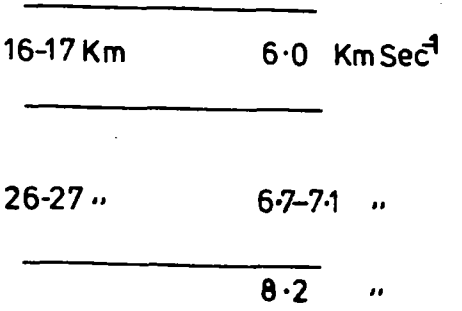

Bonjer et al 1970
Crust under Nairobi

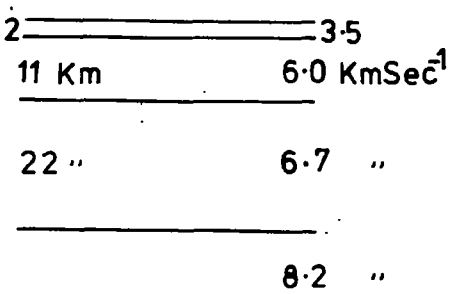

Bonjer et al 1970
Crust under Lwiro

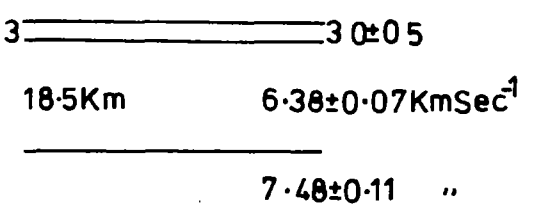

Griffith et al 1971
Gregory Rift

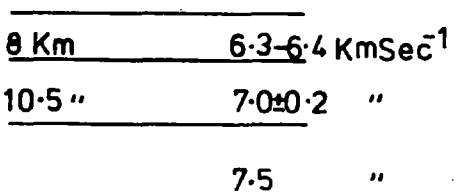

Maguire 1974
Gregory Rift

Crustal Models
Derived from Seismic
Studies

Fig 1:3

anomaly is probably due to doming, under the Gregory Rift, of the eastward extension of the low velocity mantle material found under the East African plateau. As the negative anomaly is traced northward its amplitude decreases and, in doing so, correlates well with the decrease in height of the topography (Khan and Mansfield, 1971). South of the centre of uplift the anomaly dies out between 5°S (Girdler and Sowerbutts, 1970) and 4°S (Darracott et al., 1972). Darracott et al., (1972), also suggested that the anomaly is rotated by 25° east of north. On to the negative anomaly is superimposed a positive Bouguer anomaly coincidental with the axis of the rift. This positive axial anomaly has been interpreted by Searle (1970), Baker and Wohlenberg (1971), Khan and Mansfield (1971), and Darracott et al., (1972), as an intrusion into the crust (Fig 1:3). This axial intrusion is probably derived from the mantle anomaly. Possible confirmation of a crustal anomaly comes from magnetic surveys carried out in the Gregory Rift by Wohlenberg and Bhatt (1972). In the Lake Magadi area they found a series of north-south anomalies varying in amplitude between +200 gammas and -200 gammas and more numerous in the north of the area. Superimposed on the primary anomalies are a series of NW-SE trending secondary anomalies. The half-wavelength of the secondary anomalies suggest a deep crustal origin for the secondary anomaly. In the Lake Hannington area, the NW-SE trending anomalies become dominant and again a deep crustal origin is suggested for the anomaly by their half wavelength. Refraction studies by Griffith et al., (1971), have shown that the crustal structure within the rift is different to the crustal structure outside the rift. They have suggested that the structure within the rift can be represented by the model in Fig (1:3). Griffith (1972) has suggested a modification which is illustrated in Fig (1:3). These models must

be regarded with caution as the refraction lines were effectively unreversed. Maguire (1974) using the apparent velocities measured across the Kaptagat array of earthquakes located within the Gregory Rift, suggested that the crust could be represented by the model illustrated in Fig (1:3). All the models for the Gregory Rift clearly suggest that the crust within the rift is different to the shield crust outside. Teleseismic studies have confirmed the difference between the Gregory Rift and the shield. Gumper and Pomeroy (1970) found that Sn was evident on the records for all paths less than 3000 Km in length that did not cross the African Rift zone or the Red Sea. South of latitude 10°S they found that Sn propagated across the rift. Sn was not seen for paths that crossed the rift north of the equator. In between the equator and 10°S Gumper and Pomeroy found that Sn propagation was dependent on path. The region of Sn attenuation can be correlated with positive travel time residuals to the tables of, (I) Herrin and Taggart (1968), (II) Lilwall and Douglas (1970). The abnormal structure of the rift is further outlined by delay times measured on teleseismic arrivals. Sundarlingham (1971) has measured the delay of teleseismic arrivals at Addis Ababa, Nairobi and Lwiro relative to the normal crust which is presumed to underlie Bulawayo. Delays at these stations indicate the existence of anomalously low velocity material under the stations. However, the delay at Lwiro is approximately half the delay measured at Nairobi and Addis Ababa. This suggests that the anomalous material on the path to Lwiro is less extensive than on the paths to Nairobi and Addis Ababa. Backhouse (1972) has made delay time measurements on teleseismic arrivals at the Kaptagat array. His value of 2.2 seconds delay on teleseismic arrivals at Kaptagat is similar to

the 2.3 seconds measured at Nairobi by Sundarlingham. Long et al., (1972), from the measurement of the slowness of teleseismic arrivals across the Kaptagat array and from dispersion studies of teleseismics, have suggested that a low velocity mantle anomaly underlies the Gregory Rift. They suggested that the anomaly has outward sloping boundaries and that the velocity of the material lies between 7.0 and 7.5 Km sec^{-1}. Knopoff and Schule (1972) have confirmed the presence of a low velocity channel under the rift but suggest that surface wave dispersion data does not allow a definite model. They also point out that the dispersion curve for the Addis Ababa-Nairobi path is similar to that for paths through the Basin and Range province.

The Western Rift, like the Gregory Rift, has an associated negative Bouguer anomaly. From the gravity data Bullard (1936) has suggested that Western Rift valleys are isostatically uncompensated. Gradients of 4 g.u Km^{-1} (Wong and Von Herzen, 1974) exist on the gravity anomaly to the west of Lake Kivu. To the east of the rift the gradients of the anomaly fall to zero. This implies that the anomaly becomes deeper to the west of the Western Rift. From earthquake data, Dopp (1964) has produced a model for the crustal structure within the Western Rift. Dopp's model, Fig (1:3), for the Western Rift is very similar to models for the crust in the shield area of the plateau. The depth to the second layer in Dopp's crustal model for the Western Rift is variable and the boundary may have a dip of 10-16° to the west.

Both the Kavirondo Graben and the Speke Gulf have been investigated by gravity surveys. These surveys have revealed negative Bouguer anomalies over the two features. The negative Bouguer anomaly over the Speke Gulf has been interpreted by Darracott (1974) as either a granitic intrusion or a Pre-Cambrian

Graben. Darracott favours the latter interpretation.

The similarity between the crustal model of the Western Rift and the shield would suggest that the Western Rift is not penetrated by a crustal anomaly. The crustal structure of the Gregory Rift is different to the shield structure of the plateau and the crust has been penetrated by relatively high density material, (Girdler et al., 1969, Searle, 1970, Baker and Wohlenberg, 1971, Khan and Mansfield, 1971, Darracott et al., 1972). The intrusions and the mantle anomaly that underlies the Gregory Rift may cause the crustal structure to deviate sufficiently from the crustal structure of the normal shield to affect the travel time of the seismic signals estimated using the normal shield model. Also if the anomaly is in a plastic state, or if the many intrusions that feed the volcanic vents form a diffraction grating, the amplitude of the seismic signal may be affected. Any such variation in the amplitude of the signal or travel time should be evident from measurements at Kaptagat and Nairobi. As the Gregory Rift crosses the Kenya Dome the stretching of the crust by the mantle anomaly may affect the local stress distribution. The pattern of the seismicity should reveal the currently active faults. From the pattern and nature of the active faults it may be possible to elucidate the local and general stress distribution.

1:6 Theories of rift formation.

A number of different hypotheses involving compression, tension, subsidence of faulted blocks and the movement of plates have been put forward to explain the African Rift system. Gregory (1921) proposed that the Kenya Rift is the result of compressional arching with the faulting resulting from extension on the top of the dome, Gregory's proposal has two serious fallings: (1) The blocks between

the faults have undergone subsidence and (ii) the existence of the Western Rift cannot be explained by the same process. Bullard, (1936), also believed the rifts to be formed by compression and suggested that the rift valleys were formed by overthrusting. However, the geological and geophysical evidence has shown that the faulting is normal and therefore not the result of compression. The doming in the Kenya Rift plays an important part in the hypothesis suggested by Willis (1936). He suggested that the faulting in the rift was the result of tension caused by doming of the crust by a subcrustal asenolith. Support for the doming hypothesis of Willis came from modelling experiments. Using models, Cloos (1939) simulated the crust in East Africa. By doming the model crust he managed to produce patterns of faulting in the model similar to the pattern of faulting in East Africa. The modelling experiments of Cloos will not explain the depth of the grabens. Freund (1966) suggests that these grabens are too deep to be explained by the doming hypothesis of Willis or the subsiding block hypothesis of Girdler (1964). From gravity data and the temporal pattern of volcanicity and faulting Girdler et al., (1969), Searle (1970), suggested that the rifts are the result of thinning of the lithosphere. The thinning of the lithosphere is probably a symptom of some other process and therefore not the ultimate cause of the faulting.

A number of well defined seismic bands are now recognized as the boundaries of lithospheric plates capable of moving over the asthenosphere. Using the pattern of seismicity part of a plate boundary has been defined running down the Dead Sea and the Red Sea, into the Afar Triangle. In the region of the Afar Triangle the seismicity splits into two trends; one trend is coincident with the East African Rift and the other is coincident with the ridge

in the Gulf of Aden. In the Gulf of Aden the edges of the continental crust are separated by at least 200 Km of oceanic crust originating from the cental ridge. In the Red Sea the presence of the oceanic crust is indicated by a basement with a p-velocity of 6.6 Km sec^{-1}. The basement is overlain by 3-5 Km of sedimentary material with a velocity of 4.3 Km sec^{-1}. However, within the Red Sea the width of the oceanic crust has decreased to 50 Km (Tramontl and Davies, 1969). This diminution in the width of the oceanic crust suggests that the movement of the plates diminishes in a northward direction. The movement of the plates relative to each other has been represented by rotating the plates about poles of rotation. From the pattern of magnetic lineations parallel to the Indian Ocean ridge, LePichon and Heirtzler (1968), found that the rate of separation of the two plates decreased from 3.0 cm yr^{-1} at the Southern Indian Ocean ridge to 1.5 cm yr^{-1} at the Carlsberg ridge. LePichon and Heirtzler combined these movement rates with the transform faults of Laughton (1966), to put the pole of rotation for the Arabia-Somalia plates at 26°N 21°E. LePichon and Heirtzler also found breaks, dated at 9-18 my B.P. in the magnetic lineations. If these dates are correct the break would correspond to the initiation of the East African Rift and the cessation of the movement of Africa against Europe. In the eastern Mediterranean the lack of compressional features in rocks younger than middle Miocene indicates the end of the northward movement of Africa. Further evidence of a change in the movement of the plates is seen in Ethiopia where the style of deformation changes in the Miocene (Gass and Gibson, 1969). The inability of a two plate model to explain the difference in spreading rates along the arms of the Afro-Arabian rift system

led to the proposal by Gass and Gibson (1969) of the Nubia, Somalia and Arabian plates. This three plate system was extended by McKenzie et al., (1970), and Roberts (1969) to include three poles of rotation. McKenzie et al., (1970), found that by matching the Gulf of Aden coastline, at the 500 fathom contour, the pole of rotation for the Arabia-Somalia plate system could be put at 26.5°N 21.5°E. The method of transform faults also gave the same pole of rotation and this is seen as confirmation of the position of the pole. By matching the coastline of the Red Sea, McKenzie et al., placed the pole of rotation for the Nubia-Arabia plates at 36.5°N 18°E. The pole of rotation for the Nubia-Somalia plates was computed, by the above authors, to be at 8.5°S 31°E. If these poles of rotation are used the crustal separation would be 30 Km in Kenya and 65 Km in Ethiopia. Freund, (1970), suggested that fitting of the Red Sea coastline was impossible because of the Danakil horst and that a pole at 36.5°N 18°E is inconsistent with present knowledge about the Suez and Dead Sea rifts. Freund suggested that the Nubia-Arabia pole could be better placed if the 2000 m contours in the Red Sea were matched. Matching the 2000 m contour would put the pole at 32°N 22°E. Roberts (1969) suggested that the pole of rotation for the Nubia-Somalia plates should be at 30°N 47°E. This pole must be incorrect as it implies that the East African Rift is spreading faster in Kenya than in Ethiopia. Mohr, (1970), in order to explain the rifting and the movement rates has proposed a four plate system. Although attempts have been made to explain the motion of plates about poles of rotation none fully explain the observed features. For instance, in Kenya the separation of the Gregory Rift is probably smaller at the north and south ends of the rift than in the centre. However, the seismicity does suggest a link between the East African Rift system and the ocean ridges.

Oxburgh and Turcotte (1974) have postulated that the East African Rift system is a product of membrane tectonics. They have suggested that strains, of the order of 0.1%, and stresses, of the order of the strength of the plates, may result when a plate moves over the 'surface' of the Earth. As the Earth is not a perfect sphere a plate of lithosphere moving to a new latitude may have a different curvature to the asthenosphere over which it lies. For a plate moving to the equator from the poles they suggest that tension will predominate in the centre of the plate and compression on the edges. The tension in the centre of the plate may give rise to rifting similar to the African rifts. This hypothesis differs from the 'plate movement' of McKenzie and others in that it requires only one plate and no extra splitting force.

The plate system explains the general rifting but not the doming which occurs in the East African Rift system. Harris, (1969), has suggested that the continental swells are the results of either convective uprise or depression of the phase transformation boundaries or both. He suggests that frictional and mechanical energy cannot provide the heat needed to cause melting as the movement rate, 0.5 mm yr^{-1}, (Baker and Wohlenberg, 1971), for the East African Rift, is too slow. Reduction of the pressure by compression will result in a small degree of partial melting, (Bailey, 1964), but insufficient to explain the continental doming and volcanism (Harris, 1969). Magnitsky and Kalashnikova, (1970), have suggested that, after allowing for erosion and isostatic relevelling, a phase change resulting in the displacement of the transitional zone at 400 Km depth will result in displacement at the surface. For an initial displacement of the transitional zone of 200 m, the surface of the crust will show a displacement of 1 Km. Osmaston (1971) believes the uplift to be due to heating

within the mantle and perhaps the crust. He calculates that an overall rise in temperature of 200°C of the mantle will give an uplift of 1.5 Km. The heat is provided by the penetration of hot material from the asthenosphere into the lithosphere. Initially the continental lithosphere will be cold and most of the heat of the intrusion will be dissipated in the wall rock. As the walls become hotter the intrusion rises higher. The heat lost to the wall may go toward aiding the domal uplift of the crust. Gass, (1970), has suggested that the mantle under the ocean ridges is in a state of thermal inequilibrium. The body resulting from the thermal inbalance may start at 300-400 Km depth and may not have a defined base. Confirmation of penetrative convection within the mantle may come from swarms of earthquakes, with focii at 50 Km depth, which occur under a volcano before eruption (Elder, 1966).

The seismicity of the Grefory Rift will reveal the active faults within the graben. The pattern of activity may give some indication as to the movement of the plates and the effect of the Kenya Dome. The penetrative intrusion, which probably forms the Kenya Dome, may weaken the crust and so affect the seismicity. Hence the seismicity and the associated seismic parameters may give some indication of the mechanics of the rift.

CHAPTER 2

DATA COLLECTION

2:1 Geology of the area around Kaptagat.

The Kaptagat array lies ten kilometres to the west of the Elgeyo Escarpment and is sited on phonolite lavas of the Uasin Gishu plateau. The origin of the array is at latitude 35.462°E, longitude 0.452°N. Three major faults lie within the immediate vicinity of Kaptagat. These faults, known as the Elgeyo, Nyando and Nandi faults, form an open box around Kaptagat. To the east of the station the Elgeyo fault runs in a NNW-SSE direction. This fault is the youngest of the three and was initiated during the formation of the Gregory Rift. West of Kaptagat and running in a parallel direction to the Elgeyo fault, is the Nandi fault. The Nandi fault is of post-Nyanzian, pre-Kavirondian age (Jennings, 1964). This fault shows signs of rejuvenation near Broderick Falls. North of Kaptagat the Nandi fault disappears under the volcanics of Mt. Elgon. The Nandi fault may be continuous with faulting in Uganda to the north of Mt. Elgon. The southern side of the open box is formed by the ENE-WSW striking Nyando fault. This fault is the northern limit of the Kavirondo graben. As the Nyando fault is traced eastwards it disappears under the phonolite lavas. However the drainage pattern on the lavas does suggest structural control which may be provided by the Nyando fault.

The phonolite lavas that the seismometers rest upon are the older of two flows that were errupted, during the mid-Miocene, from fissures to the east of the Elgeyo escarpment. Near the Kingwall swamp the lower lava flow is approximately 166 metres thick. Both the upper and the lower lava flow dip slightly to the west. This dip is consistent with their volcanic origin. The

lavas rest upon lower Miocene lacustrine sediments. These sediments in turn rest upon a Pre-Cambrian basement consisting of paragneiss, granitoid gneiss and metamorphosed Nyanzian basaltic lavas. The gneisses are the product of regional metamorphism upon semi-pelitic sediments. Evidence of intense folding and faulting can also be found in the Nyanzian lavas (Jennings, 1964).

Both normal faults and thrust faults occur in the immediate vicinity of Kaptagat. The thrust faults are restricted to the Pre-Cambrian and are not associated with the latest phase of faulting that gave rise to the Eastern Rift.

2:2 The recording and playback equipment.

The Kaptagat array consists of two arms of five vertical Willmore Mk II seismometers with a natural period of two seconds. One arm is aligned approximately east-west and the other arm is aligned in a north-south direction. Each arm of the L-shaped array is approximately five kilometres long. The seismometers forming the arms were positioned using a compass and line method which gave an accuracy in location of $\pm$ 30m except for seismometer Y5 where the accuracy in location is $\pm$ 60 m.

The signal from the seismometer is fed into an amplifier package located in the seismometer pit. This amplifier package consists of a pre-amplifier, a bandpass filter, a modulator and a buffer amplifier. The response of the filter is similar to that given in LONG (1968). Each seismometer is connected to a central recording station by twin telephone cable. This cable served a dual purpose in that it carried the frequency modulated signal and the power, which is derived from twelve six-volt accumulators and delivered down the line as D.C., to drive the

amplifier package at each pit. At the seismometer pit there is a battery pack into which the line power is fed. This acts as a reservoir and back up in case of line damage and limits the line voltage. The system is so designed that it remains operative if the lines are in poor condition or even if one of the cables is broken. The frequency modulated signal was recorded along with the signal from a long period instrument, a binary time code, a reference signal and a radio signal on 14 track one inch magnetic tape. A quartz crystal clock with drift less than 1 part in 10^8 was used to generate the time code, (LONG, 1968). Tape speed was 15/160 inches per second allowing signals of frequency up to 20 Hz to be recorded. Standardization of time was achieved by comparing the binary time code with G.M.T. time pips recorded on the radio channel. Each day the condition of the seismometer package was checked using an impulse calibration method.

The analogue magnetic tapes were played back, in the laboratory in Durham, at a speed ten times faster than that at which they were recorded and the signal displayed using a 16 channel jet pen recorder. Ten of the jet pens were used to write the signal from the ten seismometers of the Kaptagat array. Of the remaining six channels three were used for the binary time code and three for output from three Krohn-Hite filters. The three Krohn-Hite filters were used in bandpass mode to emphasize the signal when the signal to noise ratio was low. Because at any one time only three seismic channels could be filtered each event was written a number of times. Each time the event was played out the seismic inputs to the Krohn-Hite filters were changed. In order to produce the best possible set of traces for each event the limits on the bandpass filters were varied until the optimum

response was found. The bandpass limits were the same on each of the filters and kept constant during the playback of an event. Prior to each session of playback of records the alignment of the traces on the jet pens were checked. It was important to the method of analysis that the traces were correctly aligned or that the relative offset of the traces was known. Each set of seismic event records were preceded by a written display of the calibration pulses recorded on each of the seismic channels.

2:3 Readings made on the Kaptagat records.

The signal onset time at each seismometer was measured relative to an arbitrary base line. These measurements were used to find the direction of approach of the signal. To facilitate the measurement of the relative onset time of the signal the traces of the binary time code were utilised to draw an arbitrary base line. A magnifying glass and half millimetre scale were used to measure the offset of the onset of the seismic signal from the arbitrary base line. For events with the onset represented by an instantanious break in the trace the offset was measured to an accuracy of $\pm$ 0.05 mm ($\pm$ 0.002 seconds). However this accuracy was not possible for all events, the majority of the offset measurements being made to an accuracy of $\pm$ 0.01 seconds.

The onset time of the signal at the crossover point of the arms of the array was estimated from the arrival time of the signal at seismometer Y1. A correction was applied to this measurement to allow for drift of the clock that generates the time code. The corrected onset time at the crossover point was designated as the arrival time of the event at Kaptagat and has a reading error of $\pm$ 0.04 seconds.

The body-wave magnitude of each event was determined from the amplitude and period of the first six cycles of the signal (see Chapter 6). The amplitude of the signal was measured to an accuracy of ± 0.5 mm and was converted to ground motion using the response curve indicated by Fig (6:2). The period of the signal was measured to an accuracy of ± 0.08 seconds.

2.4 Data from other stations.

Nairobi seismic station is a member of the World Wide Standard Seismograph Network (W.W.S.S.N.). The equipment at the station consists of three long period Spregnether seismometers nd three short period Benioff seismometers. The records from the ong period instruments were not used in this study. Two of the enioff seismometers are operated in horizontal mode and the hird in vertical mode. The output from the Benioff seismometers, hich have a free period of one second, is fed into galvanometers ith a free period of 0.75 seconds. The light beam from the alvanometers then describes a trace upon photographic paper. hese paper records are photographed and the negatives used to roduce the seventy millimetre film chips used in this study. To roduce the film chips the negatives are reduced in size by a actor of approximately eight.

To view the film chips a microfilm reader was used to display he traces on a ground glass screen. The magnification of the icrofilm reader is such that the image on the ground glass screen s approximately 1,41 times the original paper record. As the recording system at Nairobi has a magnification of 50K the signal displayed as a trace on the ground glass screen has undergone a total magnification of approximately 70.5K. Time on the Nairobi

records is formed by minute and hour marks superimposed upon the seismic trace. The clock from which these pulses are taken experiences a drift of between 0 and 600 milliseconds per twenty-four hour period. The onset times of the events were measured relative to the nearest minute mark. This measurement was performed using a half-millimetre scale and a magnifying glass and gave a reading accuracy of ± 0.18 seconds. Besides the onset time of the event the maximum trace amplitude and the period of the first six cycles of the signal were measured in order to estimate the body wave magnitude. The trace amplitude was measured to an accuracy of ± 0.50 millimetres and reduced to ground motion using the response curve for the Nairobi instruments indicated in Fig. (6:2). The reading accuracy on the period measurements is approximately ± 0.18 seconds.

The seismic observatory at Nairobi is sited on a series of Tertiary lava flows, pyroclastic rocks and intercalated sediments. This series lies directly upon the Pre-Cambrian basement. The average noise level at the Nairobi observatory is 0.01μ of ground motion with a predominant period of 0.5 seconds. This value of the average noise level was used to check the calculated total magnification of the Nairobi records when displayed using the microfilm reader at Durham.

CHAPTER 3

LOCATION OF EARTHQUAKE FOCII

3:1 Introduction.

To locate the epicentre of an event using only one station requires knowledge of the azimuth of the epicentre from the station and the epicentral distance. With an array station it is possible to determine the azimuth of approach and the apparent velocity of a signal as it crossed the array. If the velocity structure of the crust is known the apparent velocity of the signal can be used to give the angle of incidence of the signal. Traditionally the epicentral distance is determined from the time separation between the Pg and Sg arrivals on the record. These arrivals have travelled the direct path from the focus of the event to the station. The Pg-Sg time can be converted into the travel time for the Pg arrival. If the velocity structure of the crust is known the travel time of the Pg arrival can be used to estimate the distance between the focus and the station. At large distances the travel path distance for a Pg arrival approximates to the epicentral distance. If Sg is not visible the Pg-Surface wave time can be used to estimate the epicentral distance. The Pg-Sur time represents the difference in travel time of the Pg arrival and the travel time of the surface waves between the epicentre and the station. The Pg-Sur time has been limited empirically with the Pg-Sg time which enables the epicentral distance to be determined.

Two methods can be used to determine the azimuth and apparent velocity of the signal. One of the methods, velocity filtering, is based on the correlation of the signal between each of the seismometers. Velocity filtering can be performed

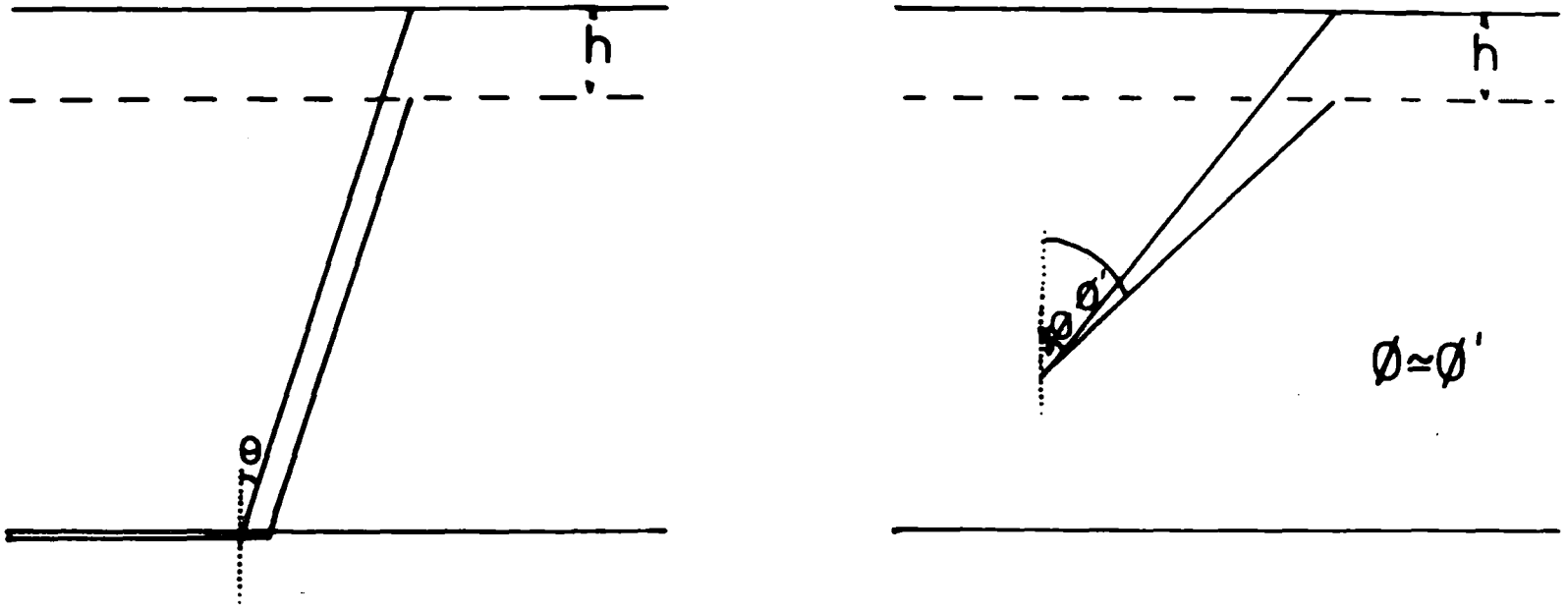

Travel Path for Height
Correction

Fig 3:1

on the Department's Modular One computer. The signal at each seismometer is delayed so that it represents a signal arriving at the origin of the array. The delay is derived using an assumed velocity and azimuth for the signal. The delayed signals are summed to give a measure of the correlation. By stepping through velocity and azimuth a matrix of correlation is formed. The maximum correlation corresponds to the apparent velocity and azimuth of the signal. In the second method, onset time analysis, a plane wavefront is fitted to the onset times of the signal at each of the seismometers. Corbishley (1969) found that the onset time analysis method provided a more accurate determination of the azimuth of an event than correlation methods. Throughout the following discussion onset time analysis was used to determine the azimuth and apparent velocity of the signal.

3:2 Height correction.

The seismometers of the Kaptagat array are each at different heights. Before any operation is performed on the onset times of the signal at each seismometer the onset time has to be corrected to effectively place each seismometer on the same arbitrary horizontal plane. Fig (3:1) illustrates the travel path of a direct wave and a head wave to a seismometer which is at a height h Km above an arbitrary horizontal plane. The diagram also shows the two paths required to reduce the seismometer to the arbitrary horizontal plane.

For a head wave the height correction is given by,

$$t = \frac{h \cos\theta}{V_s} \qquad \text{where,}$$

V_s is the velocity of the surface rock and θ is the angle indicated in Fig (3:1).

Similarly, the height correction for a direct wave is given by,

$$t = \frac{h \cos\phi}{V_s}$$

Because the nature of the arrival is not known before the onset times are analysed the height correction has been approximated by h/V_s. The difference between the true height correction and the approximation is,

$$\xi = \frac{h}{V_s}(1 - \cos\phi) \qquad \theta \equiv \phi$$

Assuming a value of 4.5 Km sec^{-1} for V_s (Backhouse, 1972), the maximum value of ξ for a head wave is given when $\cos\phi = 0$. For a seismometer 0.06 Km above the arbitrary horizontal plane ξ is approximately 0.01 seconds for a moho head wave. This error is of the order of the reading errors on the onset times of the signal.

3:3 Determination of the azimuth and apparent velocity of the signal.

Suppose that the positions of the n seismometers of the Kaptagat array can be designated by the coordinates x_i y_i. If a signal of constant velocity V, and azimuth α, crosses the array the apparent velocity V_A, along the radial i is given by,

$$V_A = \frac{V}{\cos(\alpha - k_i)}.$$

The angle, measured clockwise, between the radial i and true north is designated by k_i. Relative to the origin, taken at the crossover point of the two arms, the arrival time at the i^{th} seismometer is,

$$t_i = \frac{-R_i \cos(k_i - \alpha)}{V}$$

$$t_i = -x_i \frac{\sin\alpha}{V} + y_i \frac{\cos\alpha}{V} \qquad \text{where}$$

R_i is the radial distance from seismometer i to the origin.

As the arrival times are normally measured relative to an arbitrary zero and not the origin, the observed arrival time, 0_i, can be written as $0_i = t_i + \tau$ where τ is the arrival time at the origin. If 0_i is in error by e_i,

$$0_i + x_i \frac{\sin\alpha}{V} + y_i \frac{\cos\alpha}{V} - \tau = e_i \quad \text{(Carpenter, 1966).}$$

his equation which contains three unknown variables, $\sin\alpha/V$, $\cos\alpha/V$ and τ can be solved by least squares if the array has ore than three seismometers. In a least squares solution,

$$\frac{d\, e_i^2}{da_k} = 0 \quad \text{giving the normal equation}$$

$$\sum_{i=1}^{n}\sum_{j=1}^{m} x_{ik}x_{ij}a_j = \sum_{i=1}^{n} x_i t_i$$

n the above equation a_j represents the variables $\sin\alpha/V$, $\cos\alpha/V$ nd τ, t_i is the arrival time at the ith seismometer and x_{ij} j = 1, 3) are unity and the coordinates of the ith seismometer. his formula can be represented by the general matrix equation A = Y which can be solved by matrix inversion to give the variables a_j (j = 1, 3).

If the event occurs close to the station the approximation of a plane wavefront is not correct. For a curved wavefront crossing the array the azimuth of the signal varies for each seismometer. If the focus of the event is at or near the surface the angle of incidence of the signal will remain constant across the array. However if the focus lies deep within the crust the angle of incidence of the signal will vary from seismometer to seismometer. Hence the direction of approach of the signal will not be constant across the array, Fig (3:2) shows the error

Error on Azimuth and Velocity
Due to Assuming a Plane Wavefront

Fig 3:2

in azimuth and apparent velocity, calculated by the method of onset time analysis assuming a plane wavefront, for events at an epicentral distance of 50 and 100 kilometres. Fig (3:2) clearly shows that the error, due to the assumption of a plane wavefront, is a function of the true azimuth, which is plotted as the abscissa of the graph. The graphs also show that the error, due to the assumption of a plane wavefront, decreases as the epicentral distance increases. For an epicentral distance of 100 Km, the maximum error, due to the assumption of a plane wavefront, in the azimuth and velocity are ± 1.3 degrees and ± 0.08 Km sec^{-1} respectively. The corresponding values for an epicentral distance of 50 Km are ± 2.9 degrees and ± 0.2 Km sec^{-1}. A curved wavefront program has been developed to process close in events and this program will be discussed in section (3:4).

3:4 Curved Wavefront analysis.

The crust under the Kaptagat array approximates closely to a simple horizontally layered structure, (see section (3:5)). If the focus of the event is a point source the wavefront emitted from the focus will form a sphere. For a uniform layered structure the spherical wavefront should retain its shape, within each layer, as the signal travels through the crust. The locus of the intersection of the sphere with the surface forms a circle with the epicentre as its centre. In the curved wavefront program the onset time of the signal at each seismometer is calculated for an assumed azimuth, epicentral distance and velocity. These calculated onset times are compared with the observed onset times to give an error of fit. The azimuth, epicentral distance and velocity which corresponds to

the minimum error of fit are taken to represent the parameters of the signal.

To achieve a stable answer requires accurate picking of the onset times at the seismometers. The azimuth and velocity quickly attained a stable value but the stability of the epicentral distance was strongly dependent upon the accuracy of the onsets. The advantage of the curved wavefront program over the plane wavefront analysis is limited by the accuracy of the measurement of the onset times. Consider an event with a surface focus and the epicentre aligned such that the azimuth is at right angles to the strike of one arm of the array. On the plane wavefront analysis there should be no difference between the onset time of the signal at the centre of the arm and the onset time at the extremities of the arm. However there is a difference in the onset times because the wavefront is curved. For an epicentral distance of 25 Kms the difference in the onset times of the middle and the extreme seismometers is approximately 0.02 seconds. In general the reading accuracy on the onset time is ± 0.01 seconds so the error on the difference of the onset times at two seismometers is ± 0.02 seconds. Hence the curved wavefront program is no more accurate than the plane wavefront program at epicentral distances greater than 25 Kms.

3:5 Errors in the measured azimuth and velocity.

The measured azimuth and velocity may contain errors due to incorrect reading of the onset times, mislocation of the seismometers and effects due to the local geology.

The measured azimuth of the event may contain an error introduced by an error in the coordinates of each seismometer. Maguire (1974) and Backhouse (1972) have studied extensively the

effect of incorrect pit coordinates upon the azimuth and apparent velocity of the signal across the array. By varying the position of each seismometer within the estimated accuracy on the coordinates of the seismometers, Maguire found that the maximum error due to incorrect pit locations was ± 1.05 degrees on the azimuth and ± 0.15 Km sec^{-1} on an arrival with apparent velocity of 8.0 Km sec^{-1}. The error on the azimuth is independent of the apparent velocity of the signal. The error of ± 1.05 degrees on the azimuth implies that for an epicentral distance of 600 Km the epicentre will be located on an arc, centred on Kaptagat, approximately 21 Km in length. For an epicentral distance of 60 Km the arc is reduced to 2.1 Km.

An error exists in the measured azimuth due to reading errors on the onset time of the signal at each seismometer. Kelly (1964) has shown that if the reading errors are Gaussian variables, the r.m.s. error on the slowness is given by,

(i) $$\frac{K\sigma}{\sqrt{mD}}\left((XX)\cos^2 A - 2(XY)\sin A\cos A + (YY)\sin^2 A\right)^{\frac{1}{2}}$$

In the above expression,

m is the number of seismometers,

A is the azimuth of the event,

σ is the variance in the onset time,

K is the wave number,

$$(XX) = \frac{1}{m}\sum_{i=1}^{m} (x_i - \bar{x})^2$$

$$(XY) = \frac{1}{m}\sum_{i=1}^{m} (x_i - \bar{x})(y_i - \bar{y})$$

$$(YY) = \frac{1}{m}\sum_{i=1}^{m} (y_i - \bar{y})^2$$

$$D = (XX)(YY) - (XY)^2$$

Equation (i) has been rearranged to give an equation (equation (ii))

for the r.m.s. error on the azimuth.

(ii) $$\frac{V\sigma}{\sqrt{mD}}\left((XX)\sin^2 A + 2(XY)\sin A\cos A + (YY)\cos^2 A\right)^{\frac{1}{2}}$$

where V is the velocity of the signal across the arry. The variance was calculated by repeating five times the measurement of the onset times. This procedure was performed for a number of events and the maximum variance was found to be 0.009 seconds. As the error due to random readings is not single valued the variation of the random reading error with azimuth and velocity has been plotted in Fig(3:3). From the diagram it can be seen that the maximum reading error in the azimuth is 1.1^{o} for a signal with an apparent velocity of 8.0 Km sec^{-1}. The random errors plotted in Fig (3:3) may be regarded as a maximum as events with clear onsets will have a smaller variance.

The expected arrival time of a plane wavefront at each seismometer can be calculated from the measured azimuth, velocity and the arrival time of the signal at the origin of the array. The difference between the expected and the observed arrival time of the signal at each seismometer gives the residual at each seismometer. When the residuals are plotted against the calculated azimuth of the event they appear to follow a sinusoidal function with an imposed D.C, level. Corbishley (1969) has shown that the residuals on the seismometer onsets can be fitted to a function of the form,

(iii) $$\eta_i = A_i + B_i \sin(\alpha_k + \beta_i) + e_i$$

where η_i are the residuals for the ith seismometer,

α_k is the azimuth of the kth event,

β_i is a phase angle for each seismometer,

e_i is the remaining error,

A_i and B_i are constants for each seismometer.

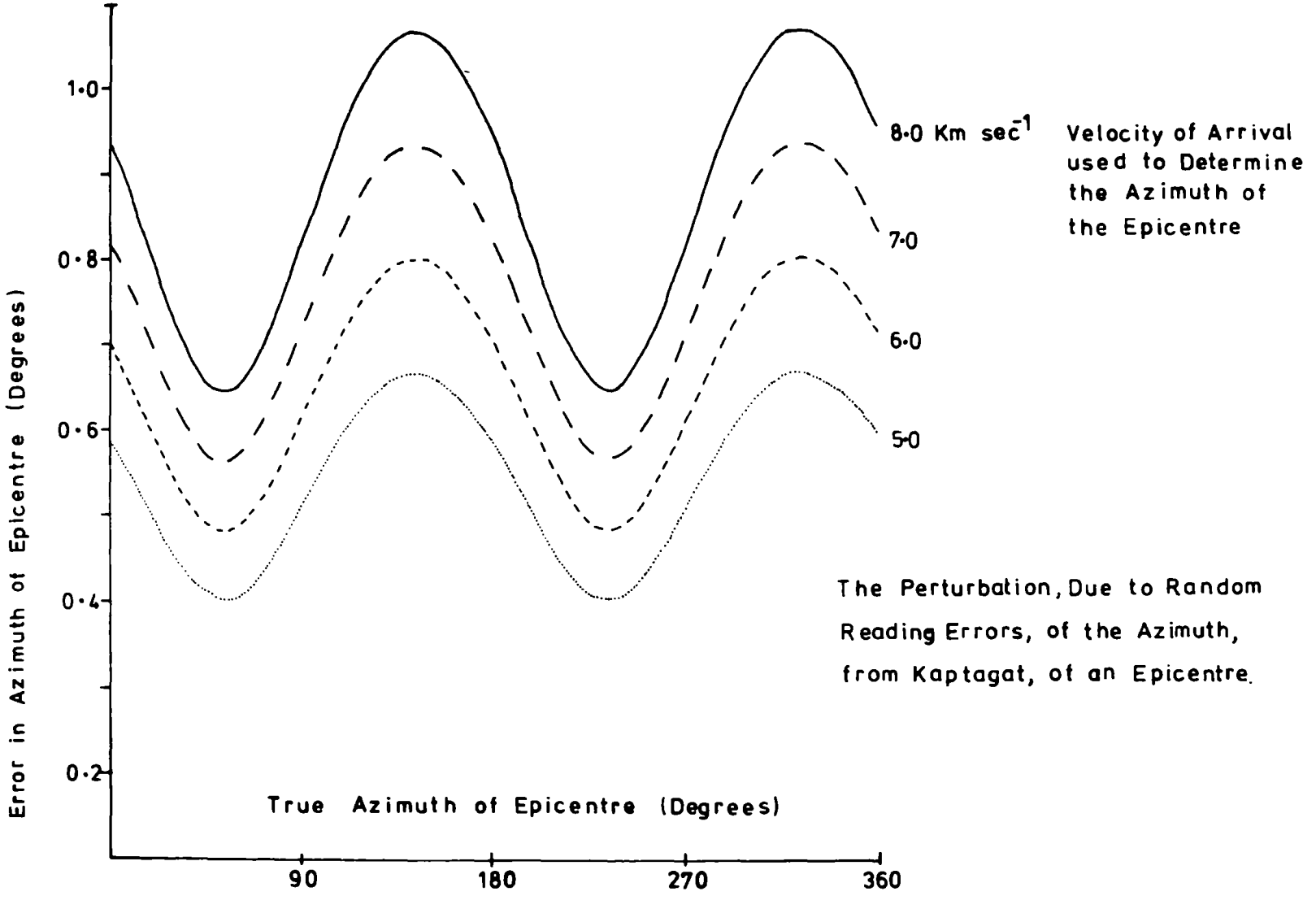
1·0
0·8
0·6
0·4
0·2
Error in Azimuth of Epicentre (Degrees)
8·0 Km sec⁻¹
7·0
6·0
5·0
Velocity of Arrival used to Determine the Azimuth of the Epicentre
The Perturbation, Due to Random Reading Errors, of the Azimuth, from Kaptagat, of an Epicentre.
True Azimuth of Epicentre (Degrees)
90
180
270
360

Fig 3:3

Before the plane wavefront analysis is performed the onset times are corrected so that the seismometers are reduced to the same horizontal plane. In the above equation A_i may be considered as representing thererror on the height correction for each seismometer. The error A_i may arise from three factors. If the p-wave velocity used for the surface material is in error the height correction on the onset times will not compensate for the relative heights of the seismometers. The height correction also depends upon the relative heights of the seismometers. An error in the relative height may contribute to the D.C. residuals. Lastly as shown in section (3:2) the height correction employed is only an approximation to the true height correction. Because the height correction does not fully compensate for the relative heights of the seismometers there will be a residual error. This residual error gives the A_i term. The sinusoidal part of equation (111) may represent the effect on the onset time of a dipping layer beneath the array. Maguire (1974) found that the values of B_i were less than $\pm$ 0.019 seconds indicating that the near surface structure under the array is nearly horizontal. This agrees with observations of the local geology. Maguire found that the A_i values were generally less than $\pm$ 0.007 seconds implying that the height correction is effective.

3:6 Estimation of epicentral distance.

As mentioned in section (3:1) the P-S time is converted to the P travel time to give an estimate of the travel path distance. The P and S velocities are related by the equation,

$$\frac{V_p}{V_s} = \frac{(2 - 2\sigma)}{(1 - 2\sigma)} \qquad \text{where,}$$

Fig 3:4

Crustal Model and Travel Paths

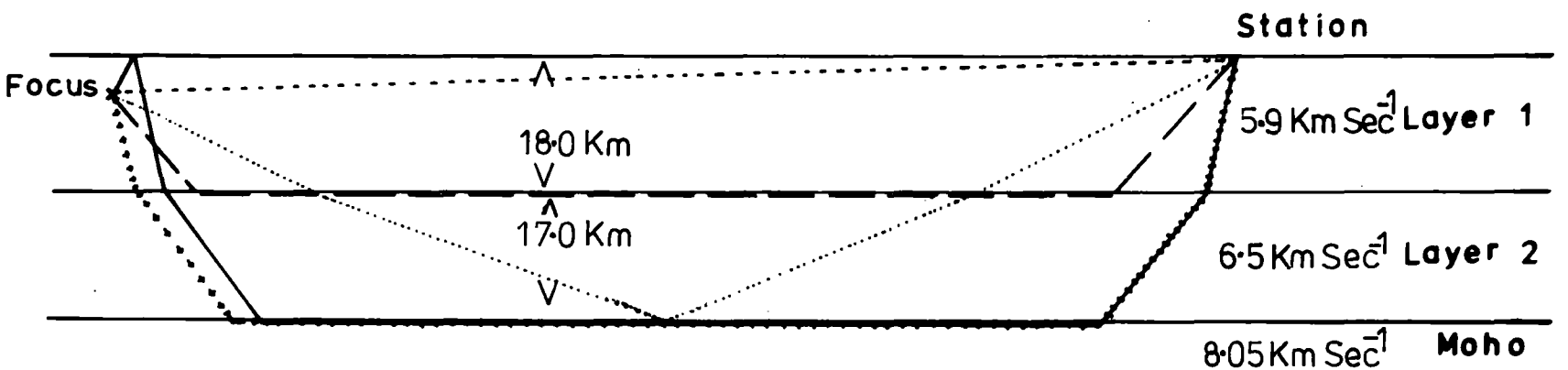

Key to paths.

- ------- P_g
- — — P^*
- ——— pP
- ------ P_n
- ..... P_m

Similar paths for S-waves.

σ is Poisson's ratio,

V_p is the p-wave velocity,

V_s is the s-wave velocity.

If σ is 0.25 the ratio $V_p:V_s$ is 1.73. In this study V_p was taken equal to $1.74V_s$, corresponding to a Poisson's ratio of 0.254, after Anderson (1965).

For close in events the first arrival is normally a P_g phase. With increasing epicentral distance the first arrival changes to P* and then P_n (Fig 3:4). In records where the first arrival was P* or P_n it frequently difficult and often impossible to identify P_g. Hence throughout this study the P-S time was taken as the time separation between the P and S wave onsets. This quantity defines the p-wave travel time for the path involved.

Frequently the S onset was not clearly visible on the record. In this case the P-Sur time was used to estimate the travel path distance for the P wave. To obtain this estimate the P-Sur time was converted to a P-S time using the empirical relationship shown in Fig (3:5). This graph was constructed using the events, located to the west of the Gregory Rift,which showed clear S and surface wave onsets. A similar empirical relationship was derived for the P-S and P-Sur time of events located within the Gregory Rift. The points that form the graph, shown in Fig (3:5), beyond a P-S time of 45 seconds show a large degree of scatter. Most of the events with a P-S time greater than 45 seconds come from the area of the Ruwenzori Mountains. This implies that the scatter cannot be due to variation in the structure of the crust. The scatter in the diagram is probably due to misidentification of the S or Surface wave onsets.

The S-wave onset is usually marked by a pronounced change in the

Fig 3:5

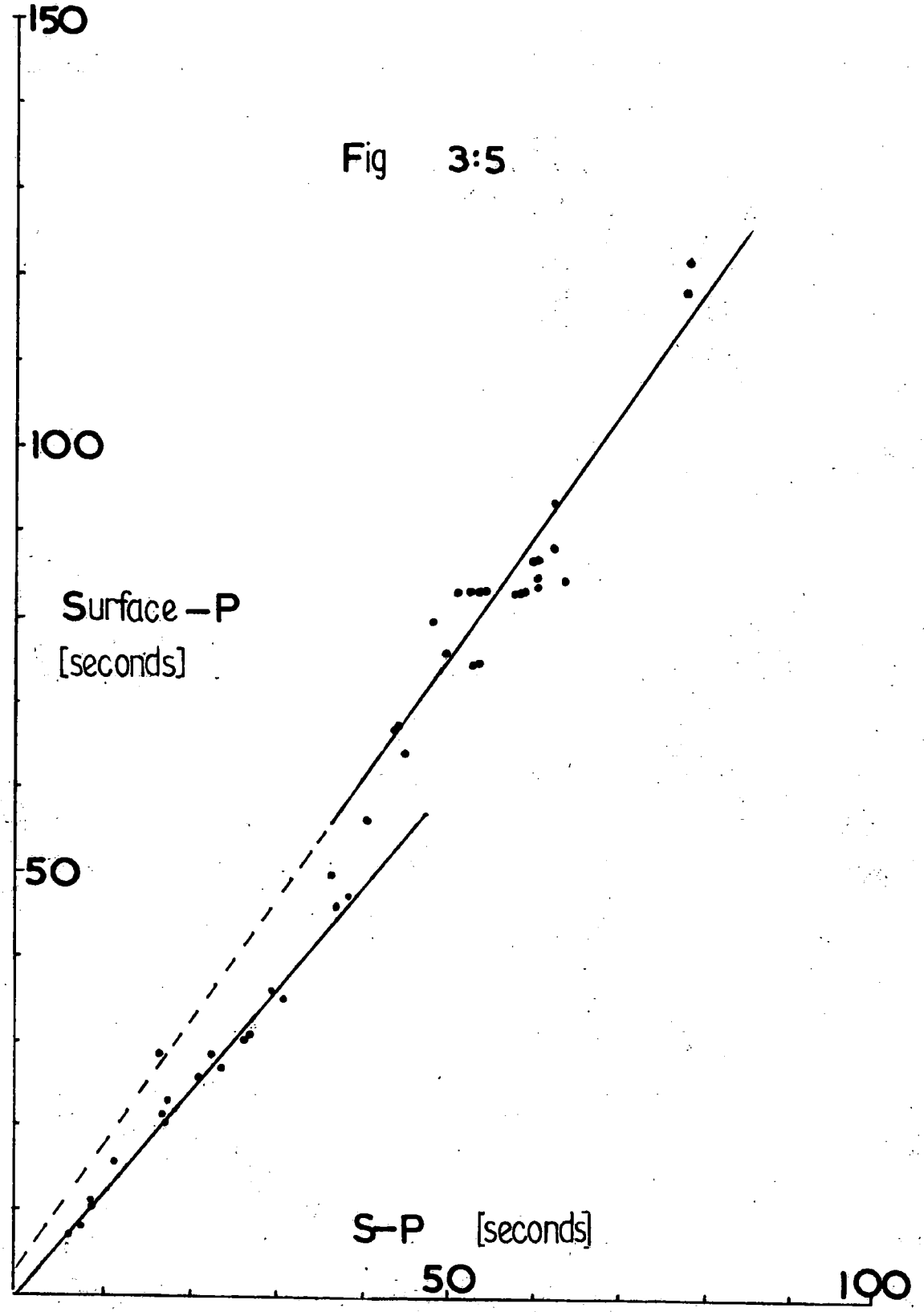

Empirical relationship between

S–P & Surface – P

frequency and amplitude of the signal (Fig 3:6). The surface waves show a clear increase in period and usually have a larger amplitude than the previous arrivals.

As defined the P-S time gives an estimate of the travel path distance. To link this distance with the epicentral distance requires a knowledge of the type of travel path and the focal depth of the event. The p-wave travel path can be found using the apparent velocity of the arrival, eg, if the initial P-wave has an apparent velocity of 6.5 Km sec^{-1} the travel path is probably P^* taking the crustal model in Fig (3:4). If the focal depth was not known it was assumed to be five kilometres. This assumption was based of the focal depths determined in this study. Also, Molnar and Aggarwal (1971) found that the majority of microseisms in the Gregory and Kavirondo Rifts lie within the top 5 Km of the crust. The effect upon the epicentral distance of an incorrect focal depth is illustrated in Fig (3:7).

The conversion of the p travel time to travel path distance and eventually epicentral distance was achieved using the model for the structure of the crust, Fig (3:4), derived by Maguire (1974). Using a range of focal depths from 0-35 Km and a set epicentral distance the travel time was calculated for the direct waves, the moho reflection and all the head waves generated by the model illustrated in Fig (3:4). The set of travel times for each focal depth were compared to find which path gave the shortest travel time. The shortest travel time for each focal depth was stored in a two-dimensional matrix and the process repeated for another epicentral distance. This travel time matrix was used to give the epicentral distance.

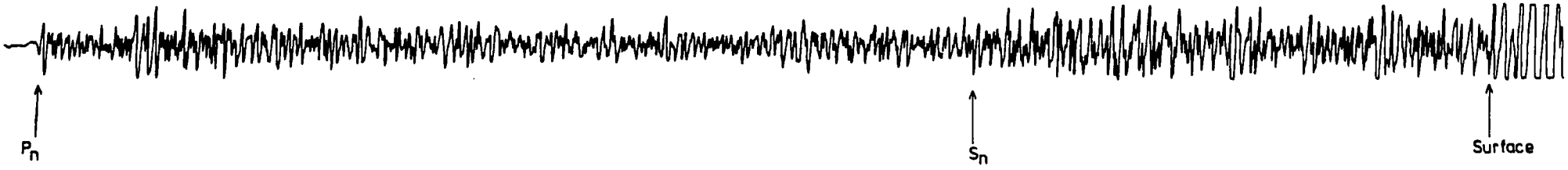

10 Seconds

Event 6243

Fig 3-6

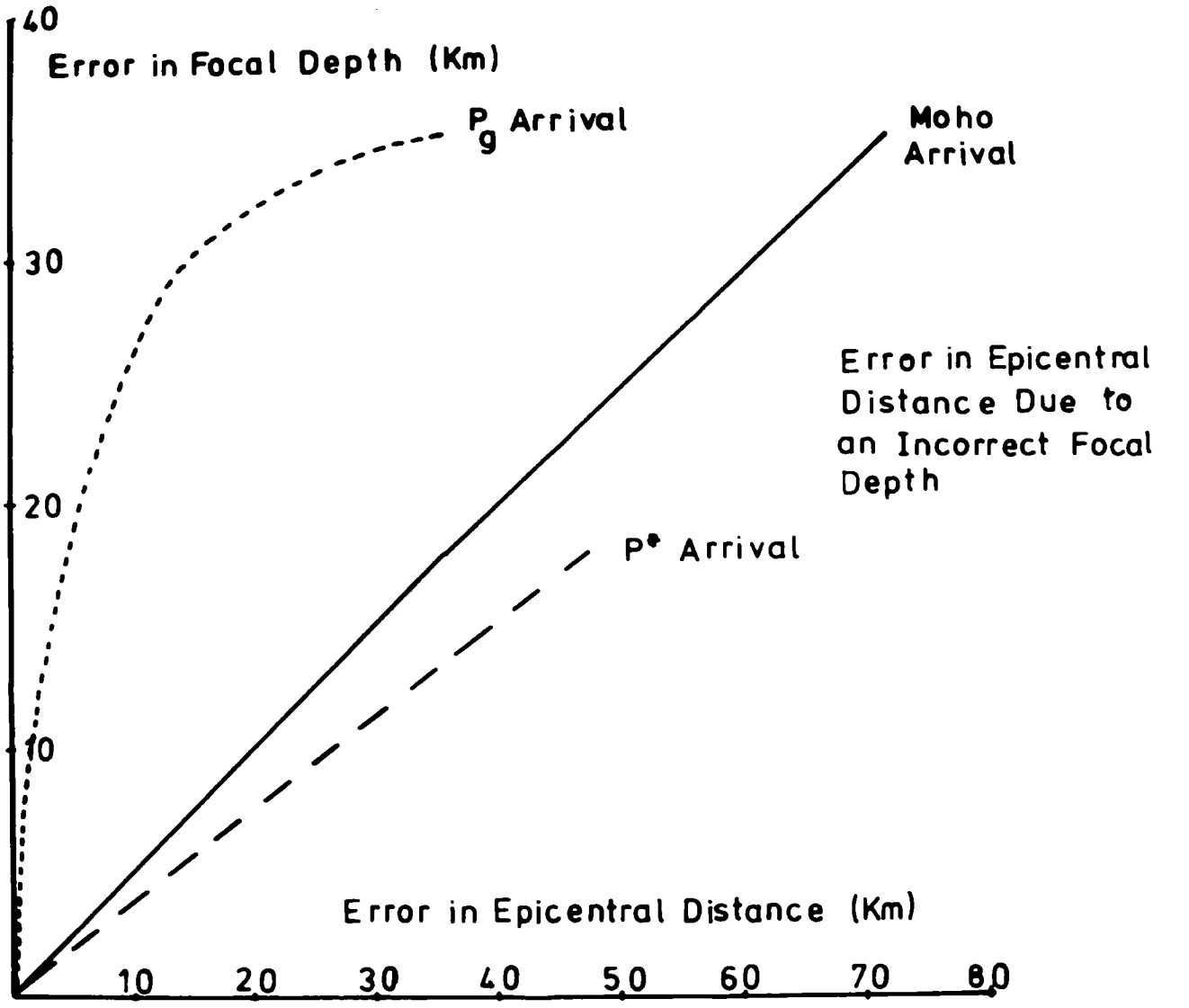
40
Error in Focal Depth (Km)
P_g Arrival
Moho
Arrival
30
Error in Epicentral
Distance Due to
an Incorrect Focal
Depth
20
P* Arrival
10
Error in Epicentral Distance (Km)
10
20
30
40
50
60
70
80

Fig 3:7

3:7 Measurement of focal depth.

The epicentral distance and focal depth are tightly bound together, an error in one affects the other. If, for a head wave arrival, the true focal depth is deeper than the measured focal depth the measured epicentral distance will be shorter than the true epicentral distance. The reverse applies to direct arrivals, ie, if the true focal depth is deeper than the measured focal depth the measured epicentral distance will be longer than the true epicentral distance. From this it can be seen that, except in a few cases, it is impossible to divorce the focal depth from the epicentral distance.

The focal depth of a large number of events can be used to define the fault plane. The events, to which the focal depths apply, must be spread over the fault plane and not clustered at one depth. Once the fault plane has been defined the nature, ie, normal, reverse or thrust, of the fault can be determined.

One or more of four methods were used in an attempt to define the focal depth of each event. All of the methods require the use of a crustal model to represent the structure of the crust. The four methods involve;

(i) A combination of the epicentral distance derived from the curved wavefront program and the P-S time,

(ii) The use of the angle of approach and the P-S time,

(iii) The use of the P-S time at Nairobi and Kaptagat and the azimuth of the event from Kaptagat,

(iv) The time separation between known first and second P arrivals.

focal depths of very close events.

The curved wavefront program gives a direct measure of the epicentral distance. As the curved wavefront analysis applies only to close in events the first arrival is a P_g phase. Hence the P_g-S_g time gives an estimate of the direct distance from the station to the focus. Knowing this distance and the epicentral distance enables the focal depth to be determined.

Like the other methods the accuracy of this method depends upon the crustal model. The calculated travel times were formed using the P-velocities given in Maguire's crustal model and may be in error if the velocities in the crustal model are incorrect. Suppose that the focus of the event lies within the first crustal layer. If the true velocity of the first crustal layer is smaller than the assumed velocity the true travel time, for a particular focal depth, will be larger than the calculated value. Conversely the true travel time is smaller than the calculated travel time if the true velocity of the first layer of the crust is greater than the assumed velocity. For the first crustal layer the assumed velocity was 5.9 Km sec^{-1}. In Fig (3:8) the error in focal depth, due to assuming a velocity of 5.9 Km sec^{-1} for the first crustal layer, is plotted against the 'true velocity' of the first crustal layer.

An error can be introduced into the calculated focal depth if the measured P-S time is in error. If the P-S time is in error by 0.1 second the observed travel time will be in error by approximately 0.135 second. In Fig (3:9) the error due to an incorrect observed travel time has been combined with possible error due to the assumption of an incorrect crustal model. This graph, Fig (3:9), shows that an error of +0.1 seconds on the travel time has the

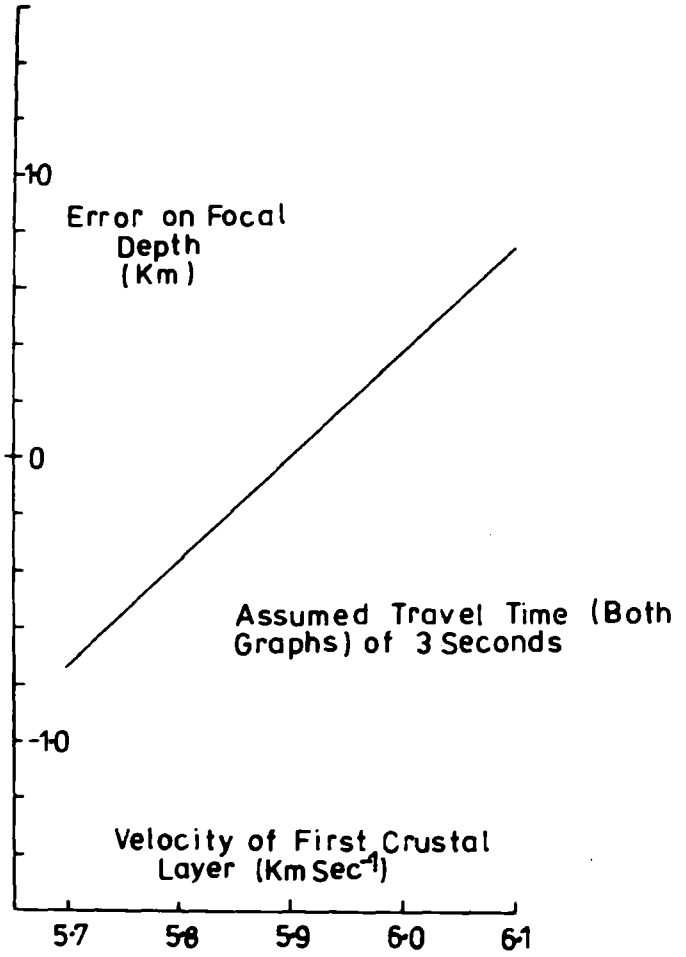

Error on Focal Depths, Determined from the Spherical Wavefront Method, as a Function of the Crustal Model

Fig 3·8

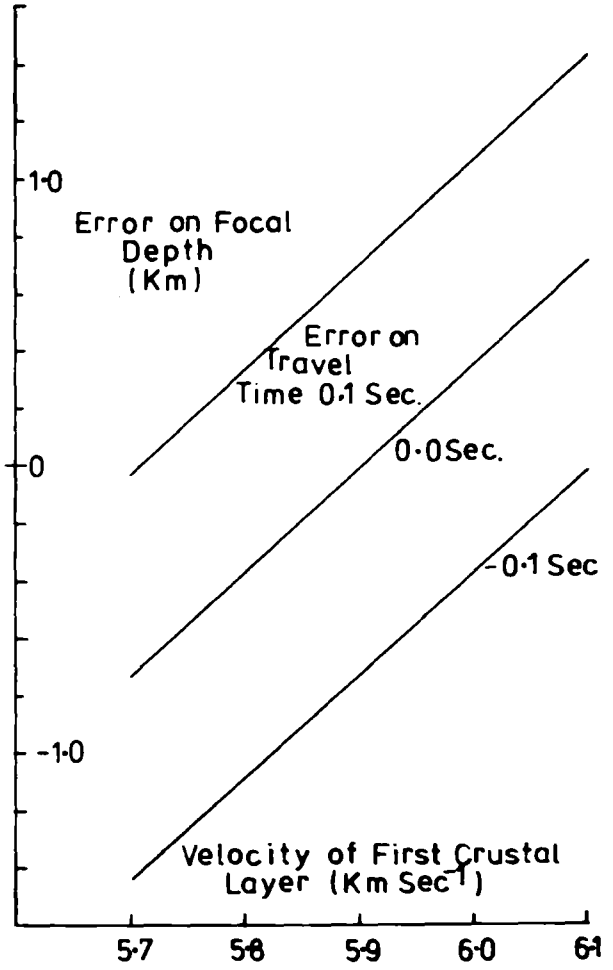

Error on Focal Depth as a Function of Error on Travel Time and Incorrect Crustal Model

Fig 3·9

effect of increasing the focal depth by approximately 0.7 Km. The error analysis for this method can be extended to include the second layer. This extension of the error analysis has not been included here as the method, for available earthquakes, did not yield focal depths in excess of 18 Km.

The curved wavefront program gave a stable epicentral distance for five close in events. These events had focal depths in the range 14 to 17 Km. These focal depths compare favourably with values of the focal depth determined using the velocity of the signal across the array and the P_g-S_g time.

3:9 Focal depths using the apparent velocity and P_g-S_g time of an event.

The angle of incidence is defined as the angle between the direction of approach of the signal and the horizontal plane on which the seismometers are standing. The cosine of this angle is given by the ratio of the velocity of the signal across the array and the p-velocity of the surface rocks. If the first arrival has travelled a P_g path the P_g-S_g time gives a measure of the path distance. This path distance can be employed along with the angle of approach to give the focal depth.

The accuracy of the method depends upon three factors,

(i) the accuracy of the crustal model used to give the angle of approach and the travel time of the signal,

(ii) the accuracy of the measured apparent velocity,

(iii) the accuracy of the P-S time.

In Fig (3:10) the error on the focal depth, due to incorrect velocities used in the crustal model, has been plotted

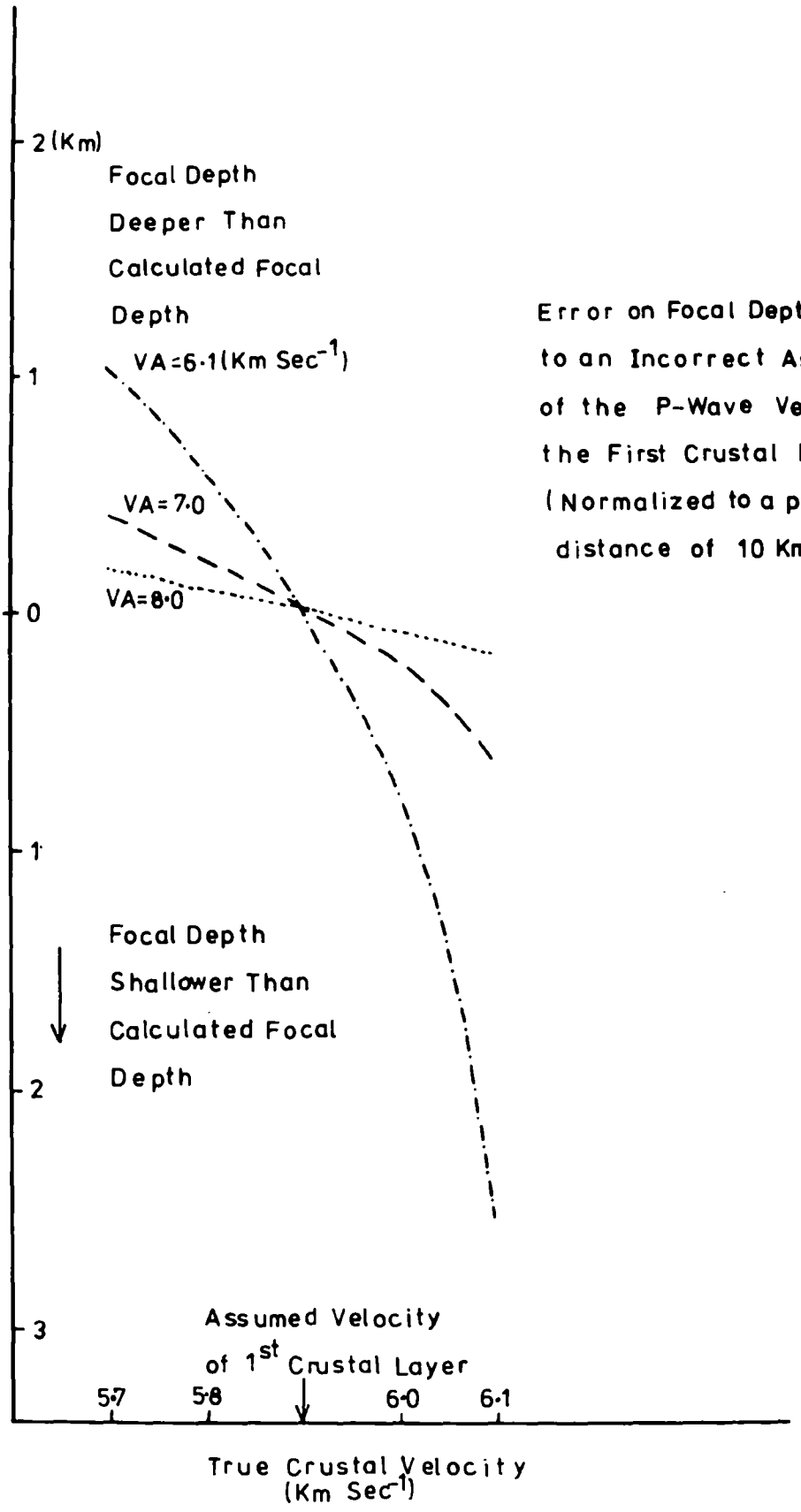

Error on Focal Depth Due to an Incorrect Assumption of the P-Wave Velocity of the First Crustal Layer (Normalized to a path distance of 10 Km)

Fig 3:10

against the p-velocity of the first layer for four apparent velocities. This error has been calculated on the basis that a velocity of 5.9 Km sec^{-1} was used to represent the p-wave velocity of the first crustal layer. A path distance of 10.0 Kms has been used to convert the error in the angle of incidence to error in focal depth. From the graph, Fig (3.10), it can be seen that the error in the focal depth, due to an error in the assumed crustal model, decreases as the measured apparent velocity of the signal increases. This indicates that, providing the path distances are the same, events with deep calculated focal depths will have a smaller error in the focal depth, due to an incorrect crustal model, than shallow earthquakes. The graph, Fig (3:10), is modified if the path distance is allowed to vary with the true p-wave velocity of the crust. Consider a focus in the first layer of the crust. If the true velocity of the first layer is less than the assumed value of 5.9 Km sec^{-1} the actual path distance will be less than the calculated path distance. This implies that the error in the focal depth is less than that plotted in Fig (3:10). For a first crustal layer with a true velocity greater than 5.9 Km sec^{-1} the true path distance will be greater than the calculated path distance. This in turn means that the error in the focal depth will be increased.

The calculated angle of incidence is a function of the apparent velocity of the signal across the array. Any error in the apparent velocity will be reflected by an error in the angle of incidence and ultimately in the focal depth. Fig (3:11) is a plot of the variation of the error in focal depth against the error in apparent velocity. Again the error decreases as the

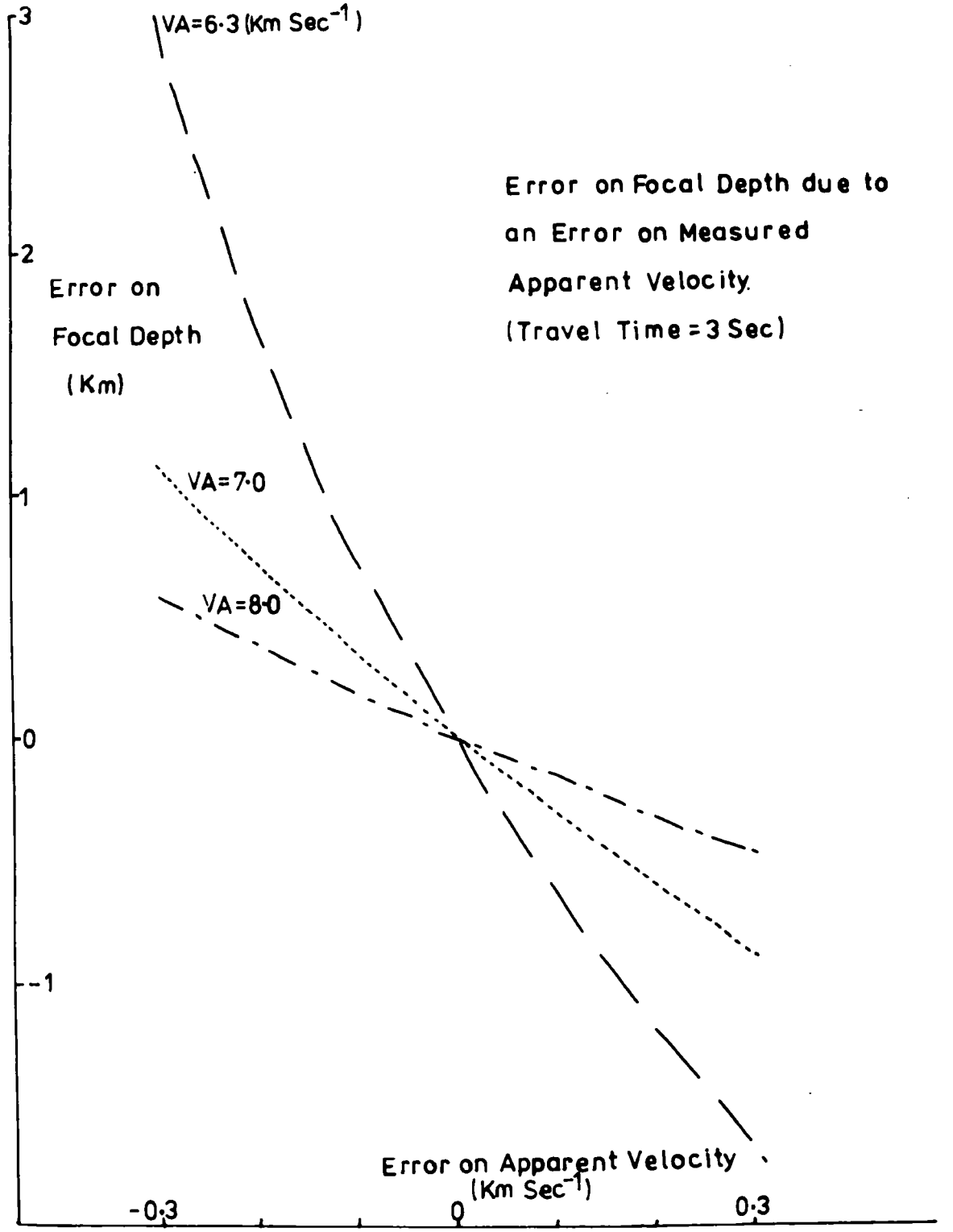
VA=6·3 (Km Sec^{-1})
VA=7·0
VA=8·0
Error on Focal Depth due to an Error on Measured Apparent Velocity. (Travel Time = 3 Sec)
Error on Focal Depth (Km)
3
2
1
0
-1
-0·3
0
0·3
Error on Apparent Velocity (Km Sec^{-1})

Fig 3:11

apparent velocity increases. This decrease in the error implies that the higher the apparent velocity the smaller the error in focal depth due to an incorrect measurement of the apparent velocity.

An error in the measured P_g-S_g time will give an error in the travel path distance via the error in the travel time. Suppose that in measuring the P-S time an error of ± 1 second is introduced into the measured P-S time. For a direct wave confined to the first layer of the crust the ± 1 second error in the measured P-S time will give an error in the calculated path distance of 7.97 Km. The corresponding error in the focal depth will be a function of the sine of the angle of incidence. As the angle of incidence increases the error in the focal depth, due to an incorrect measurement of the P_g-S_g time, also increases. If the focus lies deeper than the first layer of the crust the error on the path distance will increase because the p-wave velocity is greater. For an error of ± 1 second on the P_g-S_g time the maximum error on the focal depth of a crustal focus is 8.79 Km.

This method of determining focal depths was restricted to events within the Kavirondo Graben. These events are located within normal shield crust the structure of which is represented by the crustal model of Maguire (1974). The analysis was restricted to events that had a first arrival 6.5 Km sec^{-1} or 6.6 Km sec^{-1}. This limitation was imposed to remove P^* travel paths from the analysis. A limiting depth can be put on events with a first arrival apparent velocity of 6.5 Km sec^{-1}. Fig (3:12) shows the range of focal depth and epicentral distances for which P_g arrives before P^*. This graph has been constructed

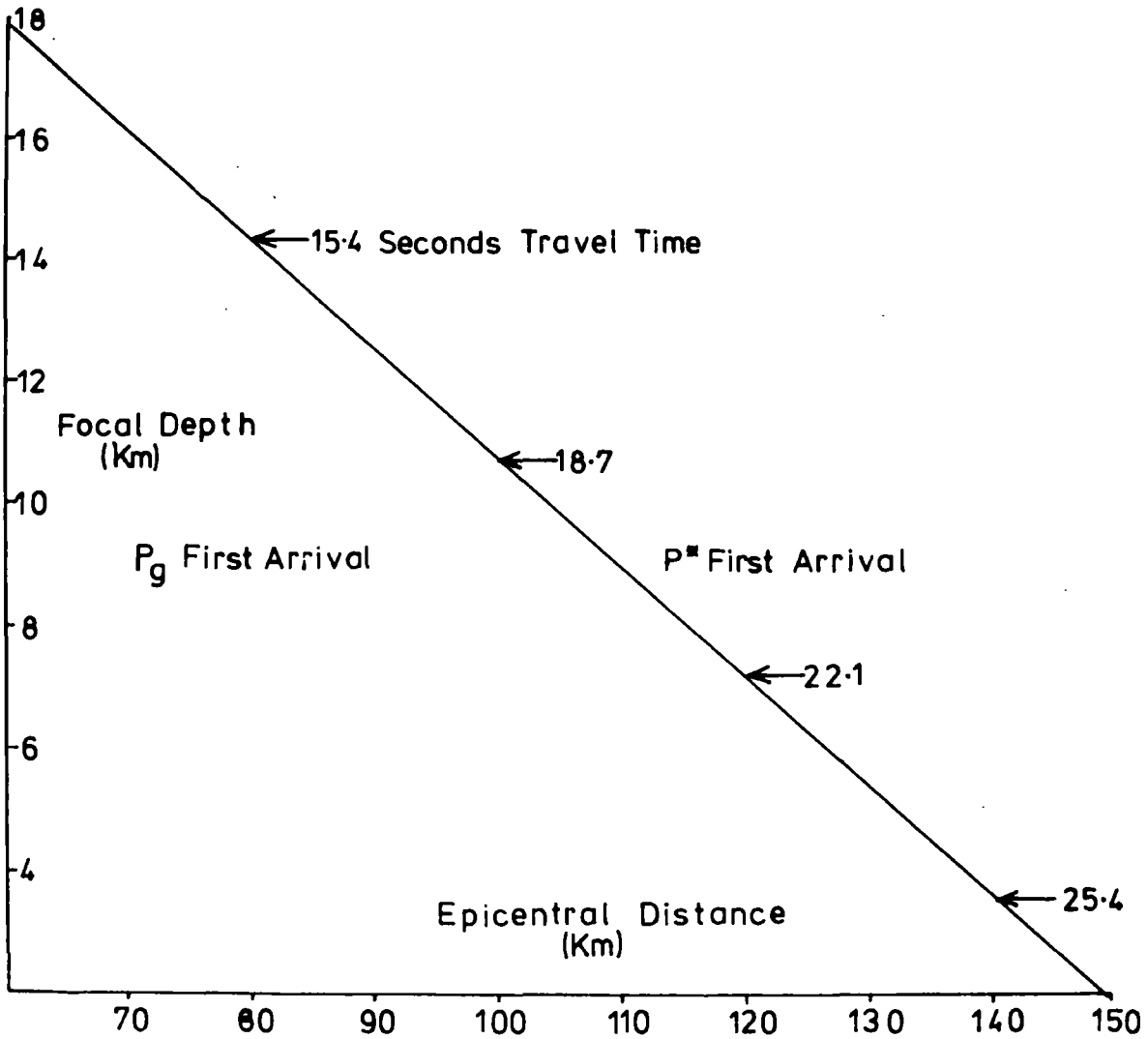

Change in First Arrival From P_g to P^* as a Function of Focal Depth and Epicentral Distance

Fig 3·12

using Maguire's model for the crustal structure. Lines of equal P-S time have been drawn on the section of the graph for which P^* arrives, at the station, before P_g. Fig (3:13) shows the range of focal depths for events in the Kavirondo Graben. The greatest number of focii apparently occur at a focal depth of 11-25 Km. The lack of earthquakes with shallow focal depths is probably due to the poor resolution of the apparent velocities. Also the maximum error on the apparent velocity is $\pm$ 0.2 Km sec^{-1} which can give a considerable error in the focal depth.

3:10 Focal depths determined using data from Kaptagat and Nairobi.

If a crustal model and focal depth are assumed the azimuth of the event from Kaptagat and the P-S time at Kaptagat can be used to estimate the hypocentral location. The travel path from the focus to Kaptagat was assumed to be the travel path of the signal that should, theoretically, be the first arrival at Kaptagat. The hypocentral location and the assumed focal depth can be used to determine the nature of the first arrival at Nairobi and the associated P-S time. This calculated P-S time at Nairobi can be compared with the measured P-S time at Nairobi. By varying the assumed focal depth the calculated P-S time at Nairobi can be adjusted until it is the same as the measured P-S time at Nairobi. When this condition exists the assumed focal depth was taken as the actual focal depth.

The accuracy of the method depends on four factors:

(i) the accuracy of the measured P-S time at Nairobi,

(ii) the accuracy of the measured P-S time at Kaptagat,

(iii) the accuracy of the measured azimuth, from Kaptagat, 66 the epicentre,

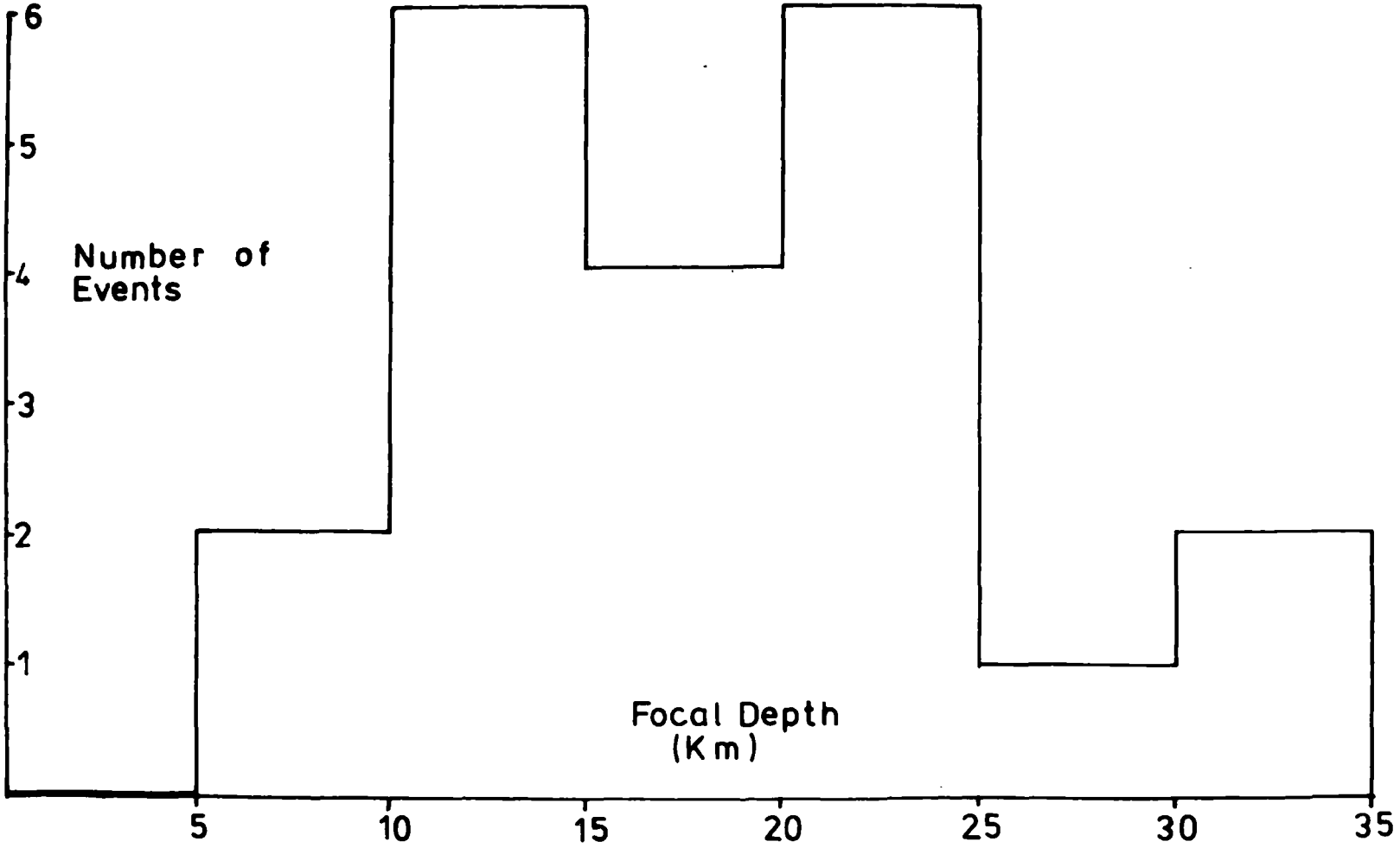

Histogram of Focal Depths in the Kavirondo Graben.

Fig 3:13

(iv) the similarity between the crust and the model used to represent the crust.

An incorrect measurement of the P-S time at either station will result in an incorrect estimate of the path distance from the focus to the station. Fig (3:14) shows the variation with azimuth of the error on the focal depth due to an incorrect measurement of the P-S time at Kaptagat. The graph considers two cases,

(a) when the first arrival at Kaptagat is a P_g phase restricted to the first crustal layer and the first arrival at Nairobi is a P_n phase,

(b) when both stations see P_n as the first arrival.

Each graph has been constructed assuming an error of $\pm$ 0.39 seconds on the P-S time. An error of $\pm$ 0.39 seconds on the P-S time corresponds to an error of $\pm$ 0.50 seconds on the travel time. The first case is applicable to events located in the Kavirondo Graben for which P_g is the first arrival at Kaptagat. Case (b) applies to events located in the Eyasi Rift or along the arc of the Western Rift. Confirmation of the P_n arrival at Nairobi, for distant events, is given by the expected onset time, at Nairobi, of the signal being approximately the same as the actual onset time. Fig (3:15) shows similar graphs for an error of 0.39 seconds on the P-S time at Nairobi. Again two cases have been considered,

(c) the first arrival at Nairobi is a P_g phase and the first arrival at Kaptagat is a P_n phase,

(d) both stations see a P_n phase as the first arrival.

Case (c) applies to events very close to Nairobi. These events have a P-S time which limits the first arrival, at Nairobi, to a P_g phase. The graphs in Fig (3:14) and Fig (3:15) show that the

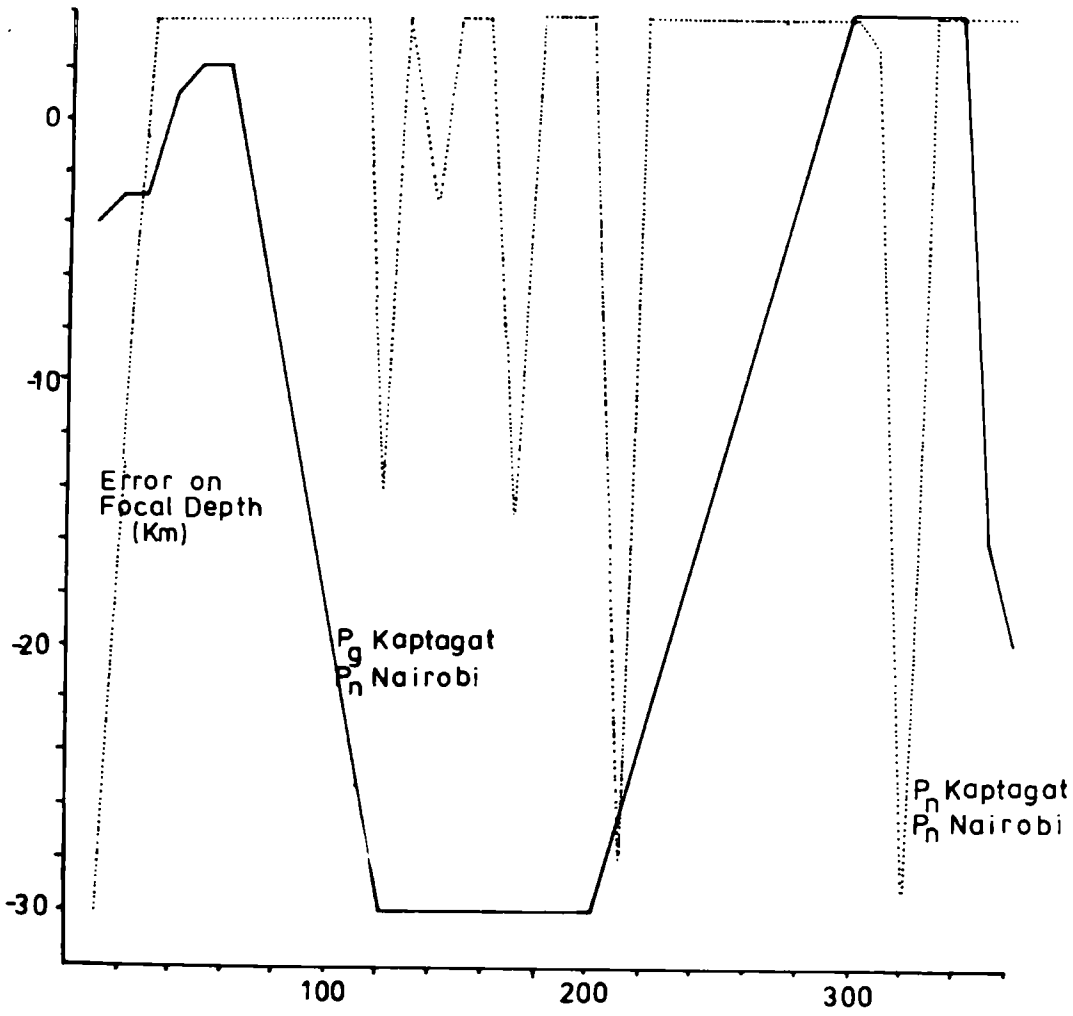

Error on Focal Depth due
to an Error of 0·5 Seconds
on the Travel Time to Kaptagat

Fig 3·14

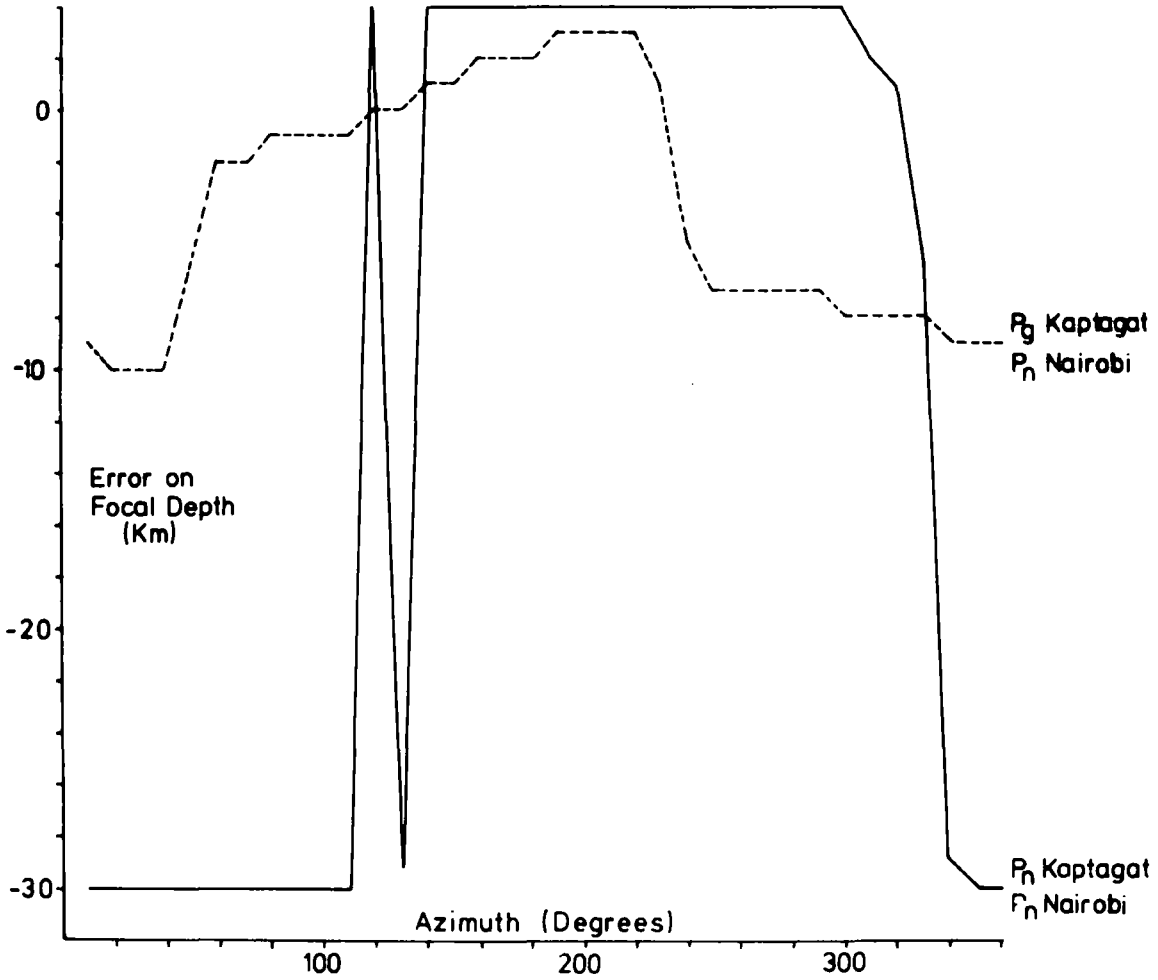

Error on Focal Depth due
to an Error of 0·5 Seconds
on the Travel Time to Nairobi

Fig 3·15

accuracy of the method is strongly dependent upon the accuracy of the measured P-S time at Nairobi.

The accuracy of the azimuth, measured from Kaptagat, of the epicentre also affects the error on the focal depth. In Fig (3:15) the error on the azimuth is assumed to be one degree. Three of the four cases listed above have been considered and are represented on the graph by a, b, c. The three graphs shown in Figures (3:14) to (3:16) are not smooth curves. This is because the computer program, based on the above method to determine focal depth, increments the test focal depth in steps of 1 Km. An error in the azimuth has a maximum effect when one of the two stations sees a P_g phase as the first arrival. The effect of an erroneous azimuth is not so pronounced when both stations see a P_n phase as the first arrival.

Fig (3:17) shows the error on the focal depth, due to an incorrect crustal model, assuming both stations see a P_n phase as the first arrival. The graph in Fig (3:17) has been drawn assuming an error of $\pm$ 0.2 Km sec^{-1} on the velocity of the first and third layers and an error of $\pm$ 0.3 Km sec^{-1} on the second layer. In these graphs the epicentral distance has been constrained to the correct value. In the case when the actual p-wave velocities are at the extreme limits of the velocities in the crustal model the error on the focal depth is $\pm$ 12 Km. This discussion assumes that the width of each layer, within the crust, is known. An error in the width of each layer will introduce an error into the focal depth. For a P_n arrival a variation of $\pm$ 1 Km in the depth to the first boundary will result in an error of $\pm$ 0.1 Km on the focal depth. For a P_g arrival the same error on the crustal model will produce an error on the focal depth equivalent to an error of

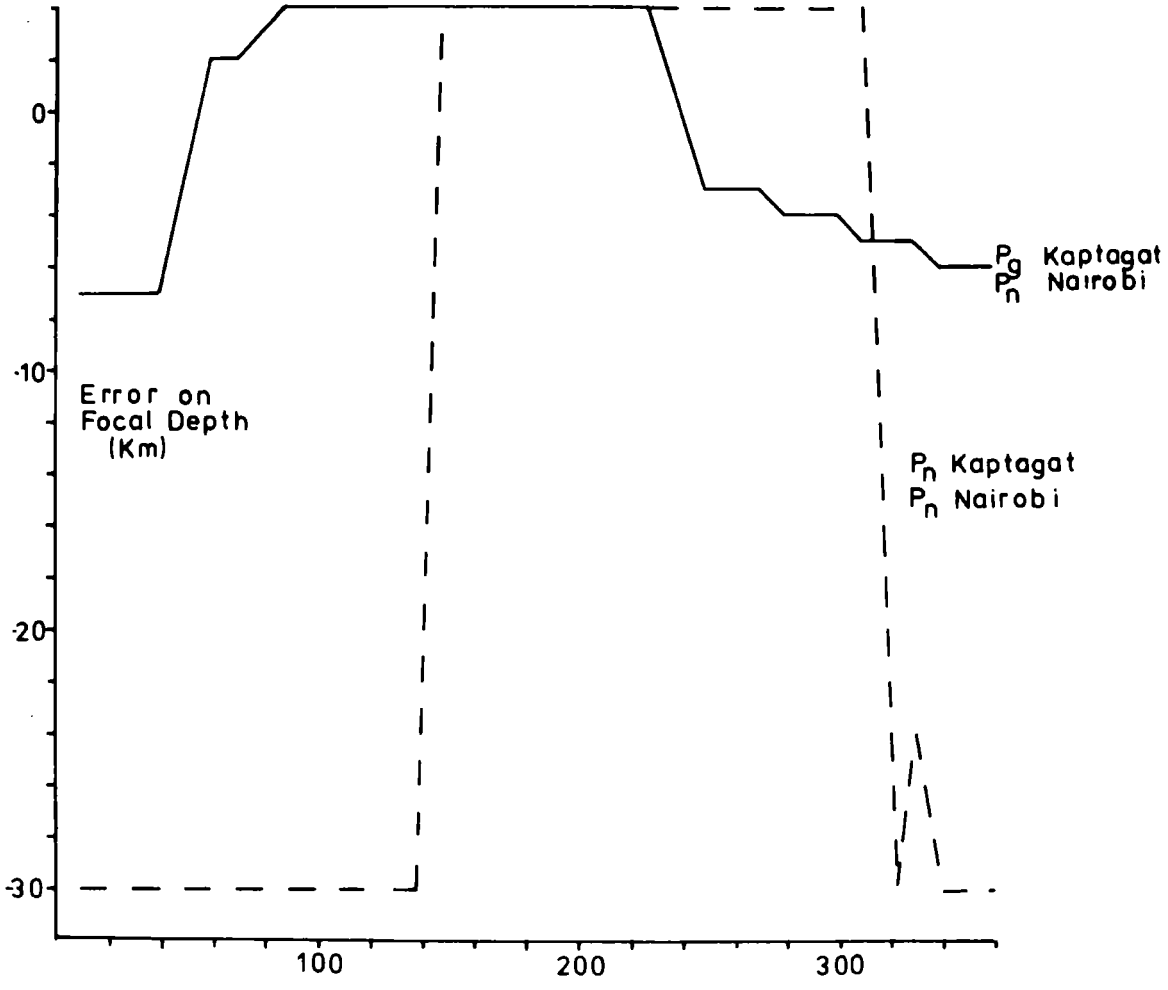

Error on Focal Depth due to
Error on the Measured Azimuth.

Fig 3:16

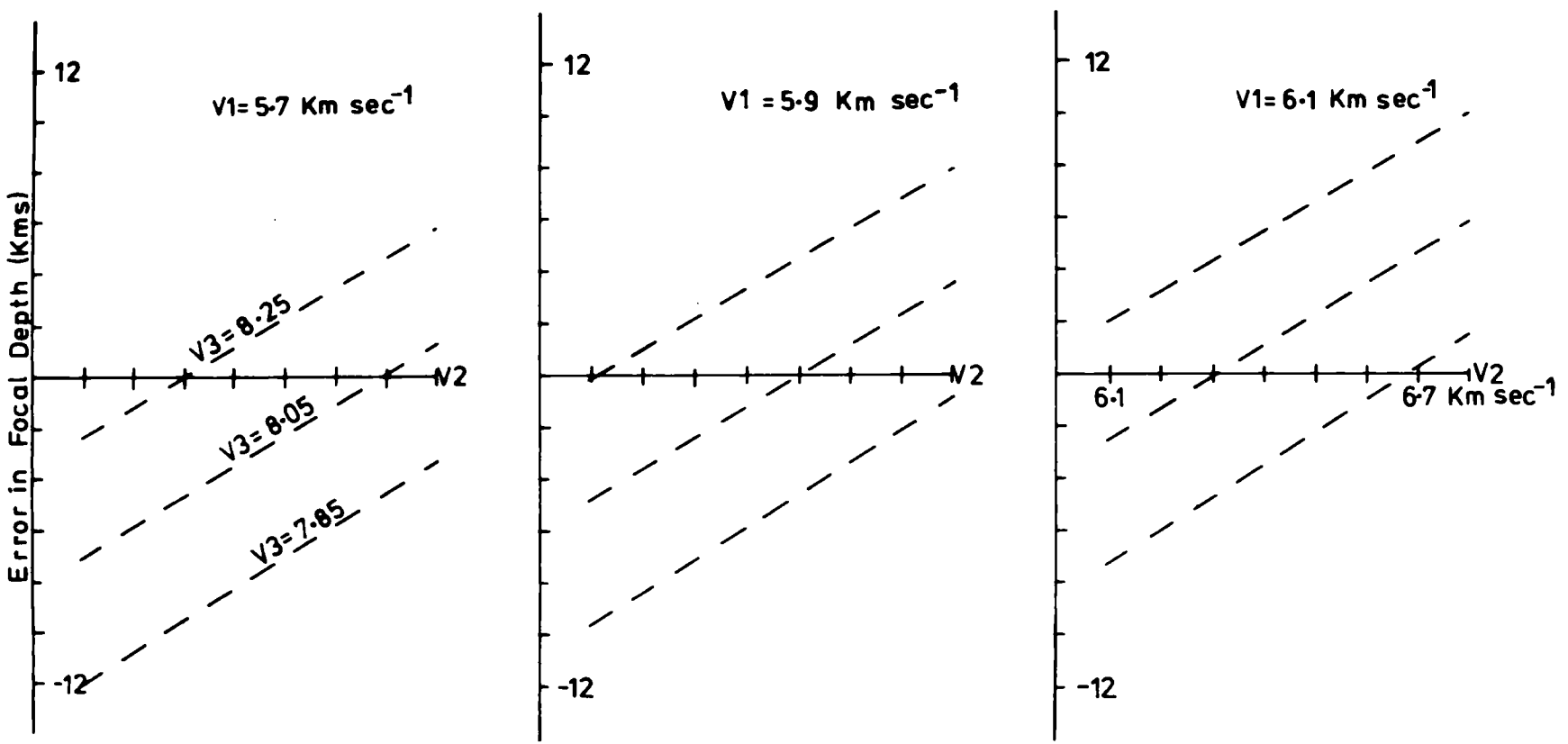

Variation of the Error on the Focal Depth Due to Variation of the P-Velocity of the Three Layers Forming the Crustal Model

Fig 3:17

± 0.32 seconds on the travel time. This error is insignificant.

The crust within the Gregory Rift is anomalous and therefore the calculated travel time to Nairobi will be incorrect. When the focal depths of events within the Kavirondo Graben are determined by this method the focus of the event is placed at or near 0 Km depth. This is due to the incorrect travel time. A similar perturbation exists on the focal depths of events located within the Ruwenzori area. Because of this perturbation, by the anomalous structure within the Gregory Rift, of the travel time of the signal the method was restricted to events from the south and southwest of Kaptagat and Nairobi. Events from these regions have travel paths which do not cross the Gregory Rift. Events from these regions have focal depths within the top 5 Km of the crust.

3:11 Focal depths determined using second arrivals.

The three focal depth methods discussed previously did not utilize any second arrivals that may appear on the record. Focal depths were determined from the previous methods using some feature of only the first arrival and the measured P-S time. A crustal model as illustrated in Fig (3:4) will give rise to a number of P-arrivals originating from different travel paths. If the event is sufficiently distant from the station these second P-arrivals may be sufficiently separated to be distinguishable on the record. Consider an event with P_n as the first arrival. Using the crustal model in Fig (3:4) it is possible to postulate a number of major second arrivals following the moho arrival. The paths followed by the second arrivals are illustrated in Fig (3:4) along with the letters by which they will be identified in the text. For an event with a focus in the first layer the second

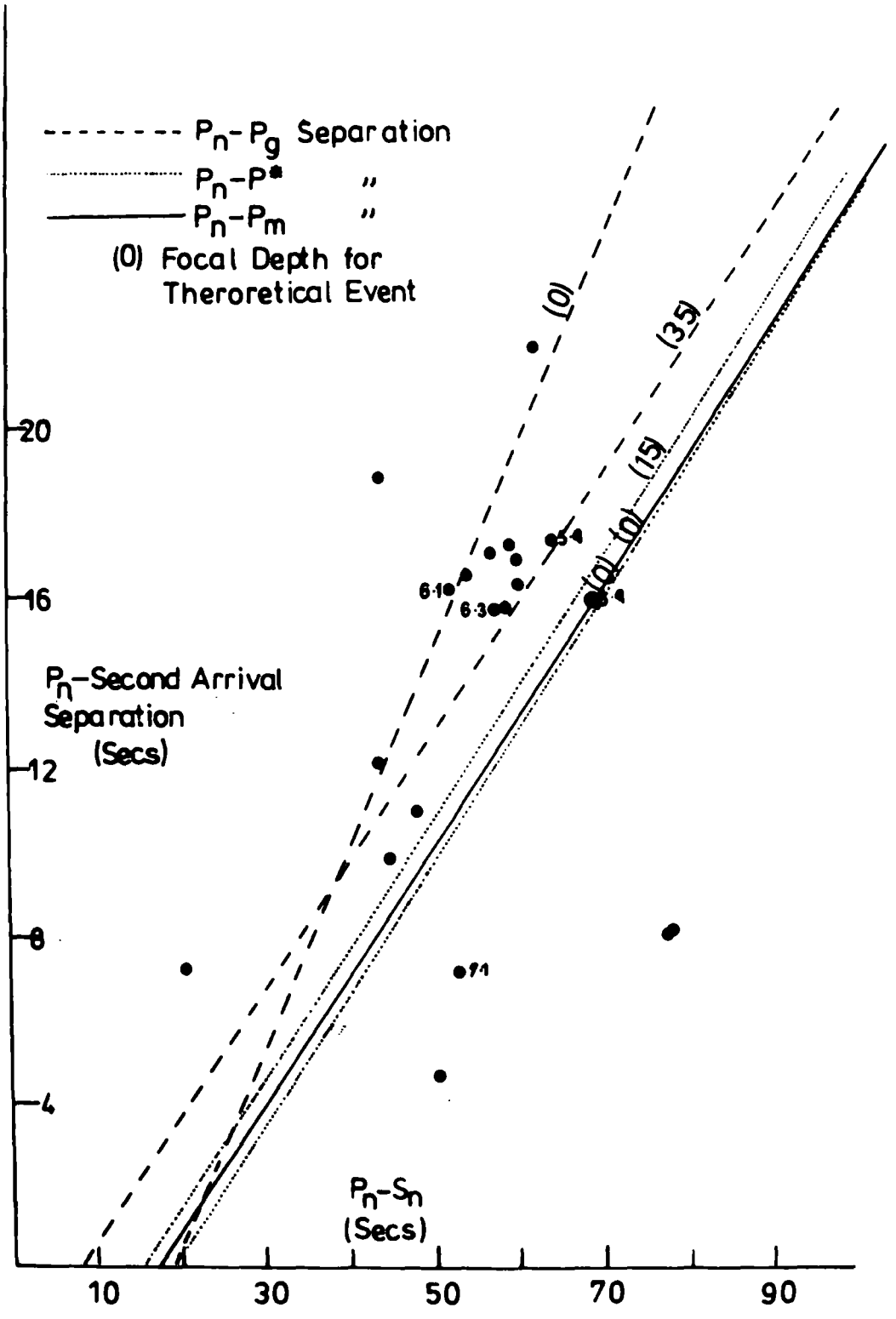

Theoretical Separation of P_n and Second P Arrivals Against P_n-S_n

Fig 3·18

arrivals may include P_g, P^* and P_m. An event with a focus in the second layer may have P_g and P_m as second arrivals. A P_p second arrival was tentatively identified for one event. This arrival had an apparent velocity of 8.0 Km sec^{-1} and was similar in shape to the P_n signal which was the first arrival. The 'P_p' signal showed an 180 degree phase shift relative to the P_n signal.

The second arrivals were identified using the apparent velocity of the signal. This means that the second arrivals were accurately defined and there is only a slight chance of misidentification.

Using the crustal model in Fig (3:4) the arrival times for P_n, P^*, P_g and P_m were calculated for a series of epicentral distances and focal depths ranging from 0 to 35 Km. The difference between the arrival times of P_n-P_g, P_n-P^* and P_n-P_m are plotted against P_n-S_n in Fig (3:18). In the case of the P_n-P_g two focal depths, 0 and 35 Km, have been considered. Similarly two focal depths, 0 and 15 Km, have been considered for P_n-P^*, and a focal depth of 0 Km for P_n-P_m. At a focal depth of 35 Km, P_n-P_g and P_n-P_m are equivalent. Against the theoretical separation between P_n and the second p-arrivals are plotted the observed differences for earthquakes recorded at Kaptagat. Fig (3:18) shows that the majority of the earthquakes have a shallow focal depth. This is confirmed by the apparent velocity of the second arrivals (see Appendix).

3:12 Discussion of focal depths.

Of the four methods available to determine focal depths, the potentially most useful method, the combination of the P-S time at Kaptagat and Nairobi and the azimuth of the epicentre from Kaptagat, is virtually eliminated by the anomalous crust in the Gregory Rift.

When this method was used, for events from the far south and south west of Kaptagat, it gave focal depths in the top 15 Km of the crust. The error graphs discussed previously have shown that an error in the P-S times or azimuth of the event forces the focal depth to the limits of the crust. That this does not happen is taken as an indication that the focal depths, determined by this method, are not wildly incorrect.

The focal depths within the Kavirondo rift cluster between 11 - 25 Km, similar to the focal depths found by Wohlenberg (1968, 1970) for the Western Rift. These focal depths are deeper than those found by Molnar and Aggarwal, (1971), for the after shock sequence in the Homa Bay area. The difference between their focal depths and those found in this survey may be due to an error in the measured apparent velocity.

In the northern section of the Eyasi Rift Rykounov et al., (1972), and Molnar and Aggarwal reported values of focal depth clustering in the range 10 - 20 Km. This compares favourably with the focal depths found for events in the Kavirondo Rift.

The second arrival method can only provide an indication of the focal depth. However, it does support the other methods in that the focal depths appear to cluster at depths of 10 - 15 Km.

CHAPTER 4

SEISMICITY

4:1 Introduction

Previous seismic studies of the East African Rift System have, because of the location of the recording stations, concentrated on the western arc of the system. Consequently little is known about the seismic activity in the Kenya section of the East African Rift System. Wohlenberg (1969) lists four seismically active tectonic areas;

1) The Semliki - Ruwenzori area.
2) North of Lake Tanganyika and the Russi Plain.
3) The Rukwa Rift.
4) The Eyasi Rift and the southern part of the Gregory Rift.

Of the four areas listed above the first three are part of the Western Rift and the fourth area is part of the Eastern Rift.

The Semliki Ruwenzori area is in the northern sector of the Western Rift and of the three seismically active areas in the Western Rift it is the nearest to Kaptagat. It should be possible to observe at Kaptagat shocks within the Ruwenzori area with a magnitude greater than 3.4. The largest earthquakes previously recorded within the area had a magnitude of 6.5-7.0 (m_b) and occurred on March 20 1966. This shock may be associated with an upthrow to the west of 40 cm on a fault running NNE for 40 Km from latitude 0.7N, longitude 29.8E (Wohlenberg, 1966). The epicentral location of the earthquake on March 20 lies on the line of the fault described above (Lahr and Pomeroy, 1970). In the 1.8 days prior to the large shock there were 35 events with a body wave magnitude greater or equal to 3.3. These shocks are so distributed in time as to suggest that they are part of a

foreshock sequence. At the beginning of this foreshock sequence the temporal frequency of events is approximately 150 events per day. Just before the main shock, toward the end of the foreshock sequence, the temporal frequency of events dropped to 1 event per day. The third earthquake in the foreshock sequence was the largest of the sequence and had a magnitude of 4.8 (m_b). If the foreshock sequence is isolated from the following shocks it takes on the appearance of an aftershock sequence. This impression is created by the large earthquake, magnitude 4.8, followed by the decaying sequence of smaller magnitude earthquakes. In the 67 days after the main shock there were 779 earthquakes with magnitude (m_b) greater or equal to 3.3 (Lahr and Pomeroy, 1970). Wohlenberg (1968) has split the aftershock sequence into a main series starting immediately after the main shock and two secondary series starting approximately 32 days and 37 days after the main shock. When the magnitudes of the earthquakes of the fore and aftershock sequence are fitted to an equation of the form $\log N = a - bm$ both the fore and aftershock sequence give a b value of approximately 1.05 (Lahr and Pomeroy, 1970). The events of the aftershock sequence are located on the Kitimbi-Semliki fault, to the west of the main shock (Fairhead and Girdler, 1971). In the period 1956-1963 before the earthquake of March 20 the Ruwenzori area was moderately active with 38 events of magnitude (M_1) greater or equal to 4 and 80 events of magnitude less than 4.0 (Wohlenberg, 1968). Sutton and Berg (1958) using data from the I. S. R. A. C. network located two earthquakes with magnitude (M_1) greater than 6 on the western side of Lake Albert. The first shock (M_1=6.0) occurred on July 22 1955 and the second shock (M_1=6.3) on September 4 1955. The three large magnitude earthquakes that have been located in the region of the Ruwenzori

may represent an upper limit to the magnitude of earthquakes in this region. Analysis of the I.S.C. bulletins for the period 1967-1970 showed that after the major shock of March 20th 1966 and its associated aftershook sequence the number of events with magnitude (m_b) greater than 4 dropped to 8 and 4 earthquakes with magnitude (m_b) less than 4. This apparent decrease in the seismic activity of the Ruwenzori region may be a function of the number of observing stations or may reflect a large stress drop due to the series of earthquakes during 1966. Microseismic activity in the Ruwenzori area has been investigated by Rykounov et al., (1972), who found a microseismic activity of 230 events in ten days. This level of microseismic activity is in agreement with the temporal frequency of the earthquakes with larger magnitudes.

As the Western Rift is traced southward the next prominent seismically active zone is the northern end of Lake Tanganyika. Providing that the earthquakes located at the northern end of Lake Tanganyika have a magnitude greater than 3.9 they will be recorded at Kaptagat. The seismic activity for the northern part of Lake Tanganyika in the years 1956-1963 is outlined in table 4:1 (from Wohlenberg, 1968). From this table the general seismic activity is approximately 12 earthquakes a year with magnitude (M_1) less than 4 and approximately 5 earthquakes a year with magnitude (M_1) greater than 4 excluding the data for the years 1960 and 1962. The number of earthquakes in the two years 1960 and 1962 are much higher than for the other years listed and are representative of aftershock sequences following earthquakes with magnitudes (M_1) of 6.25 (1960) and 5.75 (1962). Further evidence that the northern end of Lake Tanganyika is a continuously active seismic zone comes from DeBremaecker (1959). Using data from the I.S.R.A.C. network,

TABLE 4:1

TEMPORAL DISTRIBUTION OF EARTHQUAKES

AT THE NORTH END OF L. TANGANYIKA

YEAR	MAGNITUDE>4	MAGNITUDE<4
1956	6	9
1957	2	1
1958	8	17
1959	1	6
1960	54	128
1961	5	24
1962	12	53
1963	4	17

he has shown that this area was one of the most active areas in the Western Rift during the period 1953-1957. DeBremaecker also found that the earthquakes were closely related to the faults that form the margin of the Tanganyika graben. Combined with the locations of Wohlenberg (1966, 1968, 1969), the data of DeBramaecker (1959) clearly shows the continuity in the seismic activity at the northern end of Lake Tanganyika.

The southern end of the Tanganyika and Rukwa grabens are areas of high seismicity with 68% of the shocks felt in Tanzania originating from faults in these areas. Of the two areas the Rukwa graben is the more active (Fairhead and Girdler, 1971) and the majority of the seismic activity is concentrated on the eastern flanks of the grabens (Wohlenberg, 1968). During the years 1958-1963 the southern part of the Tanganyika graben and the Rukwa graben were the site of 7 shocks with magnitude (M_1) greater than 5 and 27 shocks with a magnitude (M_1) between 4 and 5. These figures suggest that the seismic activity in the southern part of the Tanganyika graben and the Rukwa graben is slightly higher than the seismic activity at the northern end of Lake Tanganyika. The southern end of the Tanganyika graben is approximately 2000 Km southwest of Kaptagat and at this distance only earthquakes with a magnitude (M_1) greater than 6.3 will show above the noise level at Kaptagat.

Within the Western Rift not all seismic regions are tectonic areas. Regions of high geothermal heat flow correlate well with zones of seismic activity (Fairhead and Girdler, 1971). These geothermal areas include the Upemba-Mweru area and north of Lake Kivu where the activity is associated with the Virunga volcanoes (DeBremaecker, 1959). Two seismic zones, one running due west of Lake Kivu (DeBremaecker, 1959) and the other in the Malagarasi

area 200 Km east of central Lake Tanganyika (Wohlenberg, 1969) show no signs of tectonic or geothermal activity.

Compared with the Western Rift the eastern arc of the East African Rift system is much nearer to Kaptagat and consequently it should be possible to detect, at Kaptagat, small magnitude earthquakes with epicentres located in the Eastern Rift. Previous work has shown that the most active part of the Eastern Rift lies between latitudes 2°S and 6°S. This section of the Eastern Rift is known as the Eyasi Rift. From Lwiro, a station within the I.S.R.A.C. network, it should be possible to detect events with magnitude (M_1) greater or equal to 4 originating from within the Eyasi Rift (Fig 4:1). During the period 1958-1963 the I.S.R.A.C. network located 14 events with magnitude (M_1) greater than 5, 38 events with magnitude (M_1) between 4 and 5, and 10 events with magnitude (M_1) less than 4 within the Eyasi Rift. If the trend indicated by the above figures for the recorded seismicity in the Eyasi Rift is extrapolated toward lower magnitudes approximately 300 events per year with magnitude (M_1) greater than 3 can be expected to occur within the Eyasi Rift. Most of the shocks located in the Eyasi Rift by the I.S.R.A.C. network are concentrated on the western flank of the Eyasi Rift or to the west of the Eyasi Rift (Wohlenberg, 1968). Sykes and Landisman (1964) have relocated four of the large earthquakes located in the Eyasi Rift by Wohlenberg. The locations of Sykes and Landisman are to the east of those of Wohlenberg (see table 4:2) and lie within the Eyasi Rift.

The microseismicity of the Eyasi Rift has been studied by Rykounov et al., (1972), who recorded approximately 30 events per day in the vicinity of the two volcanoes Ngorongoro and Oldonyo Lengai, and Lake Manyara. These shocks had magnitudes in the range

TABLE 4:2

COMPARISON OF LOCATIONS OF EVENTS IN THE EASTERN RIFT

	Sykes and Landisman		Wohlenberg		
Date	Location		Location		Magnitude
April 04 1956	04.98°S	35.44°E	05°S	35.2°E	6.5
May 10 1959	03.19°S	35.91°E	03°S	34.58°E	4.2
August 24 1959	04.24°S	35.04°E	04°S	34.5°E	6.1
October 25 1959	04.83°S	35.64°E	04.75°S	34.75°E	5.2

0.5-3.5 (M_l). Although the earthquakes in the vicinity of Ngorongoro, Oldonyo Lengai and Manyara did not correlate with known faults, further north at latitude 2°S Tobin et al., (1970), located a significant number of earthquakes near the scarps of Pleistocene faults. Tobin et al. found that the eastern flanks of the rift near the Kenya border showed the highest seismic activity with a seismicity of 47.1 events per day. Further north into the Gregory Rift the seismic activity appears to decrease (Molnar and Aggarwal, 1971; Tobin et al., 1970).

Beyond the northern limit of the microseismic surveys two large earthquakes have occurred in the rift. The earlier shock happened on January 6, 1928, and had a magnitude (M_l) of 6.2 (Tillotson, 1937a). Tillotson (1937b) has suggested that this shock was in fact a double event with a near surface focus. The second of the two major earthquakes had a magnitude (M_l) of 7.0 and occurred on September 1, 1957. This shock was located in the Gregory Rift on the same latitude as the southern boundary fault (the Lambwe fault) of the Kavirondo Gulf (Wohlenberg, 1968). Unfortunately, the U.S.R.A.C. system is too far away from the Gregory Rift to reveal any low magnitude seismicity. However, the close proximity of the Kaptagat array to the Gregory Rift does provide information on the low magnitude seismicity.

On the same latitude as the centre of the Gregory Rift but running in an east-west direction is the Kavirondo graben. Like the Gregory Rift the Kavirondo graben appears to be seismically quiet. However, during March and April, 1968, a series of magnitude (M_l) 5.0 earthquakes occurred on the Lambwe fault (Loukepine, 1968). The after effects of these large shocks is confined to a zone 2 Km wide just north of the Lambwe fault. In this zone, Molnar and Aggarwal recorded over 300 microseisms per day during March, 1970.

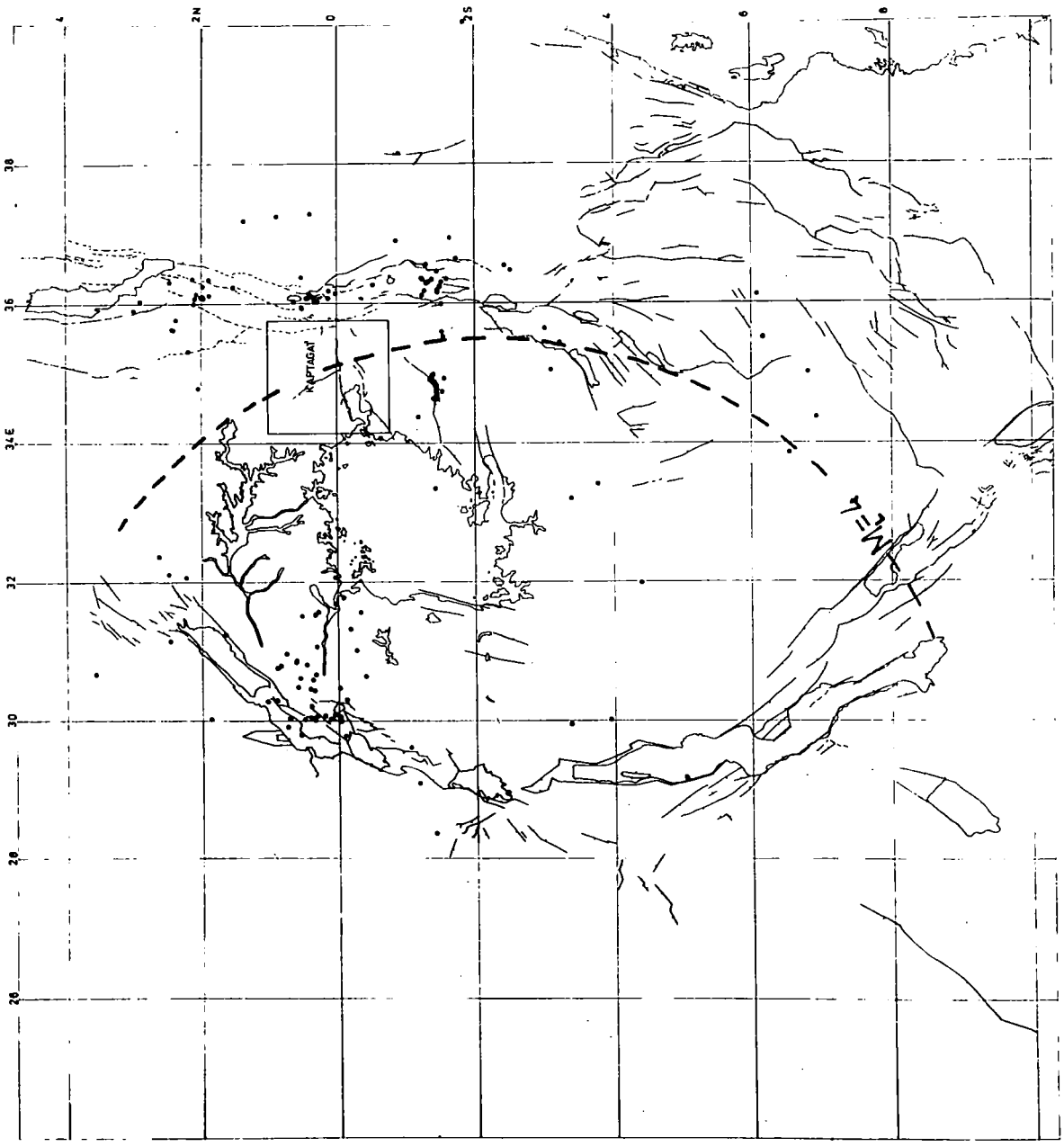

Kaptagat Location of Epicentre

Fig 4:1

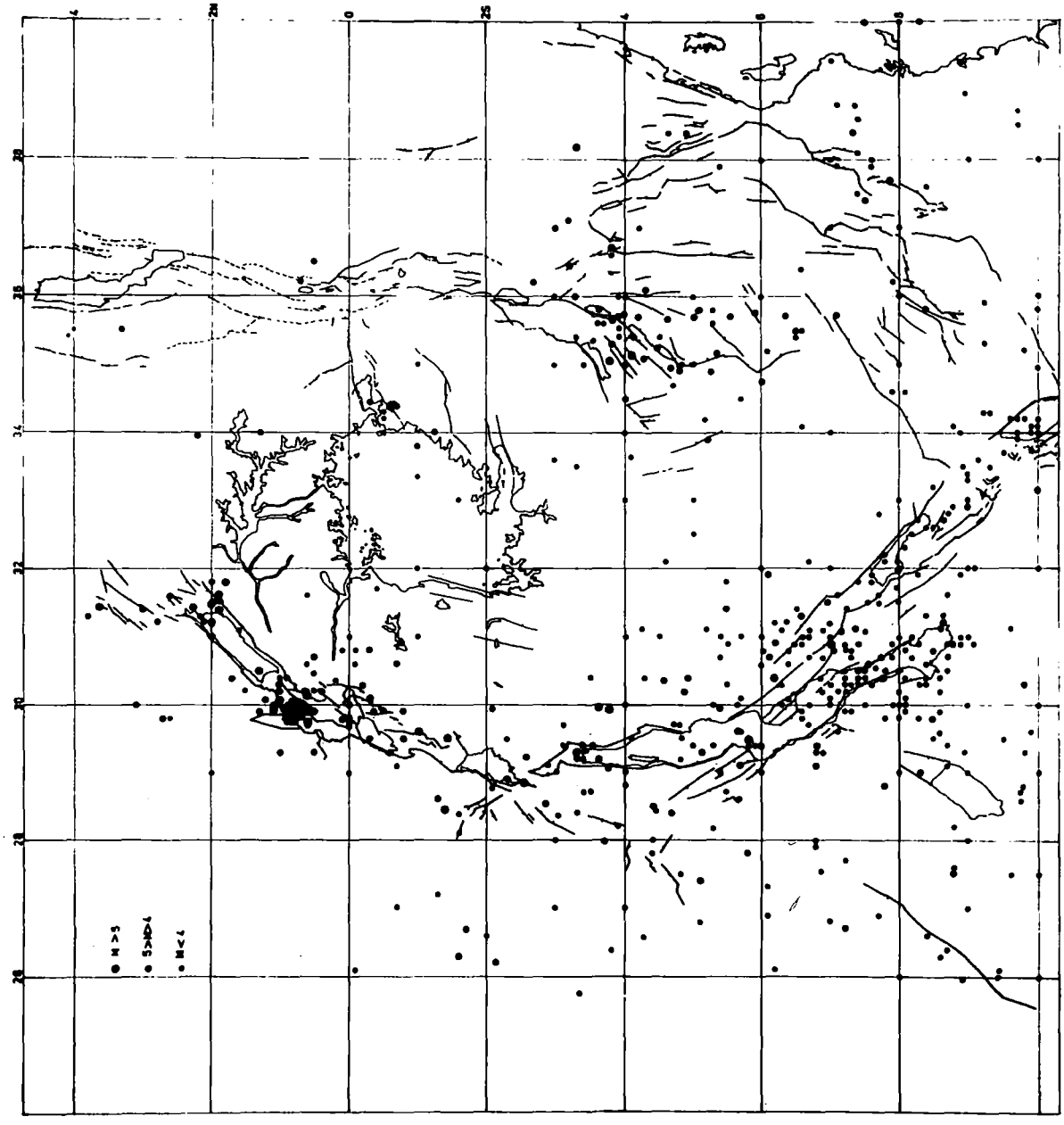

I S C Location of Epicentre 1964-1970

Fig 4·2

Earthquakes within this zone had a focal depth between 3 and 5 Km.

From previous seismic surveys the Gregory and Kavirondo Rifts appear to be areas of low seismic activity. The small earthquakes located in the area may represent a small stress build up and the large earthquakes a locking of the faults. Further south the pattern of faults and the presence of large magnitude earthquakes may indicate a change in the crustal structure and the stress build up.

4:2 The present survey.

The bulk of the data involved in this study covers a continuous period from March 12, 1971, to July 9, 1971. This data was supplemented by data from September 1, 1971, to November 14, 1971, and from July 20, 1970, to July 31, 1970. Although the study is based primarily on the data from the continuous period the secondary periods were used to confirm the seismic areas, the background activity, magnitudes and other features outlined by the continuous period.

Four seismically active areas were outlined by this study. The four areas, each of which will be individually discussed, are:-

(i) The Kavirondo Rift and surrounding areas.
(ii) The Gregory Rift.
(iii) The Ruwenzori block and the Albertine Rift.
(iv) The Siria Fault.

4:3 Kavirondo Rift.

The eastern end of the Kavirondo Rift, the Elgeyo Escarpement and the southern flanks of Mt Elgon have been grouped into one area. The Kavirondo Rift is bounded by the seismcially active Lambwe fault and the Nyando fault. Kaptagat lies between 43 and 166 Km

Two Events from the Kavirondo Rift

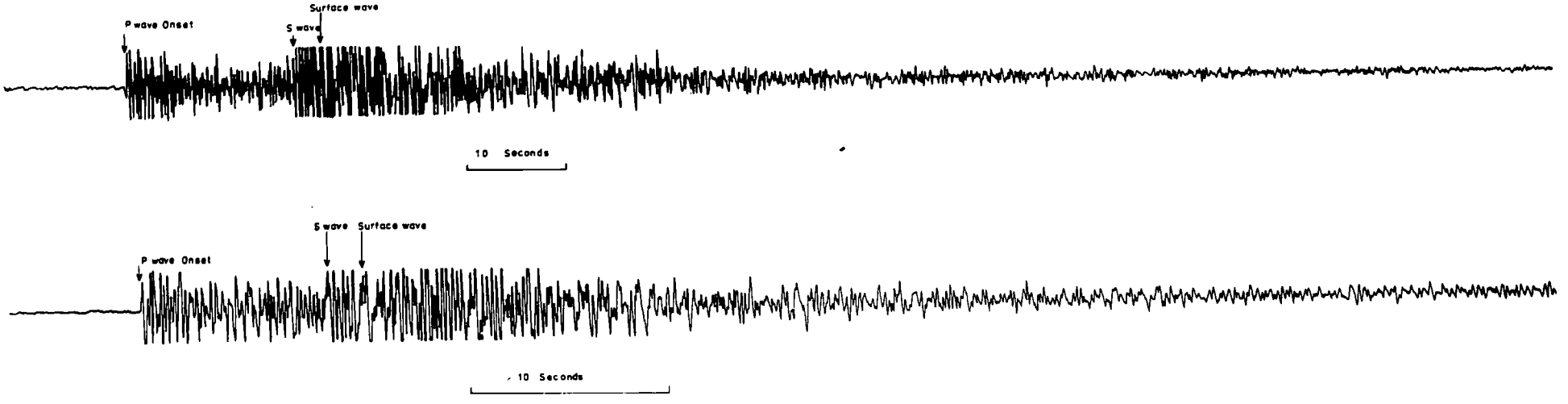

Fig 4:3

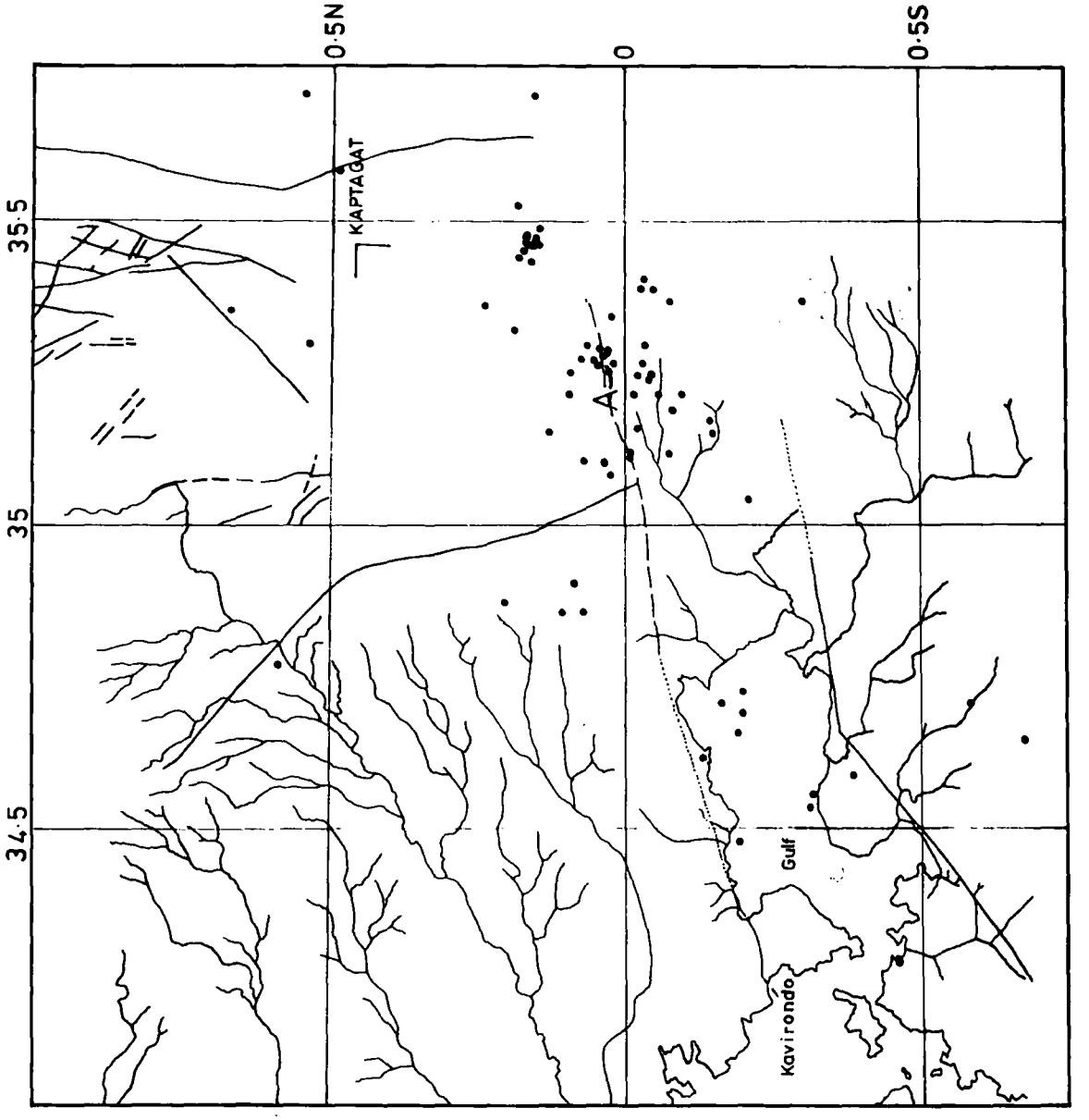

Seismic Activity in the Kavirondo Rift

Fig 4:4

from the Nyando fault and between 86 and 192 Km from the Lambwe fault. At these distances the observational cutoff magnitude at Kaptagat for events in the Kavirondo Rift lies between 2.1 and 2.4 (m_b'). Events that have been located within the Kavirondo Rift have first arrivals with a measured apparent velocity ranging between 5.9 Km sec^{-1} and 7.0 Km sec^{-1}. The majority of the measured apparent velocities are between 6.4 and 6.6 Km sec^{-1}. If the model in Fig (3:4) is applicable to the crust in this area the velocities of 6.4 Km sec^{-1} to 6.6 Km sec^{-1} suggest that the first arrival is a P* phase and the focal depths are less than 18.0 Km.

All of the events located within the Kavirondo graben show an initial impulsive P arrival. After the first arrival the amplitude of the p-wave train gradually dies away until the onset of the S or surface waves. The s-waves are not always visible on the record and this may be due to the orientation of the fault plane to Kaptagat. The frequency of the p-wave train of all the events from the Kavirondo Rift lies in the range 4-6 Hz. With the onset of the surface waves the frequency of the signal decreases. Two events which have epicentres located in the Kavirondo graben are illustrated in Fig (4:3).

A cluster of 13 events have been located approximately 25 Km south of Kaptagat and east of the Nyando fault. These events have travelled a P_g path to Kaptagat, the measured apparent velocity of the first arrival ranging between 6.3 and 7.2 Km sec^{-1}. The signal frequency of the p-wave train is approximately 10 Hz.

As can be seen from Fig (4:4) the majority of the events located within the Kavirondo graben are associated with the eastern end of the Nyando fault. Events located in this part of the graben are not concentrated on the inferred extension of the fault but

form a diffuse pattern either side of the fault line. The spread of the epicentres may be due to local small faults or incorrect focal depths. As the eastern end of the Kavirondo Rift is covered by the Uasin Gishu lava any small faults are hidden and their correlation with the epicentres cannot be confirmed. If the events located at the eastern end of the graben and the events 25 Km to the south of Kaptagat are treated as one group they form a line of seismicity aligned in a ENE direction. This line is coincident with the direction of the inferred extension of the Nyando fault, The tight grouping of the epicentres near the Elgeyo Escarpement suggests that these events are associated with a local fault. If this is correct the line of seismicity probably represents a band of local faults and not one continuous fault.

The western end of the Kavirondo Rift is apparently less seismically active than the eastern end of the graben. This apparent lack of seismic activity may be due to the increase in the observational cutoff magnitude because of the increased distance to Kaptagat. However, the number of earthquakes in the western part of the rift is still lower than the number anticipated. Even the Homa Bay area ($0.5^{o}S$, $34.5^{o}E$) of the western part of the Kavirondo rift which was the site of previous seismic activity, (section 4:1), was seismically quiet. Between 1968 and 1971 the area of seismic activity has apparently migrated eastwards by a distance of approximately 100 Km. The events that have been located within the western end of the rift are concentrated toward the centre of the rift. Geological evidence indicates minor faulting within this part of the graben and the events are probably associated with these faults.

Seven events have been located to the north of the Kavirondo Rift. These shocks are associated with small scale normal faulting

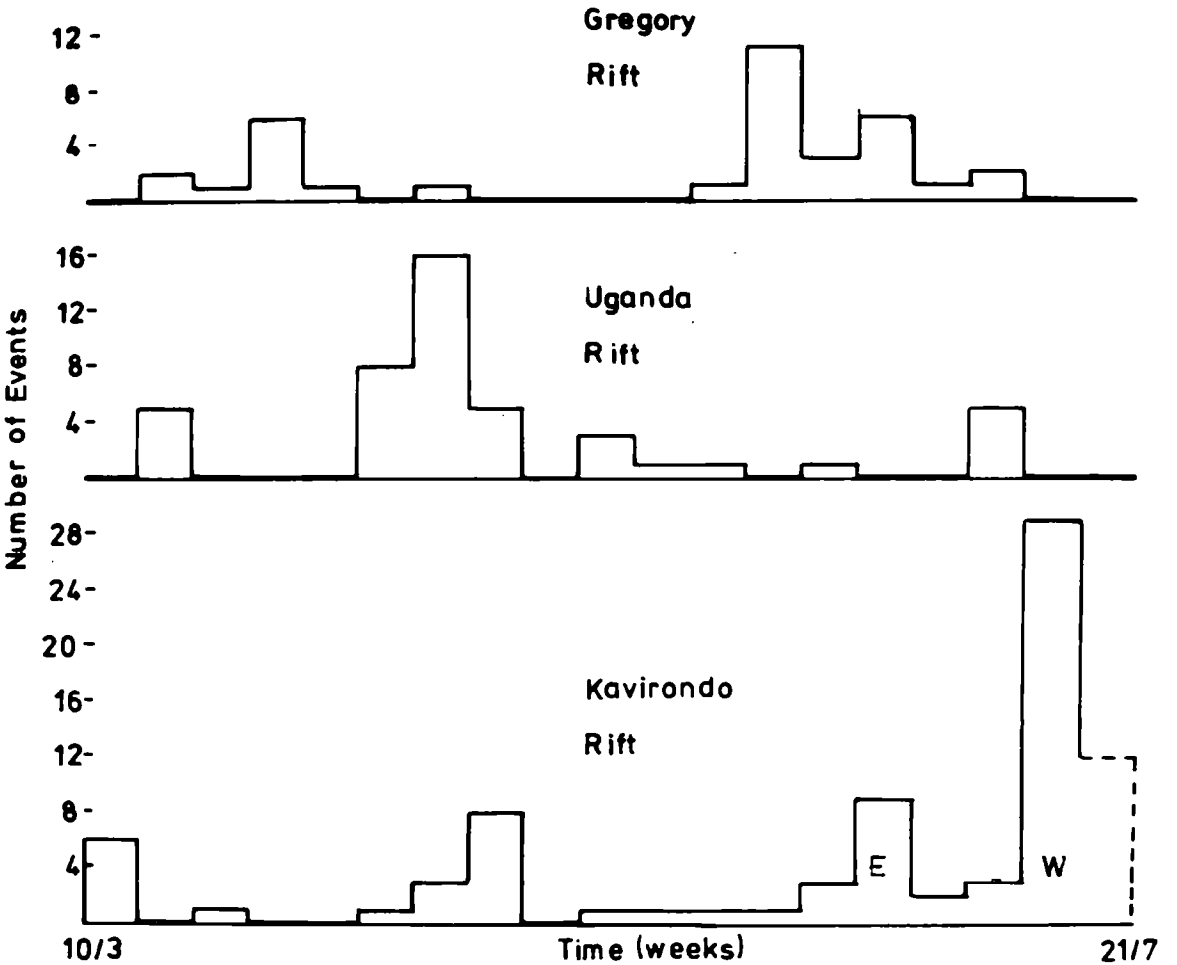

Temporal Distribution of Events within the Principal Rifts.

Fig 4:5

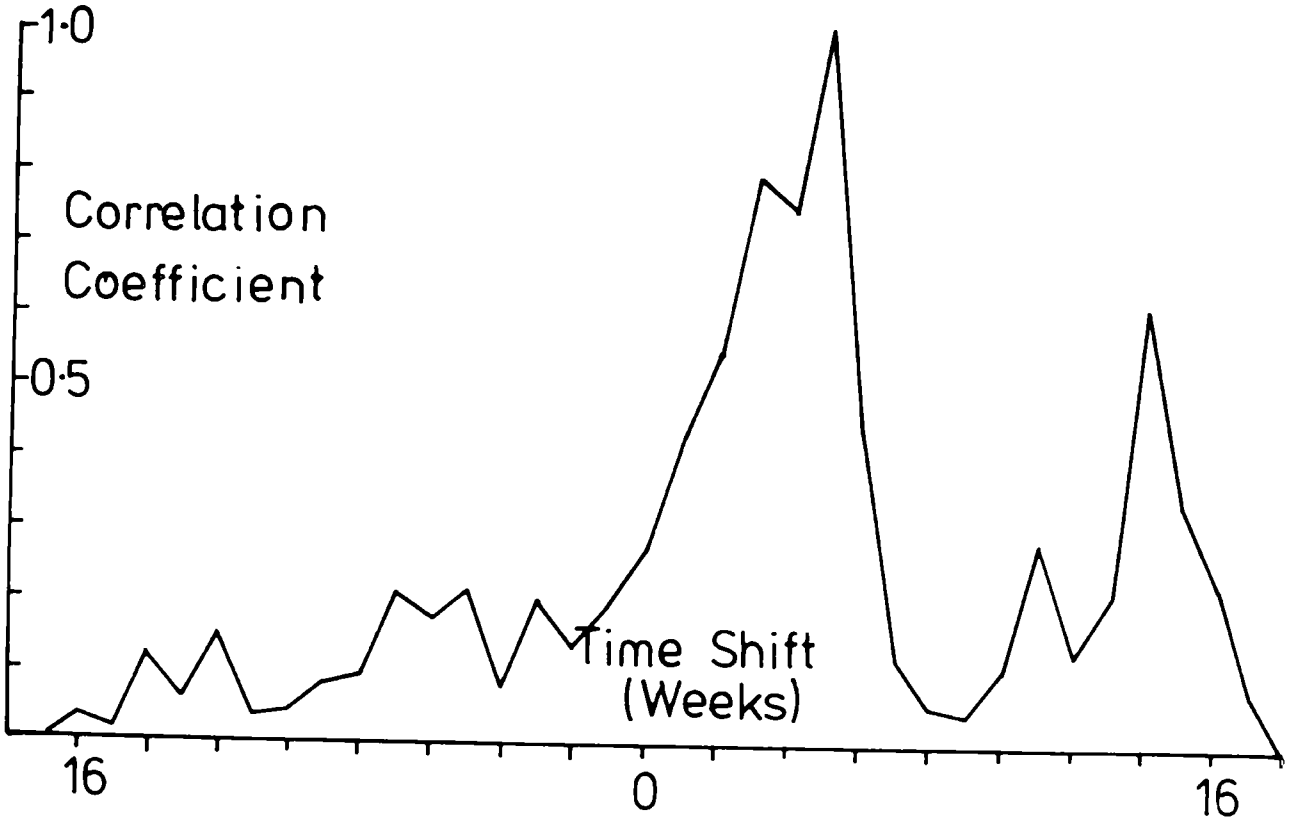

Cross Correlation of
Temporal Distribution of
Events in the Gregory
and Kavirondo Rifts.

Fig 4:6

that festoons the basement.

The temporal distibution of the events in the Kavirondo graben area is illustrated in Fig (4:5). This plot shows that the majority of the earthquakes occur in bursts, two of which have been marked E and W. Events that constitute the burst labelled E are located in the eastern part of the rift and south of Kaptagat. The burst of activity labelled W is formed by events approximately 30 Km to the west near the junction of the Nandi and Nyando faults. Within this burst there are five shocks with m_b^1 greater than 3.50. The majority of the shocks with m_b^1 greater than 3.50 occur at point A in Fig (4:4). Within burst W the events show a general shift in the epicentres from east to west. This and the position of bursts W and E suggests a migration of the activity from east to west. Of the two bursts the events in the western burst have the higher average magnitude. The events in the eastern burst have a smaller average magnitude and are probably associated with small faults.

The histograms for the temporal distribution of the seismic activity in the Kavirondo Rift and the Gregory Rift show two peaks of activity separated by ten weeks. Although the histograms cover only 19 weeks the ten week periodicity is supported by observations from tapes not included in the continuous period. The peaks in the histogram for the Kavirondo Rift are slightly displaced in time relative to the peaks in the histogram for the activity in the Gregory Rift. A cross correlation of the two histograms shows two peaks separated by approximately ten weeks (Fig 4:6). These peaks are produced when the histogram for the Gregory Rift is displaced forward in time by four weeks and reflect a similarity in the seismic activity of the Kavirondo and Gregory Rifts. This suggests that there may be a causal relationship between the seismic activity

Surface Wave Events at Nairobi (P Expected Onset Indicated by ±)

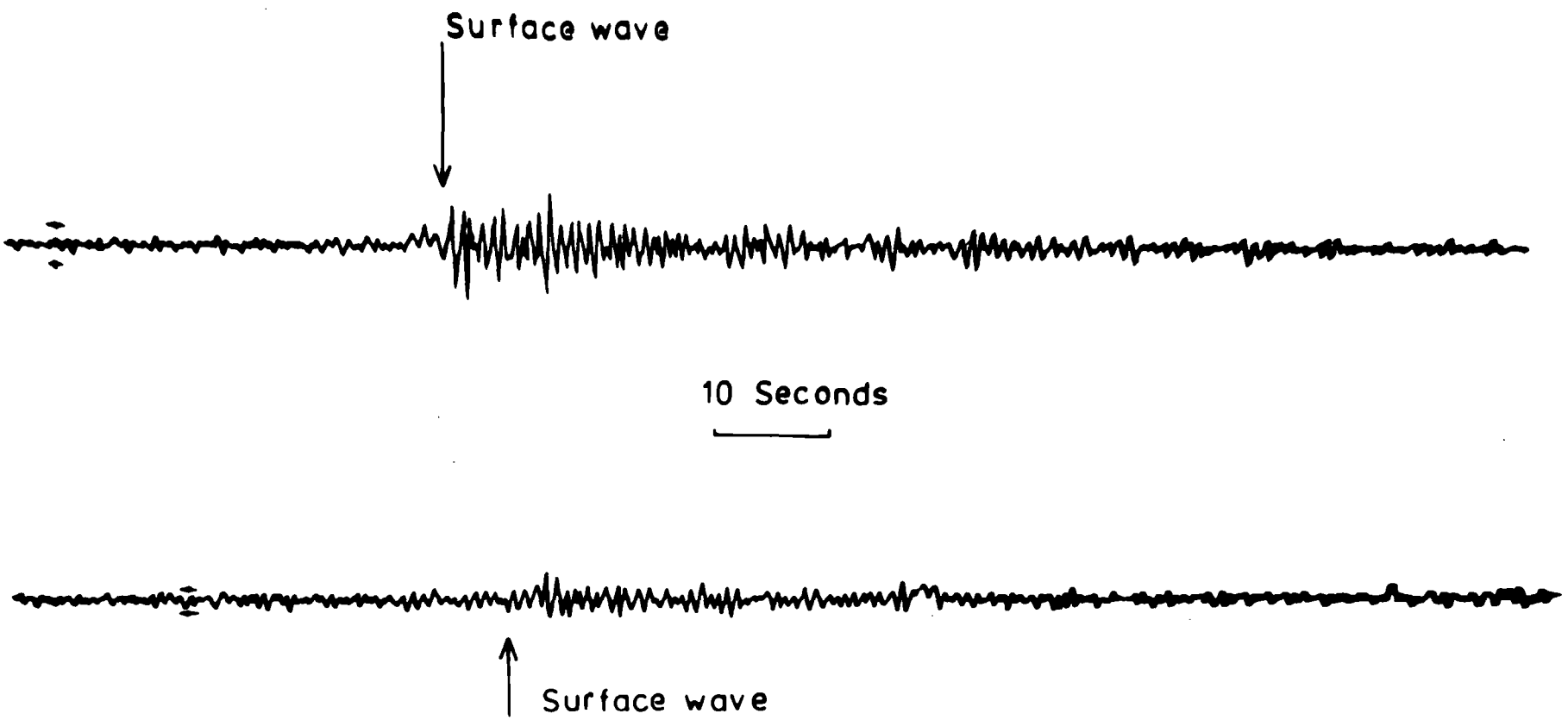

Fig 4:7

in the Kavirondo and Gregory Rifts.

Twelve events from the Kavirondo Rift were recorded by Nairobi seismic station. Of these twelve events, four did not show recognizable p-waves but were represented by surface waves. One of the surface wave only events had a magnitude of 3.5 as measured at Kaptagat. There is no apparent correlation between the position of the epicentre and the absence of recognizable p-waves at Nairobi. Two of the surface wave only events are shown in Fig (4:7). On this figure is shown the expected amplitude of the p-wave at Nairobi if the attenuation of the signal is allowed for using a modified form of Richter's curve. This reduction in the amplitude suggests attenuation of the signal as it crosses the Gregory Rift.

4:4 Gregory Rift.

During the period investigated fourty-seven events originating from within the Gregory Rift were recorded by the Kaptagat array. The epicentres of these events lie in one of three well defined seismic areas centred at latitude $1.5^{o}S$, $0.35^{o}N$ and $2^{o}N$ (Fig 4:1). These groups will be called the southern, central and northern groups respectively. The seismicity in the Gregory Rift forms a distinctive pattern with the areas of seismicity separated by regions of apparent quiet. The gaps in the seismicity within the Gregory Rift correlate closely with areas of volcanic activity. The southern gap, at approximately $1^{o}S$, is occupied by the volcanoes Suswa and Longnot. Similarly the northern gap, at approximately $1^{o}N$, is the site of two volcanoes, namely Silali and Pakka. The absence of any seismic activity within these areas is surprising as at least microseismic activity should be associated with the volcanoes. Kaptagat is approximately 90 Km from the centre of the northern

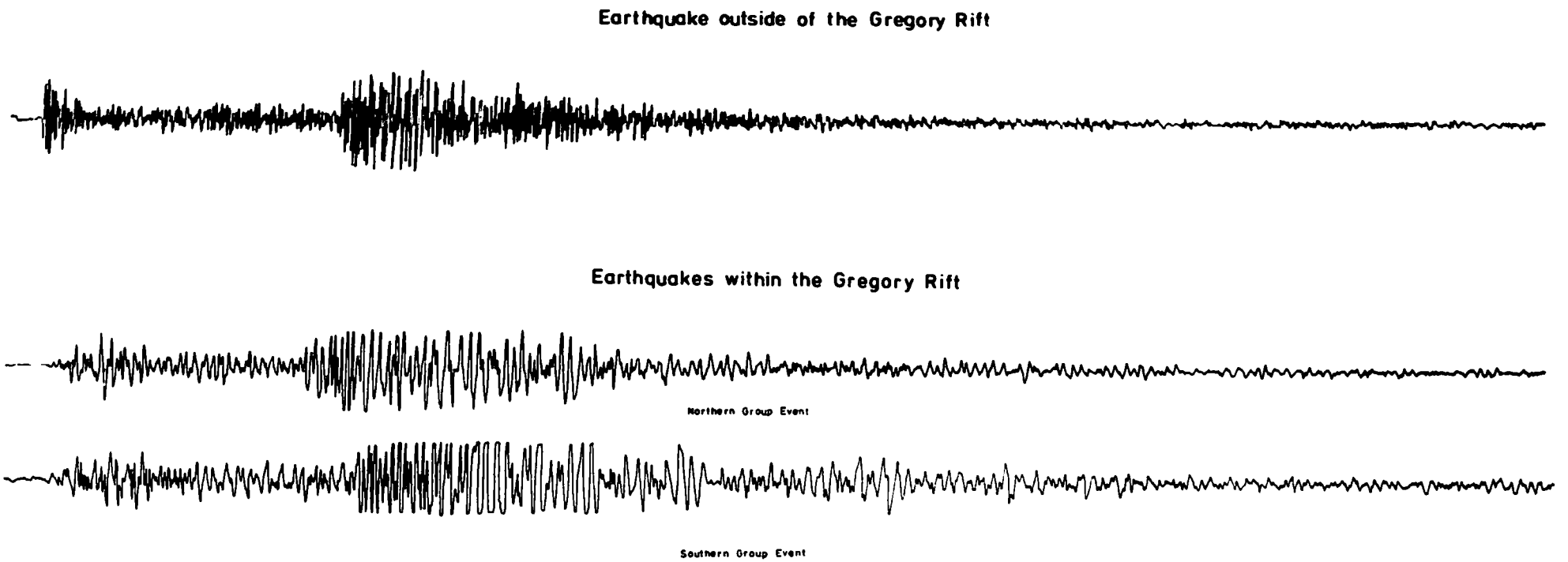
Earthquake outside of the Gregory Rift
Earthquakes within the Gregory Rift
Northern Group Event
Southern Group Event
10 Second

Fig 4:8

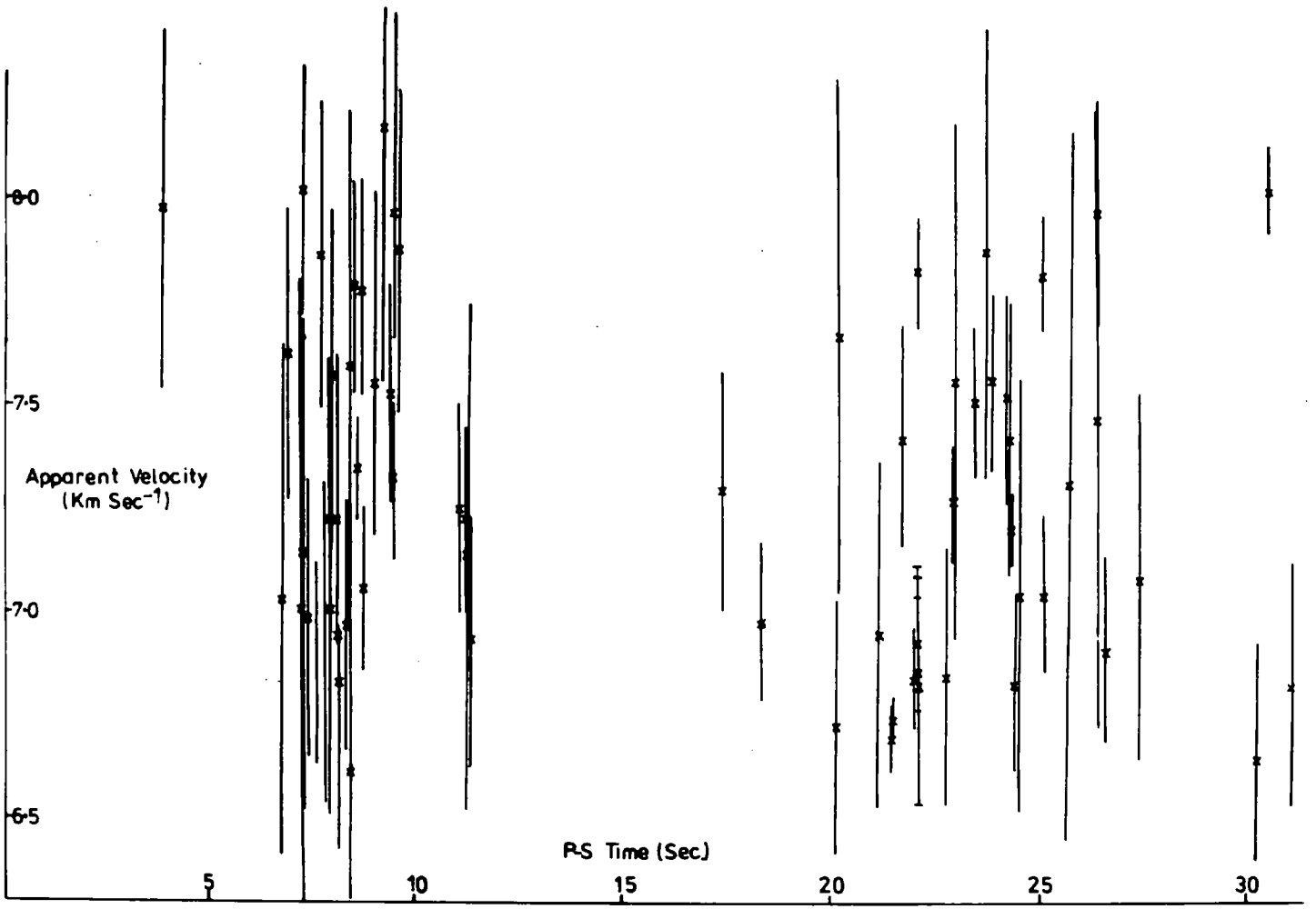

Apparent Velocity of Gregory Rift Events

Against P-S Time

Fig 4:9

gap and 150 Km from the southern gap. At these distances the observational cutoff magnitudes (m_b') are 2.2 and 2.3 respectively. The stress release, and hence the magnitude, associated with an earthquake depends upon the ability of the rock to store deformational energy. If the crust in the volcanic areas has been weakened by high heat flow and magma reservoirs, the capacity of the rock to store deformational energy may be reduced. This will result in an upper cutoff limit to the magnitudes of the earthquakes. However, it is unlikely that the volcanoes can affect the strength of the crust over the whole area of the seismic gaps. Magnitude (m_b') 3.5 earthquakes have been recorded from the central area. The southern flank of this area lies on the rim of the volcano, Menengai. If magnitude 3.5 earthquakes have been recorded from Menengai similar magnitude earthquakes may be associated with the other volcanoes.

The signal frequency of the events from the southern and northern cluster show an anomalous low signal frequency (Fig 4:8) approximately half that of events, from the same epicentral distance, outside of the rift. Events from the central area also show an anomalous signal frequency. These events have a signal frequency of approximately 5-10 Hz, in some cases nearly double the signal frequency of events, at the same epicentral distance, outside of the Gregory Rift. The anomalously low frequencies, of events from the southern and northern cluster, suggests anomalous attenuation of the signals from the rift.

Events from within the Gregory Rift show a wide variation, at Kaptagat, in the apparent velocity of the first arrival (Fig 4:9). First arrivals from the southern cluster have apparent velocities between 6.6 and 8.2 Km sec^{-1}. Events from the northern cluster show a similar range but cluster at 6.8 Km sec^{-1}. Within the

central area the first arrivals show two distinct trends in the apparent velocity. Six events have a mean first arrival velocity of 7.59 ± 0.16 Km sec^{-1} and five events a mean first arrival velocity of 6.77 ± 0.17 Km sec^{-1}. Within 95% confidence limits the two means are significantly different. These apparent velocities clearly demonstrate that the crustal structure within the Gregory Rift is different to that on the plateau. The anomalous crustal structure will be discussed in section 4:7.

4:5 The Western Rift.

A small number of events were located in the Western Rift and surrounding areas; this small number may reflect the large distance to the Western Rift. Of the earthquakes located in the Western Rift, the majority are distributed on the east side of the Ruwenzori Mountains (Fig 4:1). The events to the east of the Ruwenzori Mountains form two trends. One trend runs in a north-south direction between the Lakes Albert and Edward and the earthquakes are, in general, associated with the boundary fault of the Ruwenzori block. The second trend forms a diffuse band running from the Ruwenzori block eastward toward Lake Wamala. In this region, henceforth called the Wamala region, the basement is formed by rocks of the Toro system. These rocks have been intruded by granites. Although the Toro system in the Wamala region shows no sign of recent faulting there are a large number of small, normal and wrench faults in the Pre-Cambrian basement, (Johnson and Williams, 1961; Johnson, 1969). These faults may have been reactivated. Further north the northern end of Lake Albert is slightly active with five events recorded from this area. These events lie on the boundary fault or on the line of the boundary fault of the Albert graben.

The temporal distribution of events within the Ruwenzori area is plotted as a histogram (Fig 4:5). On average 2.5 earthquakes, from the Western Rift, per week were recorded at Kaptagat. This background level was disrupted by a burst of 24 earthquakes between April 17 and April 26, 1971. The earthquakes within this burst of activity have magnitudes (m_b') between 2.2 and 4.4 and are not associated with one large earthquake.

Data taken from the I.S.C. bulletins for the period 1964-1970, (Fig 4:2), show a similar distribution of epicentres near Lake Albert. The majority of the earthquakes occur in the region of the Semliki region. This concentration of events reflects the foreshock and aftershock sequence of the Congo earthquake of March 20, 1966. The shocks form a tight cluster indicating that the stress release is confined to a small area. To the east of the Ruwenzori block the Wamala region shows slight activity. Earthquakes within the Wamala region, generally, have magnitudes (m_b') less than 4. This agrees with magnitudes determined in this study. Further south down the Western Rift the earthquakes form a diffuse pattern of activity in the Tanganyika and Rukwa grabens. The shocks in this region lie on the NW trending boundary faults or on the line of these faults. This clearly demonstrates the continued activity of the faults in the Tanganyika graben.

4:6 The Siria Fault.

Twelve earthquakes occurred between April 2 and May 4, 1971, on the Siria fault. Outside of this period only two earthquakes with magnitudes greater than 2.7 were recorded by the Kaptagat array. The epicentres of the earthquakes are closely associated with the surface outcrop of the fault and the shocks have a near zero focal depth. The magnitude of the earthquakes range between

2.7 and 3.5. Within the period April 2 to May 4, the magnitudes are not normally distributed about a large magnitude shock. This suggests that the burst of activity from this fault is not formed by a large shock with a following aftershock sequence. Although the Siria fault is equidistant from both Kaptagat and Nairobi, only the larger shocks are recorded at the latter station. Those shocks recorded by Nairobi showed a reduction in amplitude. This suggests that the Gregory Rift contains material with a low Q value.

4:7 Crustal structure within the Gregory Rift.

The crustal model for the Gregory Rift must explain not only the apparent velocity of the first arrivals from the rift but also the quiet regions and the attenuation of the signals across the rift. The quiet regions within the Gregory Rift are approximately symmetrical to Kaptagat and resemble the shadow zones seen at teleseismic distances.

Fig (4:9) shows the apparent velocities measured in this study and those given by Long and Maguire (1976) for the first arrivals from the Gregory Rift. The data includes the velocity, across the array, of the signal of three of the eight shots let off in Lake Hannington by Griffith et al., (1971). Maguire measured the apparent velocity of the shots as approximately 8.0 Km sec^{-1} and these velocities have been confirmed in this study. The shots differ from the earthquakes in the Lake Hannington area in that the signal frequency is much lower, 2 Hz as opposed to 5-10 Hz, and is in agreement with the findings of Griffith et al., (1971).

As stated earlier the apparent velocities of events located within the central area define two groups. Those events with a mean first arrival apparent velocity of 6.77 Km sec^{-1} have, generally, either a P-S time less than 8 seconds, or are located

on the north and south edges of the central area or both. The events with a mean apparent velocity of 7.59 Km sec^{-1} for the first arrival generally have either a P-S time larger than 8 seconds, or are located toward the middle of the central area, or both. This suggests that the apparent velocity of the events is dictated by the location of the focus within the Gregory Rift.

The events from the Southern group show a wide variation in the apparent velocity and do not define average velocities as is the case of the central cluster. In contrast the events from the northern cluster have a mean apparent velocity of approximately 6.8 Km sec^{-1}. This suggests that the events from the northern cluster travel a fairly constant travel path. This wide range of velocities is suggestive of a structure which shows a velocity increase with increasing travel distance.

The symmetrical shadow zones suggests a structure which at a certain distance prevents the signal from reaching Kaptagat. In the case of the teleseismic shadow zones the travel paths, within the mantle, are deviated by a drop in the p-velocity of the 'rock'. If a similar cause is postulated for the shadow zones in the Gregory Rift there must be a velocity discontinuity within the Gregory Rift.

Lastly the model must explain the attenuation of the signals (see Chapter 6) that cross the rift and the delay times at Nairobi (see Chapter 5).

The simplest velocity-travel path distribution is given by the equation:

$$V_z = V_o + Kz \qquad (1)$$, where,

z is the depth of penetration of the ray,

K is the increase in velocity per unit increase in depth,

V_o is the surface velocity,

V_z is the velocity at depth z.

For a surface to surface travel path the travel time for a signal passing through this type of structure is given by,

$$T = \frac{2}{K} \cosh^{-1} \frac{V_m}{V_o} \qquad \text{(ii) where}$$

T is the travel time and V_m is the maximum p-wave velocity travelled by the signal. If the origin of the shock is not at the surface the travel time is given by,

$$T = \frac{1}{K} \cosh^{-1} \frac{K^2(\Delta^2 + h^2)}{2V_o(V_o + Kh)} + 1 \qquad \text{(iii) where}$$

Δ is the epicentral distance and h is the focal depth of the shock.

For the earthquakes located within the central group the lowest measured velocity for the first arrival was 6.6 Km sec^{-1}. If this earthquake has a focal depth of 0 Km, equation (ii) can be used to estimate limiting values of K providing V_o is known. Events from the western edge of the rift valley have a first arrival apparent velocity, at Kaptagat, of 6.2 Km sec^{-1}. These events may have briefly sampled the topmost part of the anomalous crust within the rift. Taking V_o as 6.2 Km sec^{-1} in equation (ii) gives $K = 0.05$ sec^{-1}. If the p-wave velocity of the topmost part of the crust is 5.9 Km sec^{-1}, K is 0.07 sec^{-1}. The minimum apparent velocity of events from the northern group of events is 6.8 Km sec^{-1}. This and the travel time can be used to put a lower limit of 0.03 sec^{-1} on K. The high apparent velocity of the shots and the earthquakes from the Lake Hannington area suggests that the simple model, for the structure within the Gregory Rift, may be locally perturbed. If a linear increase of velocity with depth is still applicable within the Hannington area, K will be 0.09 sec^{-1} for $V_o = 6.2$ Km sec^{-1}.

Into this model must be included the velocity discontinuity which will be represented by a velocity drop, VD, at a depth z. Events from the central cluster have a maximum P-S time of

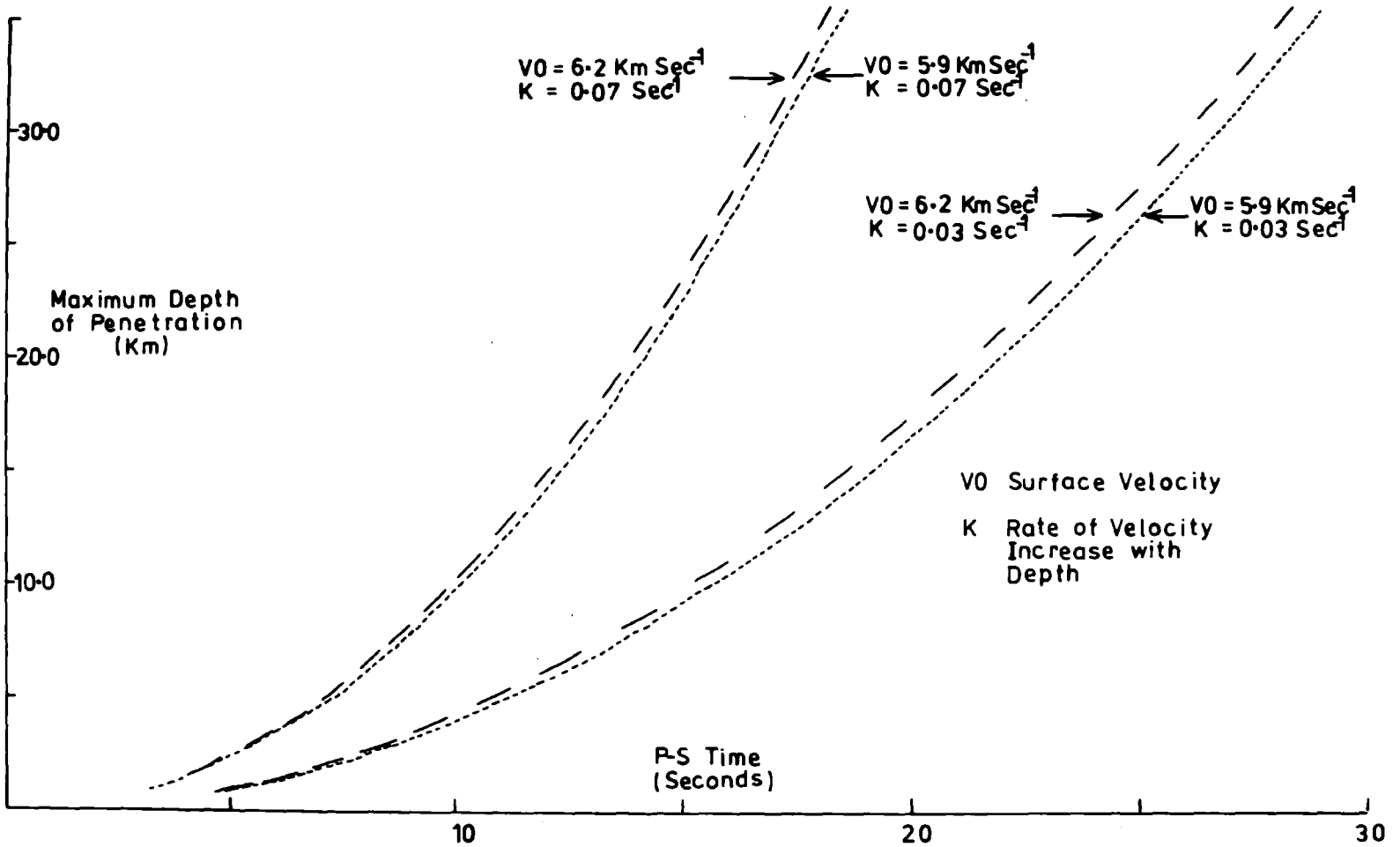

P-S Time for a Surface to Surface Travel Path Through a Velocity Increase with Depth

Fig 4·10

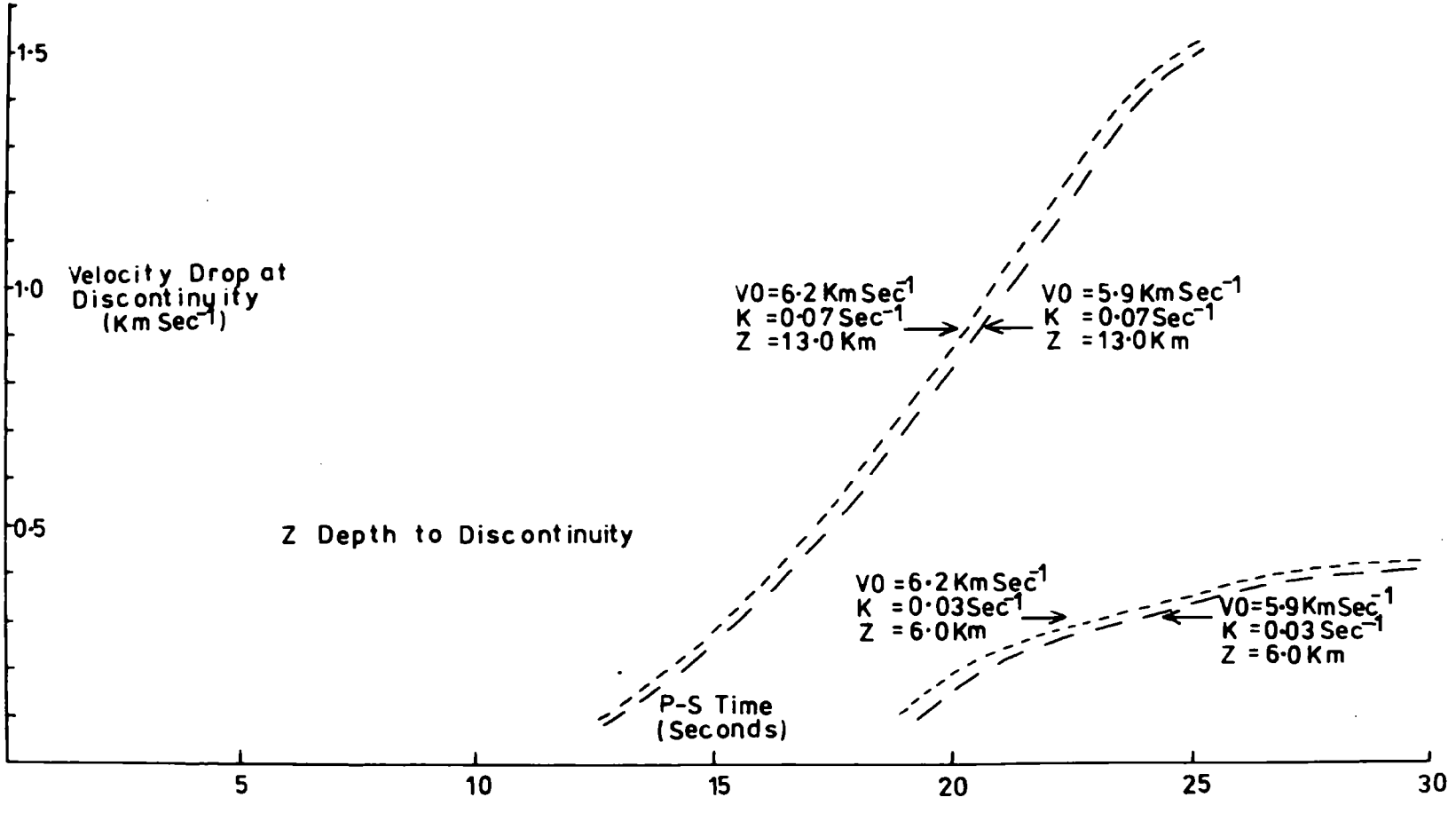

P-S Time for Surface to Surface Travel Path Through a Velocity Increase with Depth Interrupted by a Velocity Drop

Fig 4·11

11.5 seconds. This P-S time applies to events from the southern edge of the cluster. Events from the northern edge have a maximum P-S time of 8.4 seconds. The P-S time of 11.5 seconds can be used to give a maximum travelttime for events within the central zone. If K and V_o are known the maximum travel time can be used to put a lower limit on the depth to the discontinuity. Fig (4:10) is a plot of the P-S time for an event with zero focal depth against the depth to the discontinuity. This figure shows four trends each of which corresponds to a different combination of V_o and K. From the graphs the following combinations of K and V_o give the indicated maximum depth, z, to the discontinuity:

V_o	K	z
5.9 Km sec^{-1}	0.03 sec^{-1}	5.3 Km
6.2 " "	0.03 "	5.5 "
5.9 " "	0.07 "	12.5 "
6.2 " "	0.07 "	13.0 "

These figures show that the surface velocity, V_o has little affect upon the depth z. If z is smaller than the maximum value the maximum travel time, for an event with a zero focal depth, will be less than 15.54 seconds (P-S time 11.5 seconds). The reappearance of the signal from below the discontinuity is governed by the value of K below the discontinuity and the decrease, VD, in velocity at the discontinuity. Below the discontinuity K was assumed to have the same value as above the discontinuity. Fig (4:11) is a plot of the P-S time against VD for an event with a surface focus. The bulk of events, from the north and south clusters, start to appear when the P-S time exceeds 20 seconds. If this value of P-S time represents an event with a zero focal depth the graphs in Fig (4:11) can be used to give a minimum value of VD.

V_o	K	z	VD
5.9 Km sec^{-1}	0.03 sec^{-1}	6.0 Km	0.15 Km sec^{-1}
6.2 " "	0.03 "	6.0 "	0.18 " "
5.9 " "	0.07 "	13.0 "	0.83 " "
6.2 " "	0.07 "	13.0 "	0.86 " "

Fig (4:12) shows the P-S time plotted against VD for an event located on the suggested discontinuity. Events located in this position should provide an estimate for the maximum value of VD. The graphs in Fig (4:12) and the P-S time of 20 seconds give the following estimates of VD:

V_o	K	D	VD
5.9 Km sec^{-1}	0.03 sec^{-1}	6.0 Km	0.32 Km sec^{-1}
6.2 " "	0.03 "	6.0 "	0.34 " "
5.9 " "	0.07 "	13.0 "	1.46 " "
6.2 " "	0.07 "	13.0 "	1.50 " "

If the events lie below the suggested discontinuity to generate the shadow zone the limits on the above model will be modified. It is possible to stop the signal, from events from below the suggested discontinuity, reaching Kaptagat if the upward path is reflected at the discontinuity. This suggests that VD is comparitively large.

The travel path for events from within the Gregory Rift is not completely confined to the anomalous crust. At some point the signal leaves the anomalous crust and enters normal shield. For the present model any signal leaving the anomalous structure, at a level above the suggested discontinuity, encounters material with a lower p-velocity. Hence the ray will be bent towards the normal to the boundary. This means that the apparent velocity across the array is not the true maximum velocity seen by the signal. The

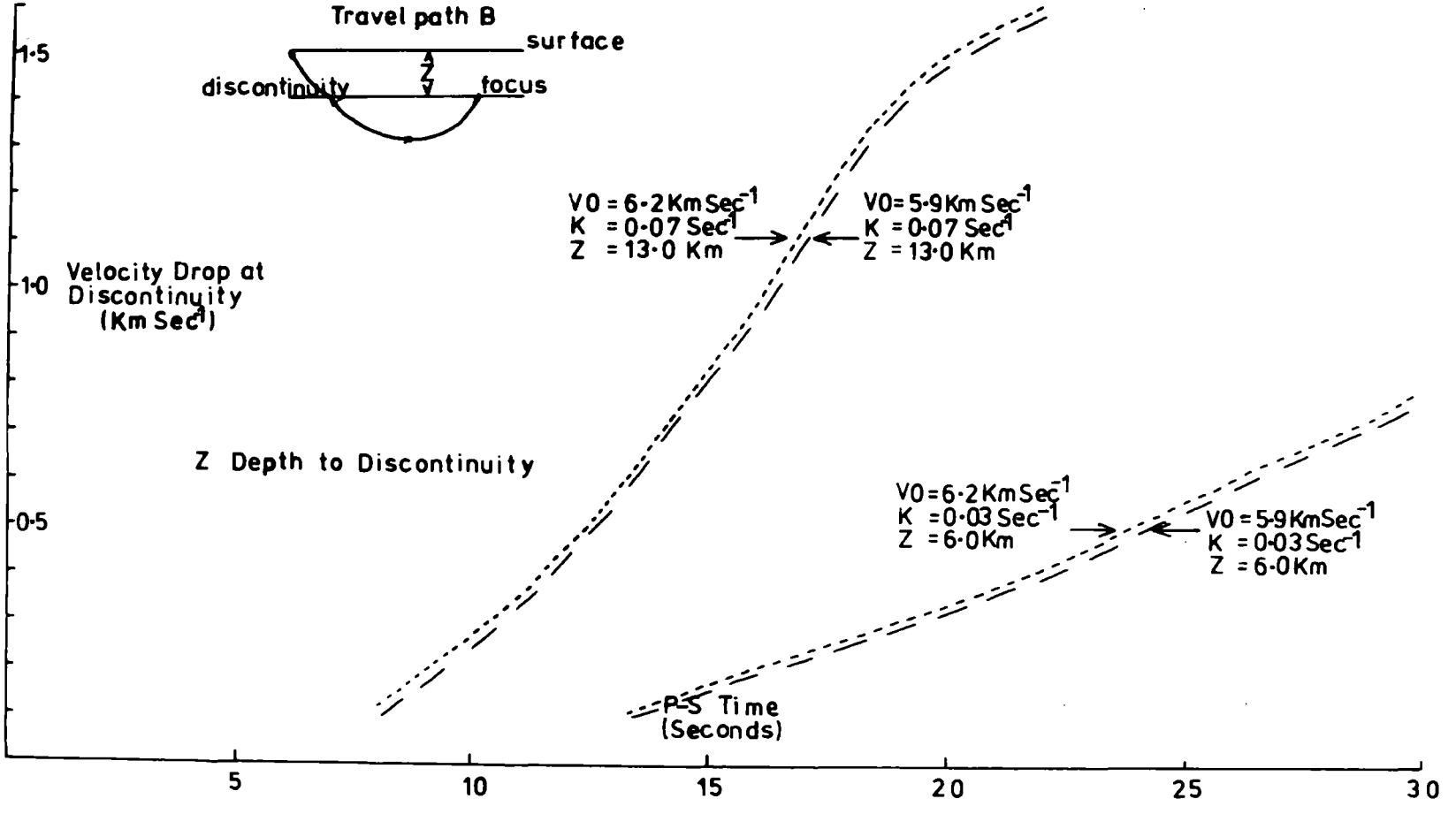

P-S Time for Travel Path B Through a Velocity Increase with Depth Interrupted by a Velocity Drop

Fig 4:12

signal will have travelled faster than the apparent velocity. The suggested deviation of the travel path implies that the epicentres, located by the array, are incorrect and that the epicentres are probably nearer to the axis of the rift than suggested. Below the discontinuity the velocity contrast between the anomalous and normal crust depends upon the model for the anomalous crust. For the upper limiting values on the general model the signal passes from a low velocity to a high velocity. This means that the signal emerging from the rift is bent away from the normal to the boundary. Also the signal is deviated in a vertical direction. This direction will, probably, increase the angle of ascent of the signal and hence the apparent velocity is greater than the maximum velocity seen by the signal. For the lower limiting values on the general model the signal, generally, passes from a higher to a lower velocity. Comparison of the travel paths for the southern and northern group events suggests that the travel path for the latter events is predominantly within the rift. This may explain why the p-velocities for the onset of the signal are fairly constant for these events. The travel path for events from the southern cluster apparently leave the rift much earlier than the events from the northern cluster. This, and the spread in epicentres, may explain the variation in apparent velocity of events from the southern cluster.

4.8 Discussion.

Within East Africa the seismicity shows two distinct trends. A north-south trend exists in both the main rift areas. This trend is in accord with the general east-west stress (Bangher and Sykes, 1969; Sykes, 1967) which is opening the Western Rift and the

Gregory Rift. At right angles to this trend is an east-west trend displayed in the Kavirondo graben, the Wamala region and on the Siria fault. If the Nubia and Somalia plates are rotating about an axis in the area of the Rukwa graben as suggested by McKenzie et al., (1970), east-west fractures should develop. These fractures will form in zones of crustal weakness such as the Siria fault, or where a local stress perturbs the regional stress pattern, for example, the Kavirondo graben and the Wamala region. In the former region the perturbation is due to the uplift of the Kenya Dome and in the latter region to the uplift of the Ruwenzori block.

The pattern of seismic activity within the Gregory Rift is the combined effect of the suggested anomalous crust and possible shallow focal depths. In section 4:7 the parameters, which define the general model, have been limited using events from within the Gregory Rift. Compressional velocities recorded from the central group of events are consistent with velocities recorded from the oceanic ridges. Across the ridges the velocity varies between 6.4 and 8.2 Km sec^{-1} (Oxburgh and Turcotte, 1968), with velocities of 7.3 - 7.7 Km sec^{-1} predominant at the centre of the ridge (Talwani et al., 1965). The latter authors found velocities of 8.2 and 8.1 Km sec^{-1}, 3 Km below the crest of the ridge, which they chose to ignore. Under the oceanic ridges the high velocity material probably corresponds to anomalous mantle material. In the Gregory Rift the velocity increase in the upper layer probably corresponds to the intrusion of volcanic material.

The anomalous crust within the Gregory Rift probably passes to normal crust to the north and south of the Kenya Dome, in accord with the findings of Rykounov et al., (1972). If the anomalous crust is to pass in to normal crust the value of K must decrease

away from the dome and the discontinuity becomes progressively deeper. This required increase in the depth of the discontinuity is probably coincident with the increased depth to the top surface of the mantle anomaly as outlined by the various gravity surveys.

Events from the northern and southern clusters, within the Gregory Rift, show a comparitively low signal frequency. If the source function for the faults in this region is similar to that for faults in other areas, the predominant low frequencies suggest selective attenuation of the high frequencies. For a partial melt Q is inversely proportional to frequency at frequencies less than the critical frequency and proportional to frequency at frequencies greater than the critical frequency (Walsh, 1969). The critical frequency for pure dilation is dependent upon the viscosity and bulk modulus of the fluid inclusions. For pure shear the critical frequency is dependent upon the shape of the fluid inclusions, the bulk and rigidity modulus of the solid and the viscosity of the fluid (Walsh, 1969). If the high frequencies are selectively attenuated by a partial melt, the viscosity of the fluid must be quite low. Alternatively if the rock is solid, Q may be independent of frequency. The attenuation of the high frequencies is then due to a decrease in Q, and the number of cycles of the signal within the anomalous material.

The absence of s-waves in the coda of earthquakes from the north and south clusters suggests that the rock on part of the travel path may be in a partially molten state. If the apparently selective attenuation is due to a partial melt, the discontinuity may represent a change from a solid state to a partial melt in magma chambers. Local perturbation of the surface of the discontinuity may be caused by magma cupolas below the main volcanoes.

The events in the Gregory Rift shown in Fig (4:1) are probably mislocated. If the model outlined in section 4:7 is applicable to the structure in the Gregory Rift, the events in the central cluster in the rift probably lie nearer to the axis of the rift than depicted in Fig (4:1). This mislocation is due to deviation of the ray path as it crosses from the anomalous to the normal crust.

CHAPTER 5

TRAVEL TIMES ACROSS THE GREGORY RIFT

5:1 Introduction.

Evidence from gravity surveys and refraction lines shot within the Eastern Rift zone suggests that the crustal structure within the rift zone is different to the structure outside of the rift zone. This difference in crustal structure may become manifest in the onset time at Nairobi of the first arrival from earthquakes to the west of the Gregory Rift. Using the hypocentral location and origin time as determined by the Kaptagat array the expected onset time of the first arrival at Nairobi can be determined if a particular model is assumed for the structure of the crust. The model in Fig (3:4) was used to represent the crust both inside and outside of the Gregory Rift and the expected onset times at Nairobi derived from this model will be termed the calculated onset times at Nairobi. As the model of the normal crust is unrepresentative of the crust within the Gregory Rift, the calculated onset times at Nairobi should be different to the measured onset times at Nairobi. This difference between the calculated and measured onset times at Nairobi will be termed the delay times at Nairobi.

Fig (5:1) shows the average delay times at Nairobi for the five main regions. The individual delays are given in Table (5:1). The 95% confidence limits on these average values are as follows: Ruwenzori, 0.24, Kavirondo Rift, 1.07, Siria Fault, 3.16, Southern Group, 1.58, Northern Group, 1.20. Events from the Ruwenzori and Kavirondo areas should have P_n as the first arrival at Nairobi. In the latter region the first arrival at Kaptagat

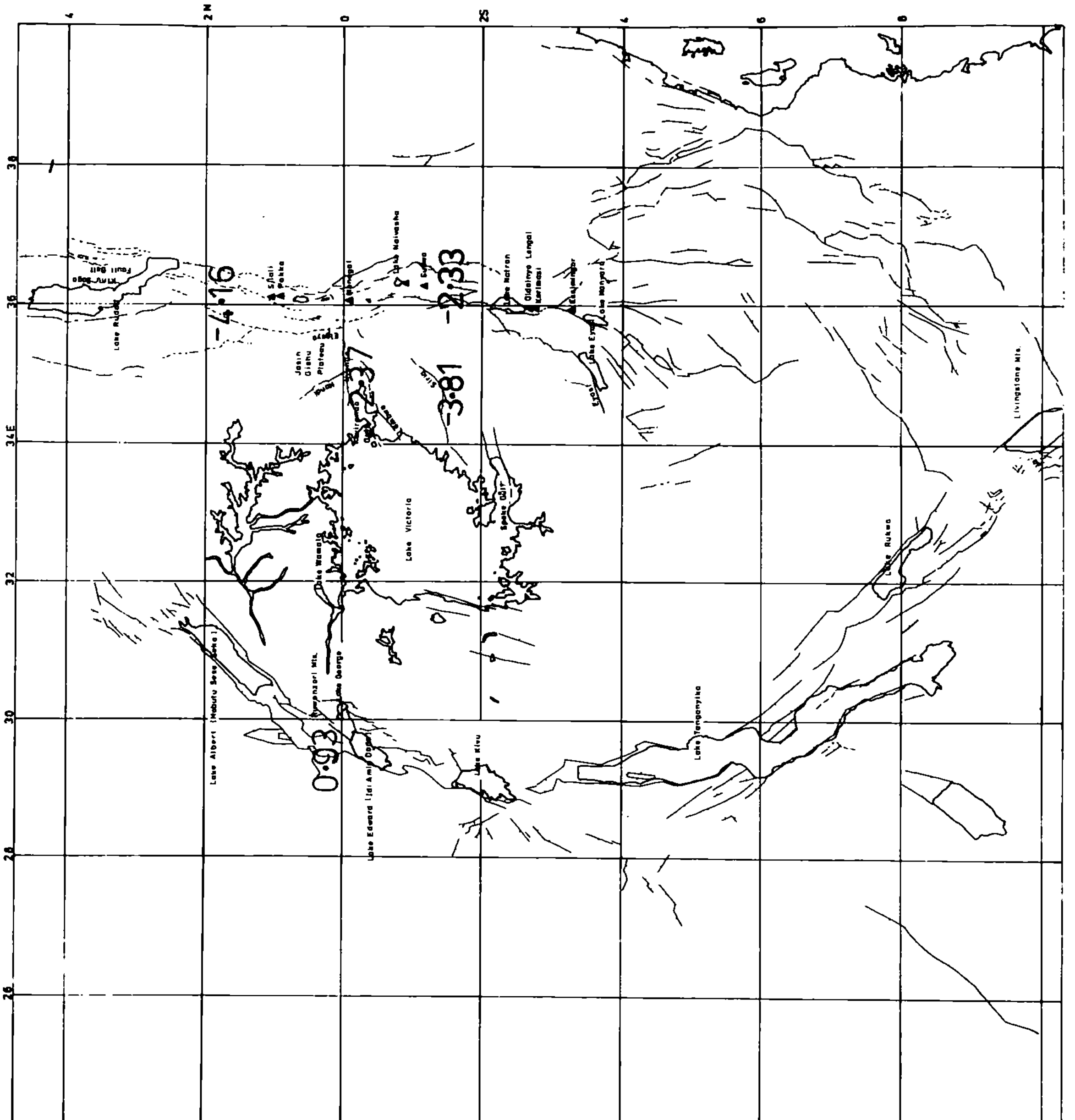

Regional Delays at Nairobi

Fig 5:1

TABLE 5:1

TRAVEL TIME ANOMALIES

Event No.	Epicentral Distance to Kaptagat	Epicentral Distance to Nairobi	Delay used in calculations
56098	216.2	211.64	-4.35
56149	215.2	212.8	-5.02
54940	212.8	209.25	-2.56
62104	50.8	220.31	2.01
62107	49.3	223.31	2.82
62108	47.1	220.08	1.97
62110	45.1	226.63	2.93
62114	46.7	224.69	0.83
62117	62.8	220.57	4.21
62135	67.1	219.91	4.70
60280	70.0	220.60	0.44
5953	210.4	66.58	-2.29
5956	219.0	53.72	-1.20
5954	242.2	33.52	-4.03
60282	215.2	54.44	-2.09
6277	285.4	45.60	-0.97
5955	208.5	66.90	-1.81
6163	347.6	142.70	1.08
6164	341.2	132.00	0.77
54902	192.1	384.81	-3.89
54906	194.0	380.80	-4.72
54901	194.0	376.70	-3.88
6263	349.2	390.91	2.09

Event No.	Epicentral Distance to Kaptagat	Epicentral Distance to Nairobi	Delay used in calculations
55987	599.5	781.70	0.58
55979	617.0	797.00	0.62
58169	639.6	793.20	0.57
58184	748.4	799.70	0.29
6219	776.6	809.70	1.22
6243	764.7	601.60	1.20
6268	928.5	942.40	0.87
6271	731.1	559.80	0.78
6278	496.2	666.40	1.07

is either P^* or P_g whilst events from the former region have P_n as the first arrival at Kaptagat. Events from the Siria fault have P^* as the first arrival at Kaptagat and from their position should have P^* as the first arrival at Nairobi. Those events from the southern group should have P_g as the first arrival at Nairobi and either P^* OR P_n at Kaptagat. These arrivals are based on the assumption that the travel path is confined to normal shield crust.

Before the delay times at Nairobi can be interpreted as the effect of an anomalous crustal structure within the Gregory Rift several alternative explanations must be eliminated. The alternative explanations are:

(i) That the hypocentral location as determined from data from the Kaptagat array is incorrect.

(ii) That the origin time of the event as determined from the onset time of the event at Kaptagat is incorrect.

(iii) The delay times are due to measurement errors on the onset times at Nairobi.

(iv) That the model used to represent the structure of the normal crust is not an adequate representation of the true crustal structure.

v) That the anomalous crustal structure is not associated with the Gregory Rift but a feature of the crust external to the rift.

The five alternative explanation listed above will be discussed in section (5:2).

:2 Discussion of possible errors.

If the crustal model for the structure outside of the rift is incorrect the calculated travel times to Nairobi will also be

incorrect and may give the measured delay times at Nairobi. Consider two cases when a) both stations see a P_n phase as the first arrival and b) when one station sees a P_n phase as the first arrival and the other a P_g phase as the first arrival.

The hypocentral location of the shock is fixed using data from the Kaptagat array. Therefore any error, in the crustal model, will give an error in the epicentral distance and the focal depth. Consider case a). If the p-wave velocity of the third layer of the model for the normal crust is in error the moho travel time to Nairobi will be incorrect. For an incorrect moho velocity the error in the calculated travel time to Nairobi is given by,

$$e = \Delta\left[\frac{1}{8.05} - \frac{1}{x}\right]$$ where,

x is the true velocity of the rock at moho level, and Δ is the epicentral distance to Nairobi calculated from the Kaptagat locations. If x differs from 8.05 Km sec^{-1} by 0.1 Km sec^{-1} the error in the calculated travel time to Nairobi is 0.15 seconds per 100 Km epicentral distance. To determine the effect of an error in the velocity of the first and second layers of the structural model the hypothetical event was assumed to have a focal depth of five Km. For this hypothetical event an error of 0.1 Km sec^{-1} on the velocity of the second crustal layer gives a maximum error of 0.13 seconds in the calculated travel time to Nairobi. A similar error on the velocity of the first layer of the crustal model will result in an error of 0.03 seconds on the calculated travel time to Nairobi. For the events from the Ruwenzori area, a true moho velocity of 7.95 Km sec^{-1}, as compared to the model velocity of 8.05 Km sec^{-1}, will explain the delay at Nairobi for events from the Ruwenzori. Events from the Kavirondo Rift have P_n as the first arrival at Nairobi and a delay at

Nairobi of 2.37 seconds. To explain this delay as an error on the moho velocity of the model for the normal crust requires the true moho velocity to be unacceptably small.

An erroneous assumption of the moho velocity will also mean that Δ is incorrect. For a true moho velocity of 7.95 Km sec^{-1} the maximum error in Δ is 5 Km for a P-S time of 50 seconds at Kaptagat. This error in Δ acts to reduce e, the error if Δ is assumed to be correct. The delay is probably not due to error on the velocity of the second crustal layer of the crustal model. If the delay is due to error in the velocity of the second crustal layer the true velocity would have to be 5.8 Km sec^{-1} to explain the delay at Nairobi.

Case b) can be split into two subsections:

(i) Kaptagat sees a P_g phase as the first arrival and Nairobi a P_n phase as the first arrival.

(ii) Kaptagat sees a P_n phase as the first arrival and Nairobi a P_g phase as the first arrival.

In both (i) and (ii) the P_g phase was usually restricted to the first layer of the crust. The following error analysis, in compliance with the above finding, assumes that the P_g phase is restricted to the first crustal layer. In case b) (i) an error in the p-velocity of the third layer of crustal model will not result in an error in the epicentral distance or focal depth. However, the travel time to Nairobi will be affected by the use of an incorrect moho velocity. For an error of 0.1 Km sec^{-1} in the moho velocity of the crustal model, a maximum error of 0.15 seconds per 100 Km epicentral distance will be introduced into the calculated travel time to Nairobi. An error of 0.1 Km sec^{-1} in the velocity of the second layer of the model will give a maximum error of 0.13 seconds on the calculated travel time to Nairobi. The focal depth of an event can be determined using the apparent

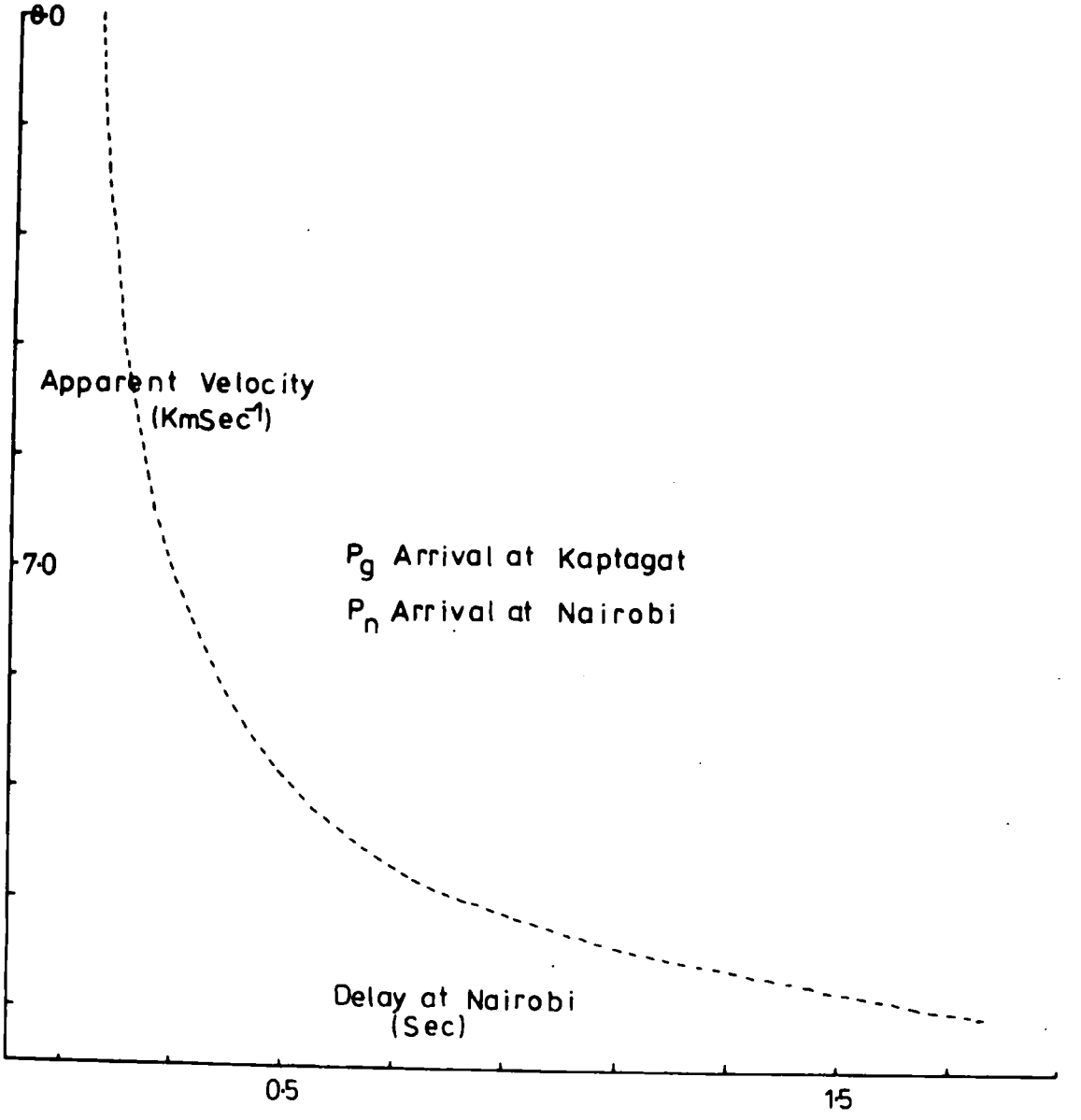

Delay at Nairobi due
to an Error of 0·1 Km Sec^{-1}
on the First Crustal Layer.

Fig 5:2

velocity of the P_g arrival across the Kaptagat array. An error in the p-velocity of the first layer of the model will introduce an error into the focal depth and the epicentral distance to Kaptagat. Therefore the effect of using an incorrect p-velocity for the first crustal layer is expressed as a function of the apparent velocity of the P_g phase at Kaptagat (Fig 5:2). The graph in Fig (5:2) assumes an error of 0.1 Km sec^{-1} in the p-velocity of the first crustal layer. From this graph it can be seen that the maximum error corresponds to low apparent velocities. For events with an apparent velocity at Kaptagat of 6.4 Km sec^{-1} the error, due to the use of an incorrect p-velocity for the intermediate layer, is approximately one-fifth of the delay at Nairobi.

In case b) (ii) an error of 0.1 Km sec^{-1} in the velocity of the third layer of the crustal model will give a maximum error in the calculated travel time to Nairobi of -0.01 seconds per 100 Km epicentral distance. An error of 0.1 Km sec^{-1} in the p-velocities of the first and second layers of the crustal model give a maximum error of 0.05 and 0.06 seconds respectively, in the calculated travel time to Nairobi.

The effect, on the calculated travel time to Nairobi, of varying the width of the crustal layers is small compared to the effect of varying the p-velocities within the crustal model.

Case b) (i) applies to events located within the Kavirondo Rift. These events have an average delay at Nairobi of 2.37 seconds and are approximately 200 Km from Nairobi. From the above figures it can be seen that this delay is probably not due to error on the crustal model. Case b) (ii) applies to events from the southern group. These events have a large negative delay at

Nairobi which cannot be explained by errors on the crustal model.

The accuracy of the hypocentral location of an event is subject to the errors on the estimate of the epicentral distance, focal depth and the azimuth, from Kaptagat, of the event. It may be possible that the delay time at Nairobi is due to incorrect location of the epicentre.

When the first arrival is a P_n phase at both Nairobi and Kaptagat the travel path between the focus and Kaptagat is similar in form to that between the focus and Nairobi. For this type of travel path the time taken for the signal to travel down to and up from the moho is the same for both the path to Kaptagat and the path to Nairobi. Hence the only difference between the travel path to Nairobi and the travel path to Kaptagat is the time spent by the signal travelling as a moho head wave. Any variation in the focal depth will be reflected by a change in the epicentral distance. As the epicentral distance to Nairobi was derived from the Kaptagat estimate of the hypocentral location an error in the epicentral distance to Kaptagat will result in an error in the epicentral distance to Nairobi. This error in the epicentral distance to Nairobi will be a function of the azimuth of the event from Kaptagat. If the two stations and the epicentre of the event are in line the error on the epicentral distance to Kaptagat is the same as that on the epicentral distance to Nairobi. When this condition exists the error on the epicentral distance will not give rise to an error on the travel time to Nairobi.

Fig (5:3) shows the delay time at Nairobi due to an error in the epicentral distance to Nairobi. This diagram has been constructed assuming a focal depth of 0 Km and can be used to give

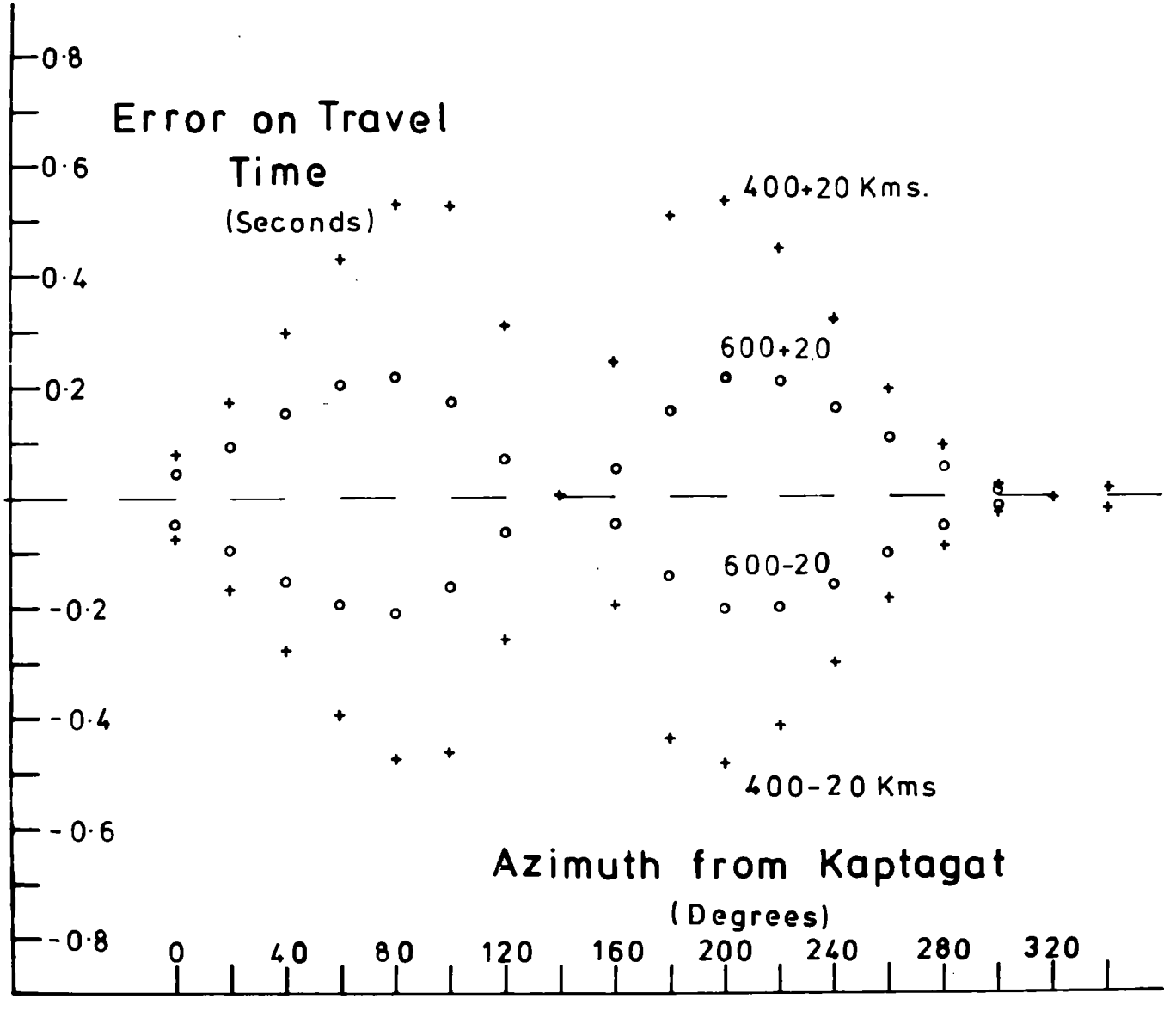

Fig 5:3 Error on Travel Time to Nairobi Due to an Incorrect Epicentral Distance

the error due to an incorrect focal depth. This is possible because of the direct link between an error in the focal depth and an error in the epicentral distance. At an epicentral distance of 600 Km the maximum error on the travel time to Nairobi is approximately 0.2 seconds. Most of the events that have two P_n travel paths and show a delay time at Nairobi have an azimuth from Kaptagat of between 280 degrees and 320 degrees. At this azimuth the error on the travel time is much less than 0.2 seconds. In the events described previously as type b) (i) and b) (ii), one station sees a first arrival which has been confined to the crust. The second station sees a moho head wave as the first arrival. This means that an error in the focal depth will introduce an error into the calculated travel time to Nairobi via the change in the epicentral distance and the time taken by the signal to travel the crustal path. For crustal arrivals at Kaptagat the signal travels a P* or a P_g path within the first layer of the crust. Crustal arrivals at Nairobi are probably P_g signals. This assumes that the signal travels through normal crust. Fig (5:4) shows the error on the calculated travel time to Nairobi due to an incorrect focal depth. The error on the focal depth was assumed to be 5.0 Km and the signal was assumed to have travelled a P* path to Kaptagat. From this graph it can be seen that for the above conditions the maximum error on the calculated travel time to Nairobi is +1.8 seconds. For the group of events which have a P_g phase as the first arrival at Kaptagat the maximum error is +0.8. Similarly for events with P_g as the first arrival at Nairobi the maximum error on the travel time to Nairobi is -1.8 seconds. The error is a function of the azimuth, from Kaptagat, for the event. In all three cases the

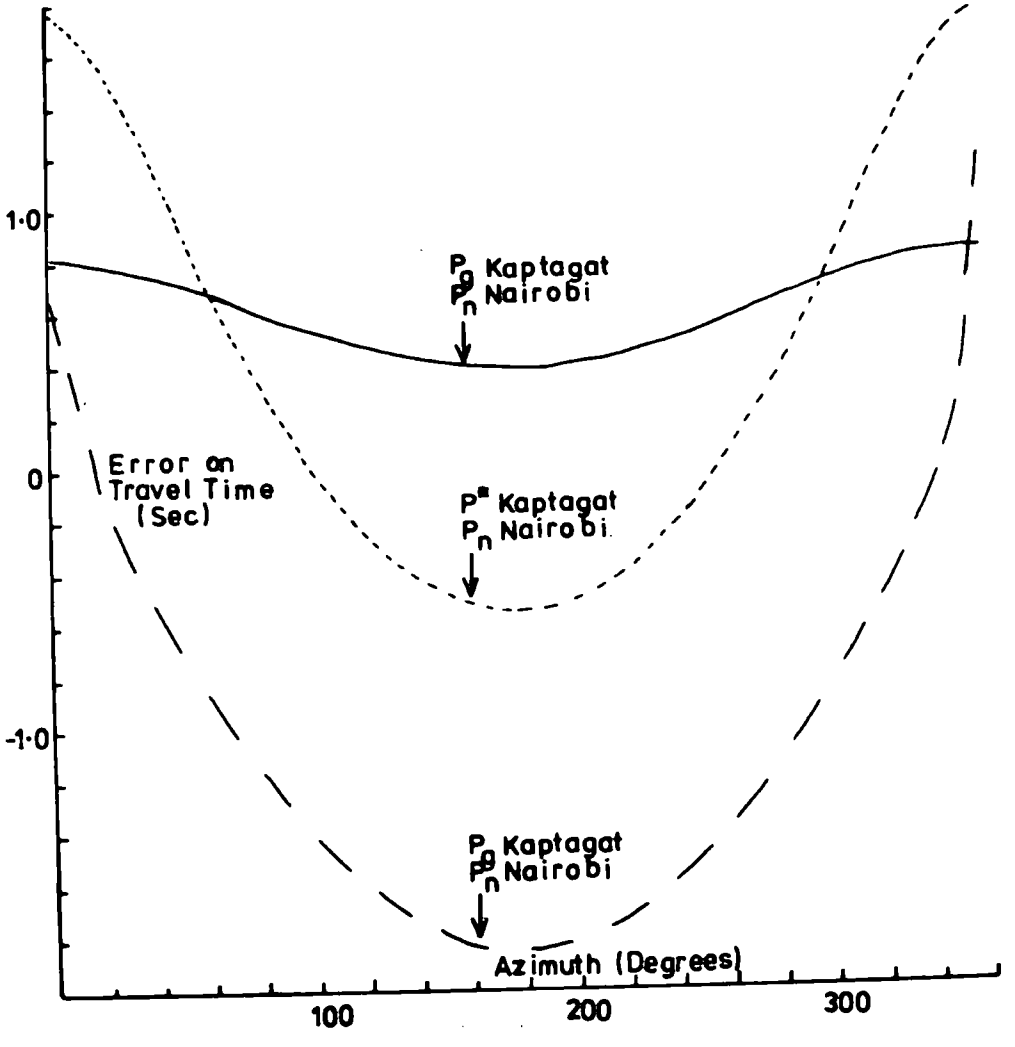

Error on Travel Time to Nairobi due to an Error of 5Km on the Focal Depth

Fig 5:4

error is less than the observed delay time at Nairobi. If the focal depth is in error by more than 5 Km the corresponding error on the travel time to Nairobi will be increased. The Kavirondo Rift events have an azimuth from Kaptagat of approximately 200 degrees. At this azimuth the delay time at Nairobi, due to an error of 5 Km on the focal depth, is -0.4 seconds for P^* arrivals and +0.4 seconds for P_g arrivals at Kaptagat. These values are considerably less than the average delay time at Nairobi of events from this region, and the focal depth would have to be in error by over 25 Km to generate this delay. An error of 25 Km in the focal depth is unlikely as the apparent velocities of the first arrival was used to give the focal depth. Events from the southern group have an azimuth from Kaptagat of approximately 150 degrees. At this azimuth the delay time at Nairobi, due to an error of 5 Km on the focal depth, is -1.8 seconds on P_g arrivals at Nairobi. The average delay at Nairobi of events from this region is approximately twice this value. Therefore the focal depths would have to be in error by approximately 10 Km to explain the delay. If this is the case, and assuming normal crust, the first arrivals at Kaptagat would be P_n. The first arrivals are not P_n and therefore the focal depth is probably not in error by as much as 10 Km.

An error in the azimuth, measured from Kaptagat, of the epicentre will produce an artificial delay at Nairobi. In Fig (5:5) the change in azimuth and epicentral distance required to compensate for the delay time at Nairobi is shown for events in the Uganda sector of the Western Rift. This graph shows that the epicentral distance has to be consistently smaller than estimated and the azimuth swung toward the north.

The accuracy of the onset times of the signal at Nairobi

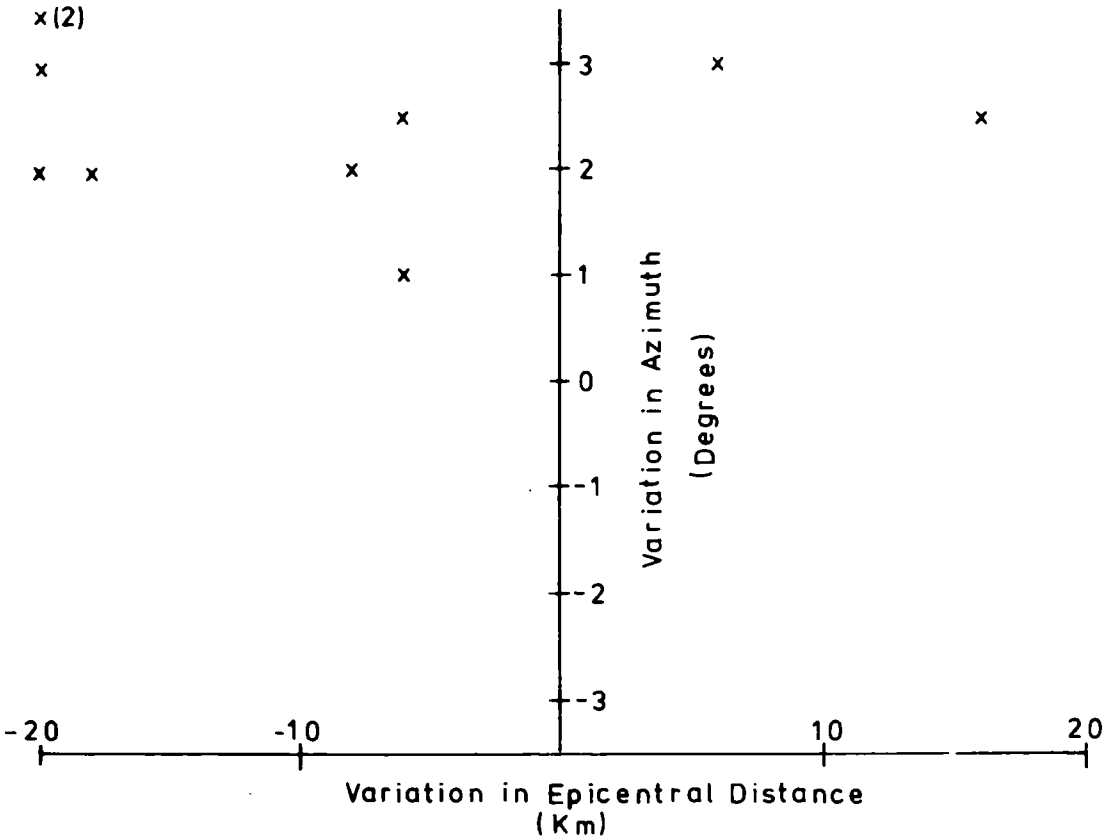

Variation in Azimuth and Epicentral Distance Required to give the Measured Delay on Moho Arrivals at Nairobi.

Fig 5:5

and Kaptagat is critical to the measurement of the delay times. An error in measured onset time at Kaptagat will be reflected in an error in the calculated arrival time at Nairobi. This error in the calculated arrival time at Nairobi will give a delay time at Nairobi. Similarly an error in the measured onset time at Nairobi will give a delay time at Nairobi. The accuracy of the onset time at each station depends upon the identification of the signal onset and the reading error involved in the measurement of the onset time. At Kaptagat the onset time was read to an accuracy of ±0.04 seconds and at Nairobi the onset time was read to an accuracy of ±0.25 seconds. The character of the onset signal varied from a sharp break, in which case it was easy to identify the onset, to a low amplitude sinusoid. When the onset was difficult to identify the maximum of the first deflection, at both stations, was chosen as the onset. This approximation produces a slight error as the signal frequency at Kaptagat is usually different from the signal at Nairobi. Comparison of the signal periods, at both stations, shows that the approximation to the onset of the signal can result in a delay time at Nairobi of ±0.1 seconds. These errors are an order of magnitude samller than the delay times at Nairobi.

5:3 Discussion of the delay times.

Fig (5:1) shows the average calculated delay time at Nairobi for events located within five regions. From this plot it can be seen that the largest delays are associated with events within the Gregory Rift. The events from the Uganda area will be treated as one unit because they are all located in approximately the same position. At the epicentral distances involved, a slight variation in the position of the epicentre hardly affects the

travel path through the rift zone.

Because of the position of the Siria fault earthquakes, ie they are equidistant from both stations, the calculated onset time at Nairobi was taken as the actual onset time at Kaptagat.

The anomalous onset times at Nairobi of earthquakes with crustal and moho travel paths indicates the possibility of an anomalous body extending throughout the width of the crust. This anomalous body is probably coincident with the intrusion which gives rise to the positive gravity anomaly along the axis of the rift. The delay times at Nairobi, on crustal arrivals from the Siria fault, indicates that the anomalous material must have a p-wave velocity greater than that of the normal crust, or the upward travel path is smaller than that of the normal path. If the anomaly is 20 Km wide, as is suggested by the gravity models, the retardation of the signal to produce the delay time at Nairobi on moho arrivals cannot take place at moho level. For an anomaly 20 Km wide the velocity would have to be 6.1 Km sec^{-1} to produce the delay time, on moho arrivals, at Nairobi. Clearly this velocity is too low to be acceptable. In the following analysis the delay time at Nairobi on moho arrivals is assumed to be due to a delay imposed on the signal as it ascends to the surface. This supposition is reinforced by the distance, 15 Km, between Nairobi and the Gregory Rift. Assuming that normal crust exists throughout this distance it is impossible for a moho head wave to emerge, at moho level, from the anomaly and ascend to Nairobi.

The moho arrivals have been split into two groups:

(1) Events from the Kavirondo graben with an average delay time at Nairobi of 2.37 ±1.07 seconds .

(ii) Events from the Ruwenzori area with an average delay time at Nairobi of 0.93 $\pm$0.24 seconds.

Two models have been tested to try and explain the delays. One model assumes a two layer crustal structure similar to that given by Griffith (1972), Griffith et al. (1971), and the other model assumes a structure similar to that used to explain the seismicity.

5:4 The two layer model.

In this model a layer of material with p-velocity of 6.38 Km sec^{-1} was assumed to overlie an anomalous layer with a higher p-velocity. If the intrusion is in the form of a wedge the model can be defined using;

VA the p-velocity of the second layer,

w the width of the anomaly,

α the angle of dip on the faces of the anomaly and

D the distance of the eastern edge of the anomaly from Nairobi.

The travel path through the anomaly will also depend upon β, the angle between the normal to the flanks of the anomaly and the approaching ray.

For moho signals the travel path was assumed to enter the anomaly immediately after leaving the moho. This gives the largest possible delay for each variation of the model and provides upper limits for the parameters. The travel path of the moho signal was traced through the model for the crustal anomaly and the associated abnormal travel time calculated. As the horizontal distance travelled by the ascending signal through the anomaly is different to that for a normal arrival a correction was applied to the abnormal travel time. A number of variations of the model were tried and an acceptable model is found when the calculated delay

time is the same as the delay time at Nairobi.

Two values of VA were considered; a lower limit of 7.1 Km sec^{-1} was based on the model of Long et al., (1972), and an upper limit of 7.5 Km sec^{-1} on the model of Griffith et al., (1971). For these two values of VA, α and w were allowed to vary until the calculated delays were 0.93 and 2.37 seconds. Initially the computations were conducted assuming that the anomaly was aligned due north-south. Under this assumption it was impossible to generate the delay time at Nairobi. Therefore the orientation, β, of the axis of the anomaly was allowed to vary.

Fig (5:6) shows the range of β and w which give the delay times of 0.93 and 2.37 seconds for the indicated values of and VA. These graphs clearly show that the axis of the anomaly has to be rotated west of north to give the required delay time at Nairobi. If VA is 7.1 Km sec^{-1} the anomaly has to be rotated by between 25 and 30 degrees to give a delay of 0.93 seconds on the moho arrivals from Uganda. The corresponding rotation required to give the delay of 2.37 seconds on Kavirondo Rift events is between 7 and 10 degrees. For VA = 7.5 Km sec^{-1} the axis of the anomaly has to be rotated by between 20 and 25 degrees for a delay of 0.93 seconds. When a velocity of (VA =) 7.5 Km sec^{-1} is employed to explain the delay of 2.37 seconds the range in the variables β and w become very restricted. The graphs in Fig (5:6) show the range of the variables β and w for three values of α. These lines show that the greatest acceptable range in β and w occurs when α = 5 degrees. Also as α increases the value of β decreases.

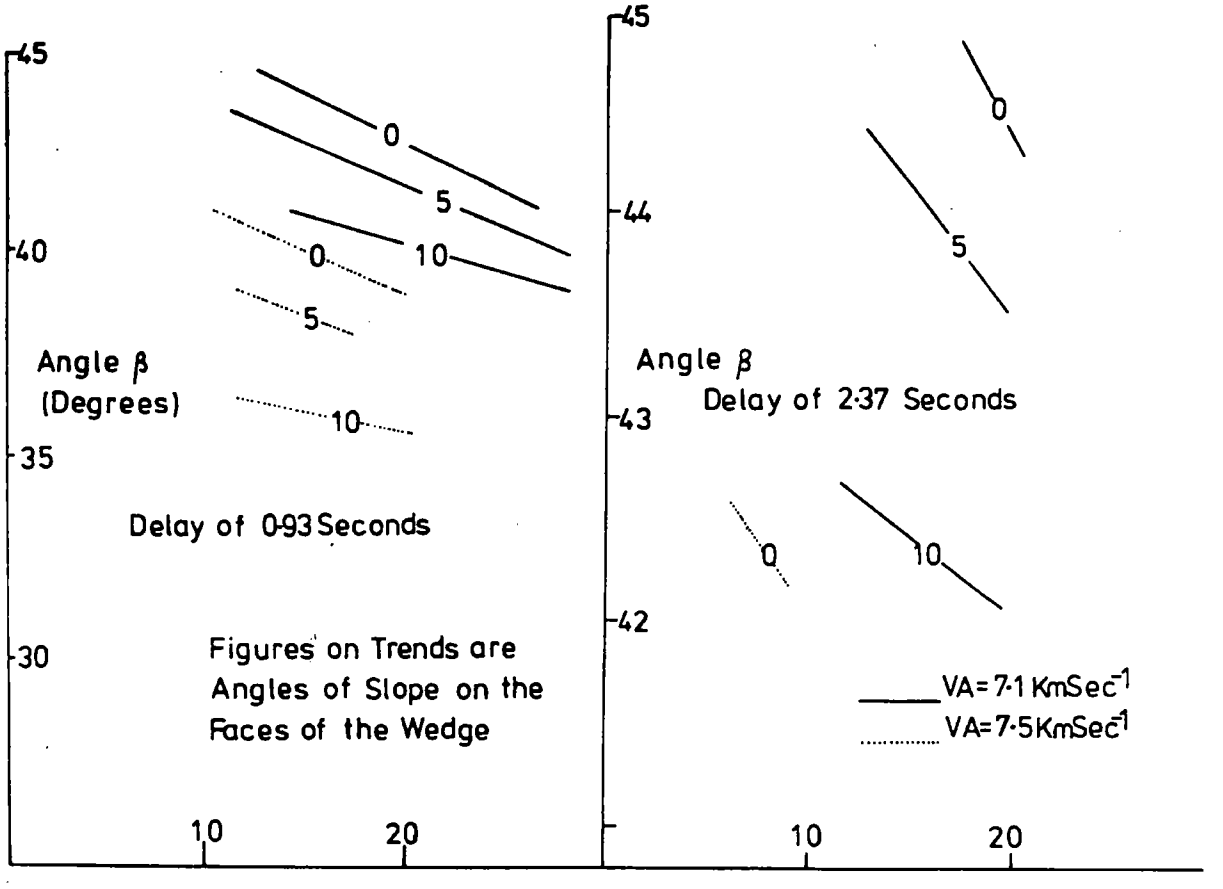

Delay on Moho Arrivals Assuming
a Two Layer Model for the
Gregory Rift

Fig 5·6

If the signal enters the anomaly immediately after leaving the moho it emerges from the anomaly into the 6.5 Km sec^{-1} layer of the normal crust. A moho signal which enters the anomaly at a higher level may emerge from the anomaly into the 5.9 Km sec^{-1} layer of the normal crust. To estimate the delay time for this type of travel path a signal was traced through the anomaly and allowed to leave the anomaly at the base of the 5.9 Km sec^{-1} layer.

Fig (5:7) shows the range in β and w required to give a delay of 0.93 and 2.37 seconds for VA = 7.1 and 7.5 Km sec^{-1}. From these graphs it can be seen that for a delay of 0.93 seconds, VA has little affect on the range of β and w. For a delay of 2.37 seconds the velocity VA becomes extremely important. A value of VA = 7.5 Km sec^{-1} will only give a delay of 2.37 seconds for this travel path if the angle, α, is 0 degrees and the wedge is between 10 and 5 Km wide. The angle by which the axis of the anomaly has to be rotated to give a delay of 0.93 seconds lies between 18 and 20 degrees for both values of VA.

The negative delay time at Nairobi of events within the Magadi area can be interpreted in two ways. Either the events are closer to Nairobi than the Kaptagat locations suggest or, the signal travels faster to Nairobi than assumed. The negative delay at Nairobi varies between -2.81 and -0.79 seconds which can be interpreted as the events being between 16.6 and 4.8 Km closer to Nairobi than expected. These distances assume a velocity of 5.9 Km sec^{-1} for the travel path to Nairobi. On the present model for the Gregory Rift the signal will see a drop in the p-velocity when leaving the Gregory Rift. Hence the true travel path will be bent away from Nairobi and not toward the station as required. To arrive at Nairobi approximately 2 seconds

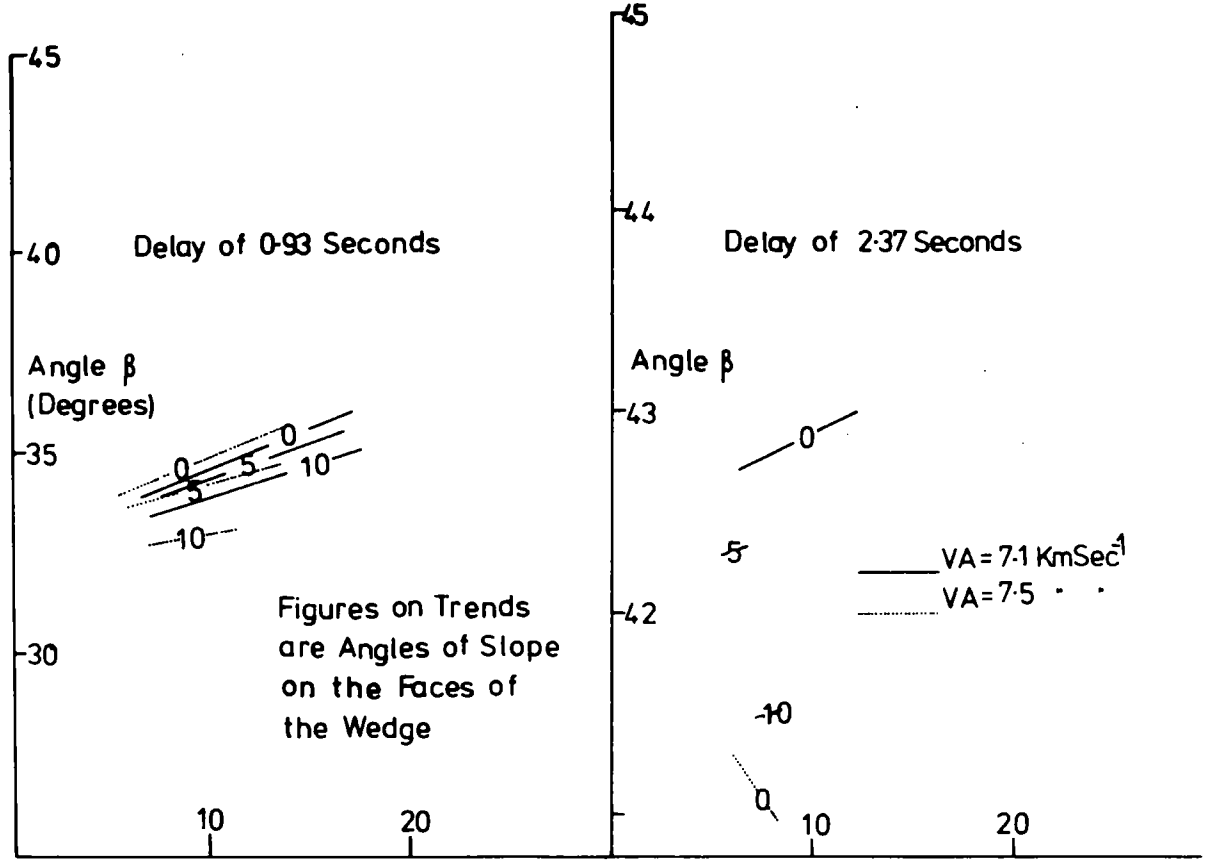

Delay on Moho Arrivals Assuming a Two Layer Model for the Gregory Rift.

Fig 5·7

early the signal must have travelled at a velocity of 7.03 Km sec^{-1} along the whole of the travel path. If the events are misplaced, as indicated above, the p-velocity along the travel path will have to be larger than 7.03 Km sec^{-1} to compensate for the increased path distance.

Events from the Siria fault arrive at Nairobi between -2.5 and 5.0 seconds earlier than expected. At Kaptagat these events have first arrival apparent velocities which suggest a P* travel path. If this is the case the travel path from the Siria fault to Nairobi should also be P*. The travel path from the Siria fault to Nairobi crosses the Gregory Rift where it is approximately 50 Km wide. Within this 50 Km wide zone the signal must be speeded up to give the negative delay time at Nairobi. The horizontal projection of the travel path to Nairobi intersects the flanks of the rift at an angle of approximately 90 degrees. Hence the horizontal projection of the travel path will not be deviated by an appreciable amount. The signal was assumed to pass through the rift undeviated in a horizontal direction. For a negative delay at Nairobi of 3.5 seconds the signal must travel within the Gregory Rift at a velocity of 11.9 Km sec^{-1}. Clearly this velocity is unacceptable. If the calculated epicentres are slightly misplaced to the west of the true epicentre the net result will be a negative delay at Nairobi. The maximum error on the azimuth, from Kaptagat, of the events on the Siria fault is ±3 degrees (±7.65 Km). If the Siria events are actually 7.65 Km to the east of the Kaptagat location the delay time at Nairobi will be reduced by 1.17 seconds. The delay time at Nairobi, of the Siria events, then gives 9.32 Km sec^{-1} for the material within the Gregory Rift. The normal P* takes a horizontal distance

of 38.9 Km to ascend to the station. If the signal from the Siria fault emerges from the anomaly as a P^* it cannot ascend to Nairobi in the distance between the rift and the station. Either the anomaly is thinner than the width of the rift or the signal starts to ascend to the surface before reaching the anomaly. Consider the latter case. If the ascending signal encounters material with a higher apparent velocity the travel path will be steepened. This implies that the western edge of the anomaly is within 39 Km of Nairobi and if the anomaly is contained within the rift it must be less than 24 Km wide. Fig (5:8) shows the variation in the calculated delay at Nairobi with change in the velocity of the intrusion. The width of the anomaly has been constrained so that the signal reaches Nairobi and the anomaly lies within the rift. If the velocity of the anomalous material is lower than the normal crustal velocity, the ray path will be deflected toward the horizontal and the resultant travel time will be larger than the normal travel time. The graph in Fig (5:8) shows that the maximum negative delay will be -0.72 seconds for a p-velocity of the anomaly of 7.5 Km sec^{-1}. A reduction in the p-velocity of the anomalous material results in a corresponding decrease in the calculated delay at Nairobi.

5:5 Delays from the model used to explain the seismicity.

The delay times at Nairobi were again treated as two groups, moho arrivals and crustal arrivals at Nairobi. The model used was the same as that employed to explain the seismicity pattern within the Gregory Rift, and was restricted to the rift zone. As before the model is defined by four variables, K, z, V_o, VD, which were varied within the limits imposed in the last chapter. Consider the moho arrivals from Uganda.

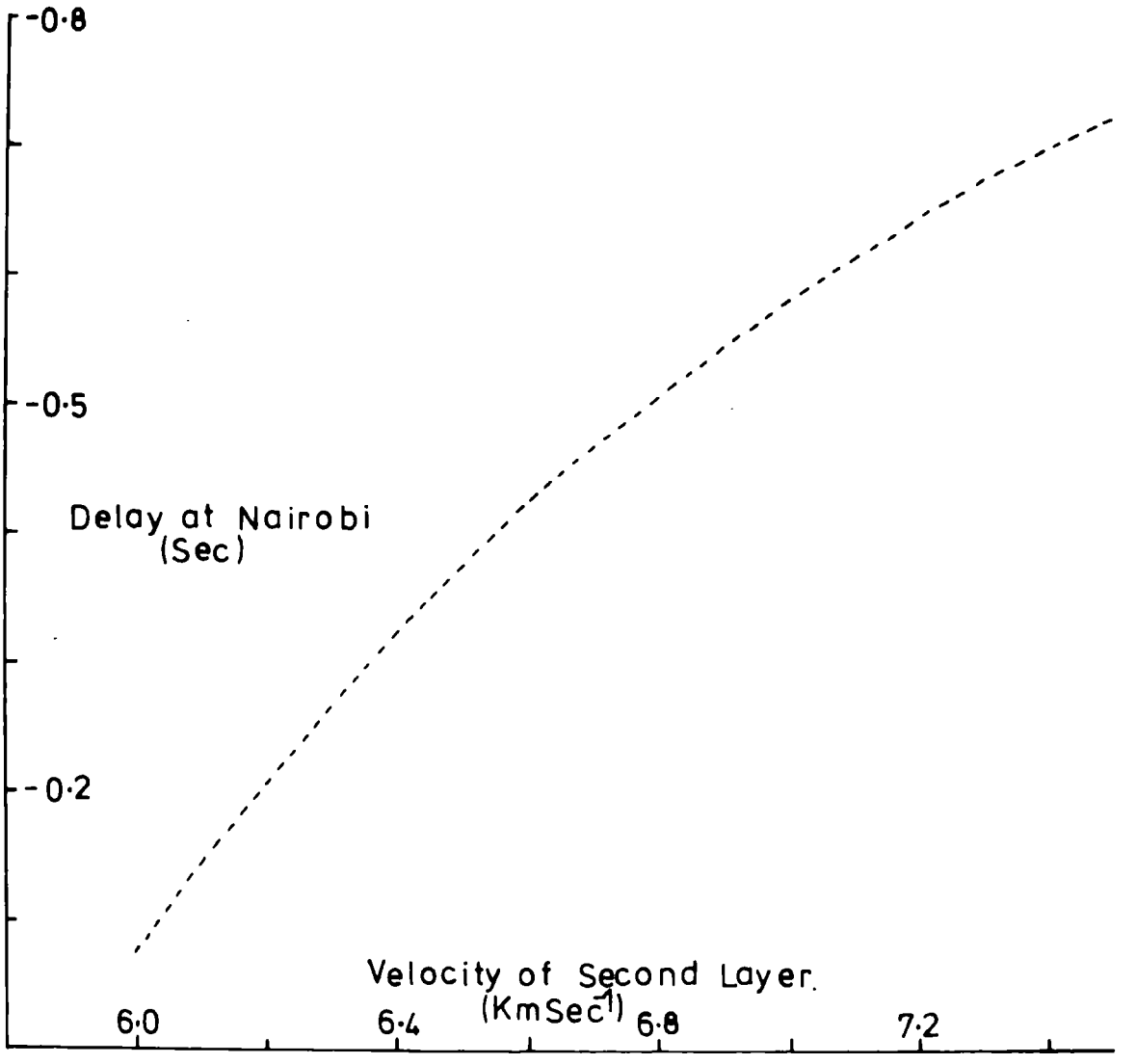

Delay at Nairobi on
Events from the Siria
Fault Assuming Two Layer
Crust in the Gregory Rift.

Fig 5:8

Fig (5:9) shows the variation of the calculated delay with z and VD for a constant value of K and V_o. The graphs in Fig (5:9) show lines of equal delay and assume that the angle between the normal to the flanks of the anomaly and the incident ray path is 15 degrees. For a constant value of K an increase in V_o decreases the range of z and VD which will give a delay of 0.9 seconds, at Nairobi, on moho arrivals from Uganda. If K is increased the theoretical delay times at Nairobi on these moho arrivals is increased and the range of acceptable values of z and VD is also increased. Although the graphs do not define the values of the parameters of the model they do confirm that the model will generate the delays.

The moho arrivals from the Kavirondo graben will intersect a north-south anomaly at an angle of 35 degrees to the normal to the flanks. Fig (5:10) shows the variation in the delay time at Nairobi for arrivals from the Kavirondo graben. The graphs in this figure show that the condition that the delay is 2.37 seconds is not satisfied until K is at least 0.06 sec^{-1}. This value can be used as a lower limit on the value of K. With increasing K the calculated delay, for the same value of VD and z, increases and, as before, the acceptable range of VD and z increases. Similarly an increase in VD increases the calculated delay at Nairobi.

The events from the Lake Magadi area, which show a negative delay time at Nairobi, have a first arrival apparent velocity, at Kaptagat, of approximately 6.9 -6.5 Km sec^{-1}. These events emerge from the Gregory Rift zone at least 60 Km from Kaptagat. This and the apparent velocity suggests that the depth at which the ray emerges from the anomaly is between 18 and 22 Km. It was shown in the last section that to give the measured negative

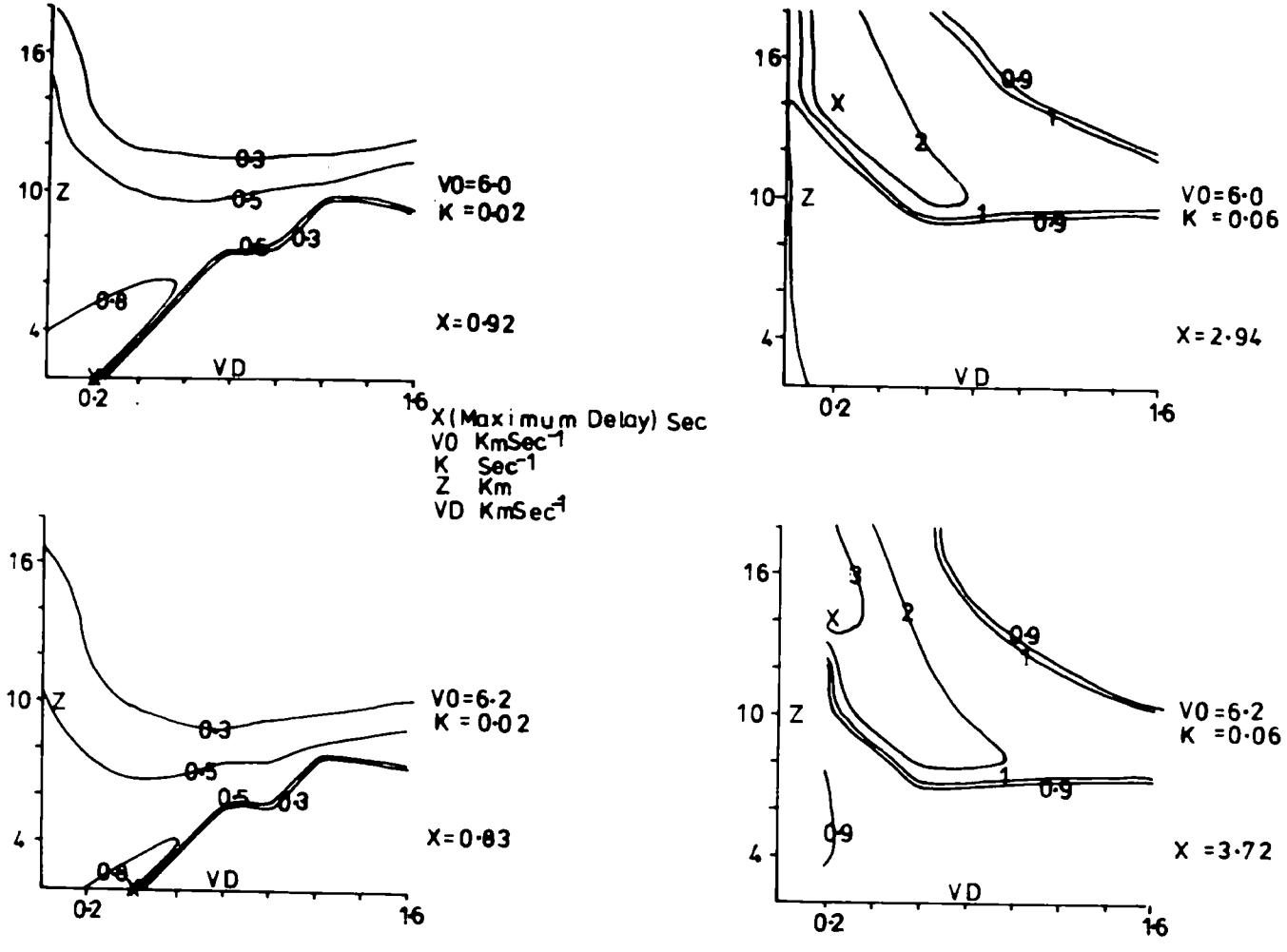

X (Maximum Delay) Sec
V0 KmSec^{-1}
K Sec^{-1}
Z Km
VD KmSec^{-1}

Delay at Nairobi as a Function of the Velocity Drop, VD, at a Discontinuity at Depth Z for Constant Velocity Increase, K, and Initial Velocity V0.

Fig 5·9

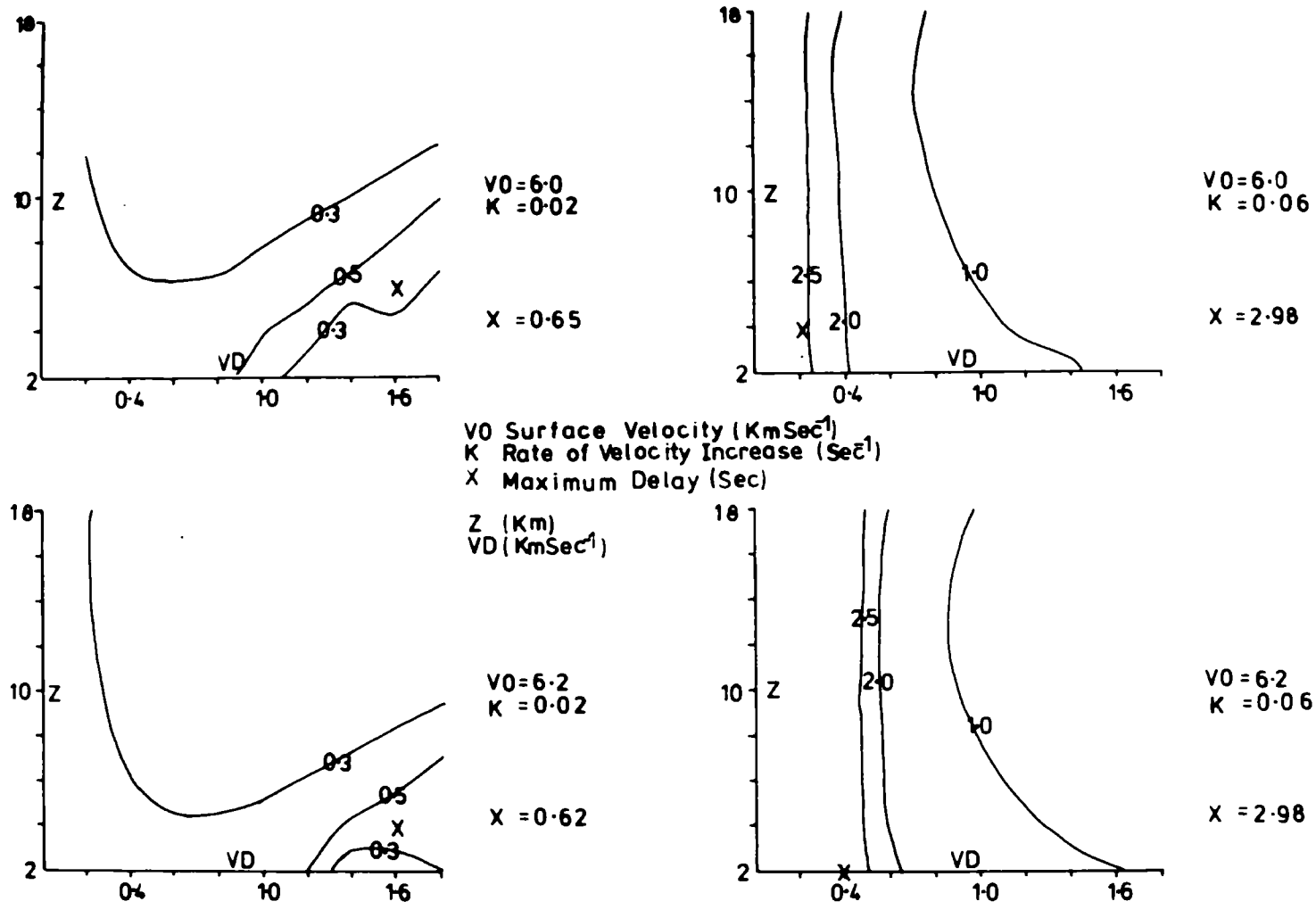

Variation in Delay at Nairobi with Velocity Drop (VD) and Depth (Z) to the Discontinuity.

Fig 5:10

delay at Nairobi the signal had to travel at over 7.0 Km sec^{-1} or the event was nearer to Nairobi than the current locations suggest. The only way to swing the locations toward Nairobi is for the signal to emerge from the Gregory Rift into a higher velocity material. As the signal must be travelling approximately horizontally when it emerges from the anomaly it is possible to calculate the horizontal distance travelled within the anomaly. Secondly there must be a negative velocity contrast between the anomaly and the normal crust to swing the travel path toward Nairobi. Fig (5:11) shows the swing, toward Nairobi, in the position of the epicentre as the parameters of the model are varied. Fig (5:11) shows that as V_o increases the velocity drop (VD) must also increase if the epicentres of the events are to be swung towards Nairobi. Similarly an increase in K also requires an increase in VD. Assuming a surface velocity of 5.9 Km sec^{-1} the size of the swing is sufficient to give the required delays at Nairobi providing the velocity drop at the boundary is sufficiently large. The delays on the first arrivals at Nairobi of the events from the southern group do not restrict the limits on the model. However they do not preclude the model.

Events from the Siria Fault probably enter the Gregory Rift as P^* signals. Fig (5:12) shows the calculated negative delay time at Nairobi assuming that the eastern edge of the anomaly is 15 Km distance from Nairobi. The width of the anomaly has been allowed to vary. Each graph in Fig (5:12) is drawn for a constant V_o, K and z with VD allowed to vary. Events from the Siria Fault should provide some indication as to the upper limit on VD because the overall upward travel time must be lower than the normal upward travel time. Large values of VD will increase the upward travel time through the anomaly. The maximum possible delay on

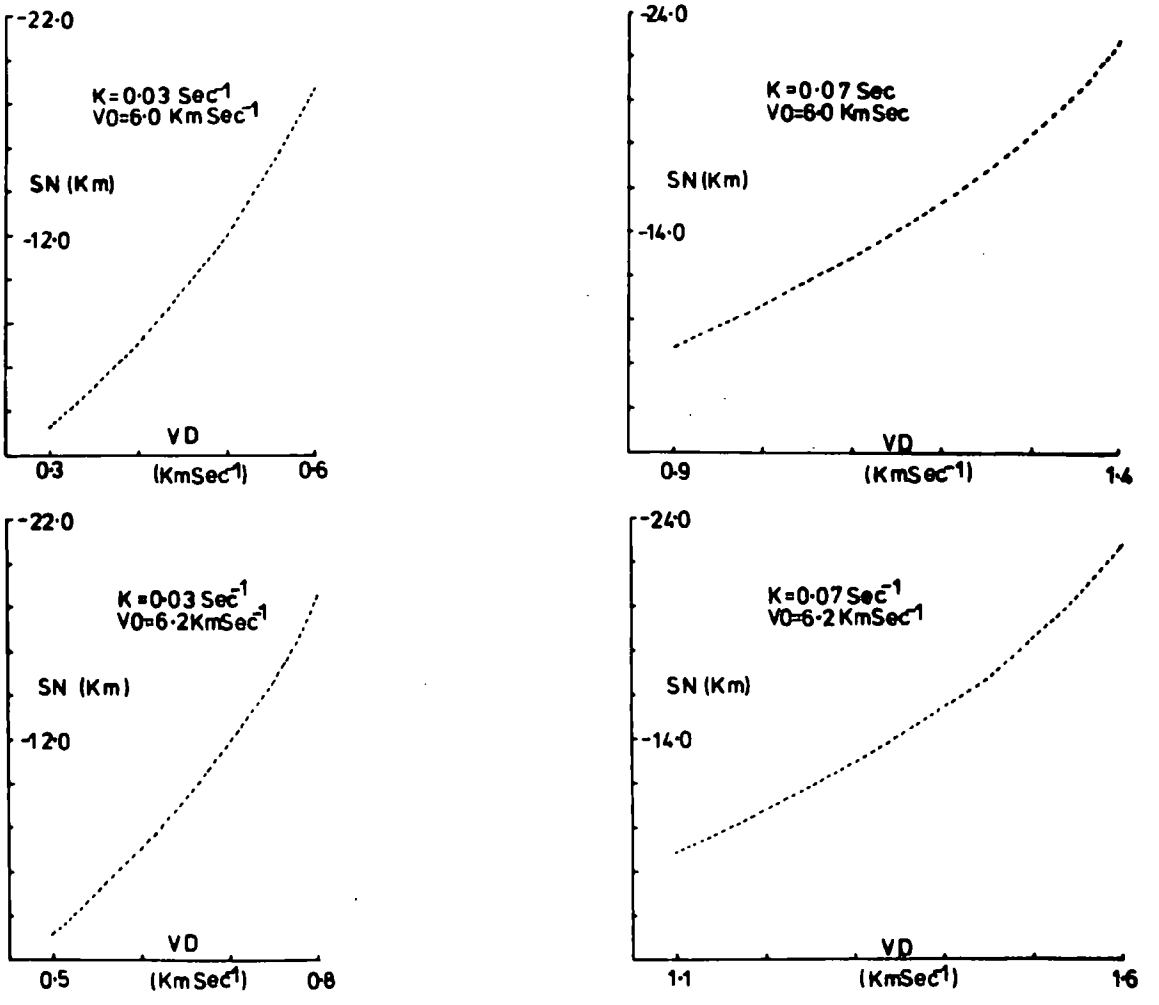

Swing (SN) of the Travel Path
Toward Nairobi Assuming an
Increase in Velocity as the
Signal Passes into Normal Crust

Fig 5:11

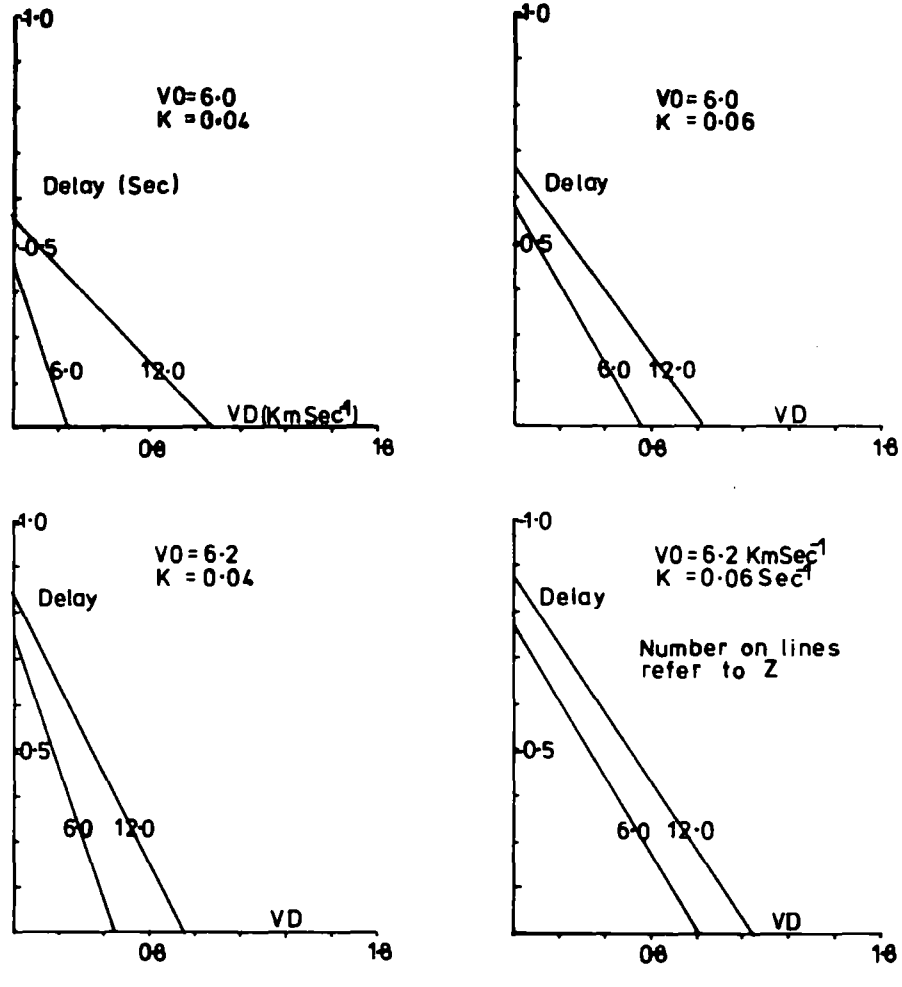

Delay at Nairobi on
Events from the Siria
Assuming the Model Above

Fig 5;12

Velocity-Depth Model
for the Gregory Rift.

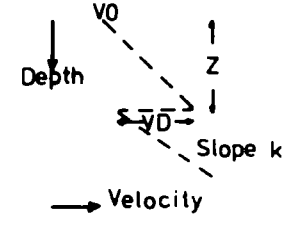

this model is approximately one quarter of the observed delay time at Nairobi. If it is again assumed that the events on the Siria Fault are mislocated the maximum possible delay, generated by the model, is approximately one-third of the observed delay.

5:6 Discussion.

Two models were considered in an attempt to explain the delay times at Nairobi. The two layered model will explain the two sets of delays at Nairobi on moho arrivals providing the axis of the anomaly is rotated in an anticlockwise direction. However the amount of rotation required will take the anomaly outside of the rift zone. Secondly the two layered model will explain the negative delay at Nairobi of the Lake Magadi arrivals only if the velocity of the anomalous material is above 7.0 Km sec^{-1} and that this material exists on the whole travel path to Nairobi. Thirdly the two layered model will not explain the negative delay time at Nairobi of the arrivals from the Siria Fault. For these reasons the two layered model is not an adequate representation of the anomaly.

The second model is the same as that used to explain the pattern of seismicity, in the Gregory Rift. This model will explain the 0.93 second delay at Nairobi providing that K is greater than 0.03 sec^{-1}. With increasing K, and V_o, the range of z and VD, which will give a delay of 0.93 seconds at Nairobi, increases. To explain a delay of 2.37 seconds, on the moho arrivals from the Kavirondo graben, at Nairobi, the value of K has to be at least 0.06 sec^{-1} and again a range of acceptable values of z and VD exists. The delays were fitted assuming that this model was aligned due north-south. If the axis of the anomaly is rotated by

a few degrees in an anticlockwise direction the minimum value of K decreases. The negative delays at Nairobi can, on this model, be explained by mislocation of the epicentres if the travel paths leave a low velocity material in the Gregory Rift and enter a higher velocity normal crust. This requirement can be used to put lower limits on the value of K and VD (see Fig 5:11). These limits lie below those required by the model to generate the pattern of seismicity. Lastly, the Siria Fault earthquakes require explanation. The negative delay at Nairobi on these earthquakes is impossible to explain on either of the models. Even if the events are shifted toward Nairobi, assuming a maximum error on the azimuth, the calculated delays are still smaller than the observed delay.

The delays at Nairobi generally support the model given in Chapter 4. However they do not refine the limits on the model but merely show that these limits are acceptable.

CHAPTER 6

MAGNITUDE DETERMINATION

6:1 Introduction.

Richter (1935) originally defined the magnitude of an event using the logarithm of the maximum trace amplitude written by a Wood-Anderson torsion seismometer. The maximum trace amplitude is taken as half the maximum peak to peak displacement on a vertical seismometer or the mean of the maximum displacements on two mutually perpendicular horizontal seismometers (Richter, 1958). To allow for the reduction in the amplitude of the trace due to absorption of the energy and geometrical spreading, Richter included a distance dependent function (Fig 6:1) into the calculation of the magnitude. Richter originally defined this measure of magnitude for epicentral distances from 0-600 Km and hence it is known as the local magnitude (M_L). Gutenberg (1945a) extended the use of magnitudes to teleseismic distances when he defined a surface wave magnitude (M_s) as,

$$M_s = \log_{10}A - \log_{10}B + C + D.$$

'A' is the maximum horizontal ground displacement of the 20 second period surface wave. 'B' is a distance dependent function to correct for the geometrical spreading of the wavefront and absorption along the travel path. 'C' is a station correction and 'D' a correction depending on the focal depth of the earthquake and anomalous absorption along the travel path.

The 20 second period surface waves were originally employed because surface waves of this period are prominent at distances of the order of 2000 Km. Also the absorption coefficient for surface waves of this period shows little local lateral variation, Evernden and Filson (1971), Solomon (1972)), and follows closely

Fig 6:1

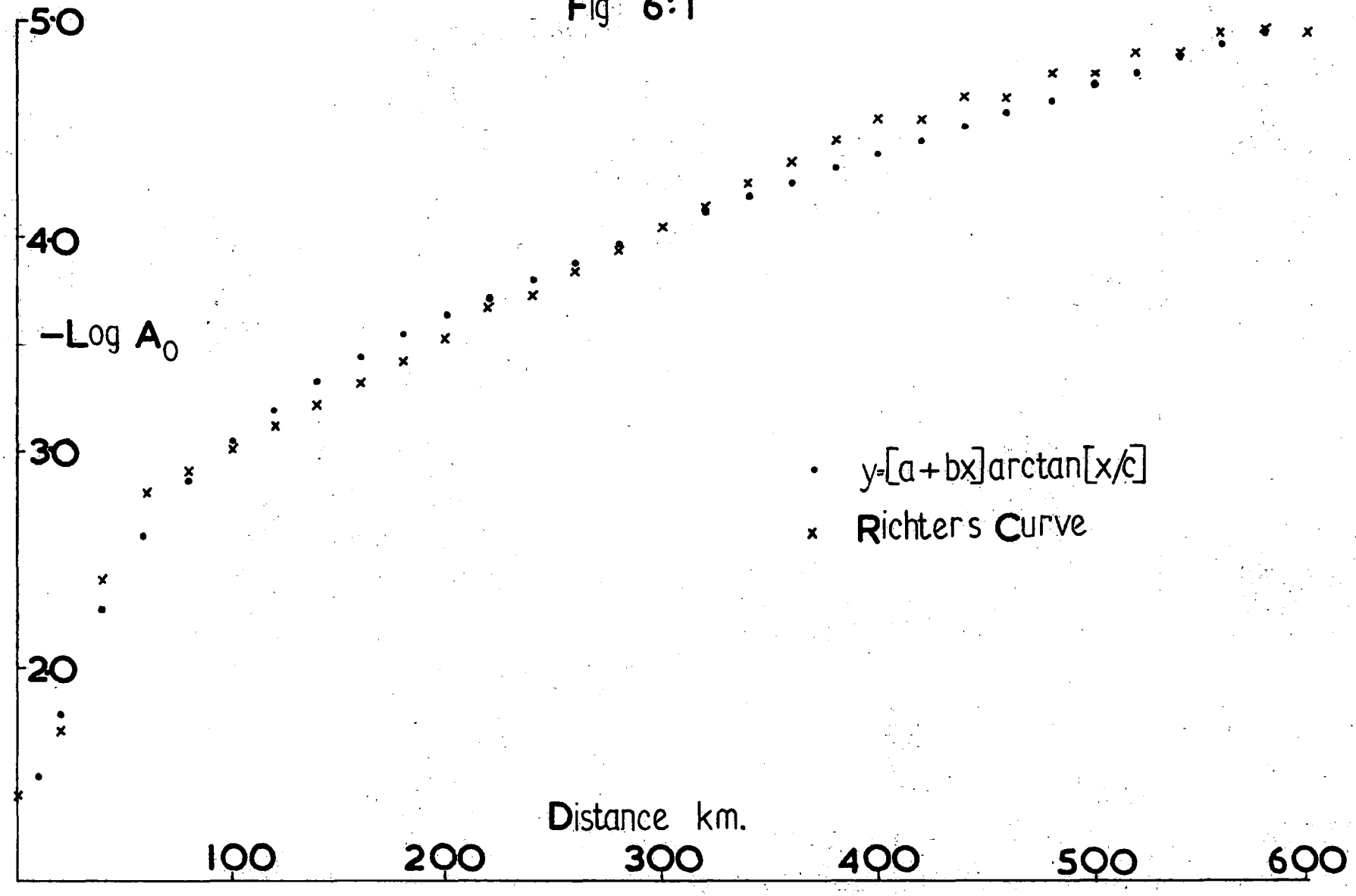
50
40
30
20
−Log A_0
Distance km.
100
200
300
400
500
600
y=[a+bx]arctan[x/c]
Richters Curve

the theoretical curves which assume constant absorption and geometrical spreading (Duda and Nuttli, 1974). The constancy of the absorption coefficient for the 20 second period wave implies that the surface wave magnitude can be universally applied. This is in contrast to the local magnitude which is a regional measure of the energy of the earthquake. The surface wave magnitude has two disadvantages. Most seismometers which operate in the twenty second period range have a gain of a few thousand and this restricts their use to medium and large magnitude earthquakes. Secondly, the amplitude of the surface waves generated by an earthquake is dependent upon the focal depth of the shock. As the focal depth increases the amplitude of the surface waves decreases. Because of the correlation between the initial amplitude of the surface waves and the focal depth, Gutenberg restricted the determination of M_s to events with focal depths less than 30 Km. A determination of M_s for deeper earthquakes can be made if a positive correction is included in the computation of the magnitude. Båth (1966), by employing a factor of 0.008 multiplied by the focal depth, has extended the determination of M_s to events with focal depths up to 100 Km. Gutenberg (1945b, 1945c) defined a body wave magnitude (m_b) which involved the use of the amplitude to period ratio of short period teleseismic body waves. As in the other methods of determining magnitude a distance dependent function is included into the calculations. This function allows for the dissipation of the energy by geometrical spreading and by absorption. Gutenberg originally calculated this distance dependent function from measurements of body wave phases at various distances. The amplitude-distance measurements were made in sets, each set confined to one earthquake for which the surface wave magnitude was known.

Usually, for the same earthquake, the magnitude m_b is not the same as the magnitude M_s. This difference between m_b and M_s is probably due to the two measurements being made at different frequencies in the displacement spectrum (Duda and Nuttli, 1974). For small earthquakes the amplitude of the displacement spectra at short periods is the same as the amplitude of the displacement spectra at long periods. However with increasing energy release, and hence larger earthquakes, the amplitude of the displacement spectra at short periods is less than the amplitude of the displacement spectra at longer periods. By linking the m_b and M_s scales at magnitude 7, Richter (1958) found the following relationship,

$$M_s = 1.59m_b - 3.97.$$

The geometrical spreading and absorption factor $F(\Delta)$ used by Richter in his determination of M_L is only applicable to areas which have a crustal structure similar to the crustal structure in Southern California. To determine the magnitude of earthquakes in East Africa, a $F(\Delta)$ factor must be determined for the crustal structure in East Africa. The $F(\Delta)$ function was determined with the help of data from Nairobi (section 6:2) after the amplitude of the signal at Nairobi had been corrected for anomalous attenuation (section 6:3). This $F(\Delta)$ function was combined with the amplitude to period ratio of the first six cycles of the p-wave ground motion to give a magnitude m_b'. The p-body waves were used in the determination of m_b' because:

(i) The S and surface waves were frequently saturated,

(ii) In some cases it was difficult to make a positive indentification of the s-waves.

To maintain consistency with other magnitude determinations the m_b' scale was tied into existing magnitude determinations

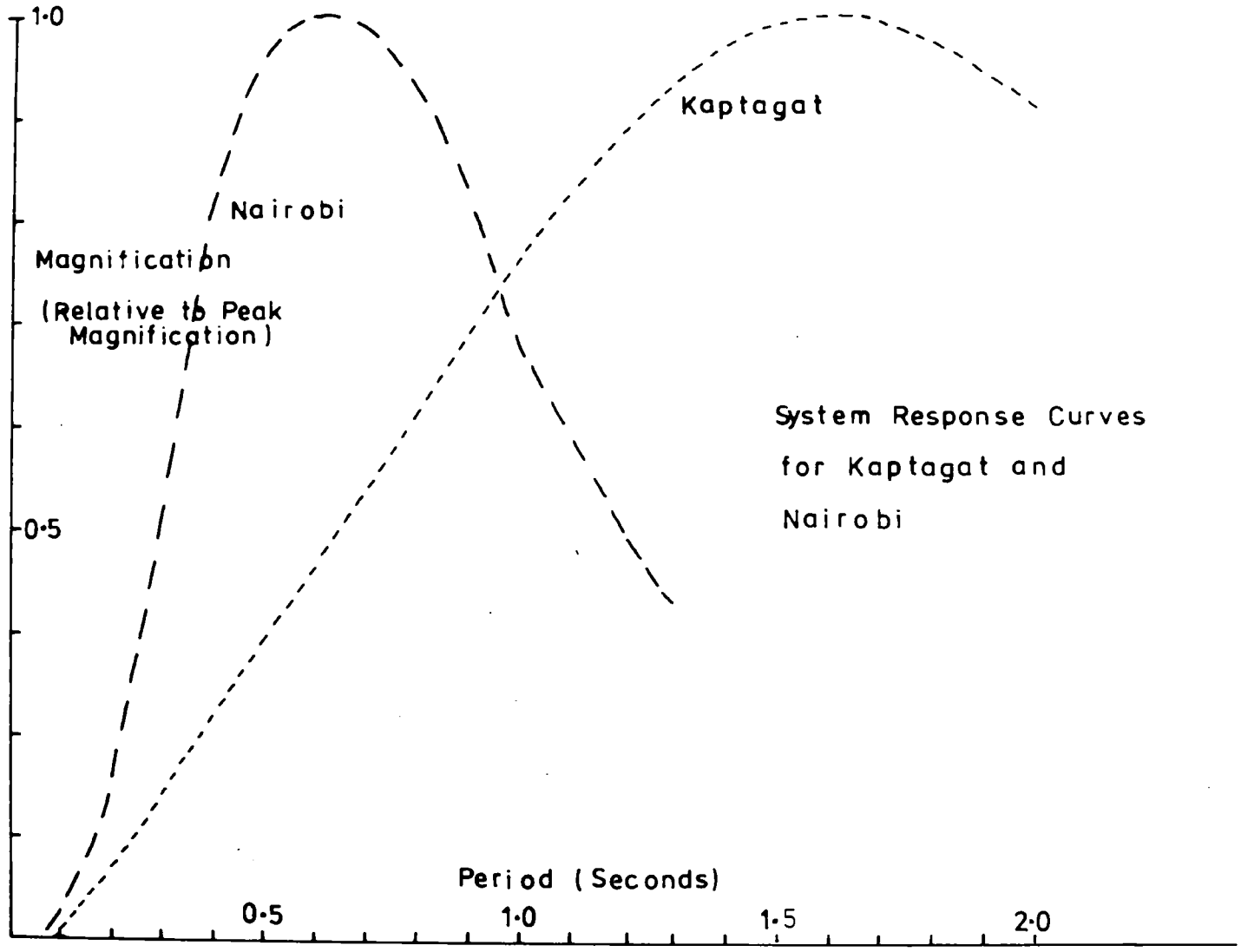
1·0
0·5
Kaptagat
Nairobi
Magnification
(Relative to Peak
Magnification)
System Response Curves
for Kaptagat and
Nairobi
Period (Seconds)
0·5
1·0
1·5
2·0

Fig 6·2

using earthquakes of known magnitude (m_b) listed in N.O.A.A. reports.

The amplitude of the ground motion was estimated using the trace amplitude, magnification of the system and the response curve shown in Fig (6:2). The response curve of the recording and playback system was determined by Fourier analysing the calibration pulse. Before the calibration pulse was digitized the curve was smoothed by hand to remove high frequency noise present in the signal. If the high frequency noise is allowed to enter the analysis the response curve shows erratic variations at the high frequency end. Even after smoothing the calibration pulse the high frequency end of the response curve showed perturbation by noise. To remove this perturbation, the high frequency part of the response curve was smoothed for a second time. The peak magnification of the system was obtained using known constants of the instrument and the current required to generate the calibration pulse.

6:2 Construction of the $F(\Delta)$ curve for East Africa.

The magnitude (m_b') of an earthquake as measured at Kaptagat is given by the formula,

$$m_b' = \text{Log}\frac{A}{T} + F(\Delta) + C_s \qquad (I)$$

where A is the maximum half peak to peak amplitude in the first six cycles of the ground motion, T is the period of the measured signal, and C_s is a station correction. For the same earthquake, the magnitude as calculated from the signal amplitude at Nairobi is given by,

$$m_b' = \text{Log}\frac{A'}{T'} + F(\Delta') + C_s' \qquad (II)$$

The amplitude of the signal at Nairobi and Kaptagat being

corrected for any anomalous absorption associated with the travel path, equations (i) and (ii) above are combined to give,

$$\text{Log}\frac{A'}{T'} - \text{Log}\frac{A}{T} = F(\Delta) - F(\Delta') + C_s - C_s' \qquad \text{(iii)}$$

From the above equation an $F(\Delta)$ curve can be defined if $C_s - C_s'$ is known. Five earthquakes of known magnitude and with P_n as the first arrival were recorded at Kaptagat. These events occurred to the west and the south of the station and the travel paths to Kaptagat did not cross the Eastern Rift zone. Using these five events the value of $(F(\Delta) + C_s)_W$ can be determined within the distance range 480 to 720 Kms. The subscript w denotes earthquakes to the west of Kaptagat. At an epicentral distance of 600 Km $(F(\Delta) + C_s)_W$ for Kaptagat is 5.04.

Seven earthquakes of known magnitude have been recorded at Nairobi. Four of the seven earthquakes are to the west of Nairobi and the remainder to the east and the south. The four earthquakes to the west were used to estimate a value of 5.42 at 600 Km for $(F(\Delta') + C_s')_W$ at Nairobi. Similarly the events from the east and south were used to give a value of 5.19 at 600 Km for $(F(\Delta') + C_s')_E$ at Nairobi. The difference between $(F(\Delta') + C_s')_E$ and $(F(\Delta') + C_s')_W$ is probably due to anomalous absorption within the Gregory Rift, (section 6:3). If signals travelling to Kaptagat from the west and signals travelling to Nairobi from the east and south have not experienced any anomalous absorption, $(F(\Delta) + C_s)_W$ and $(F(\Delta') + C_s')_E$ can be used to give $C_s - C_s'$ when $\Delta = \Delta'$. Hence equation (iii) reduces to,

$$\text{Log}\frac{A'}{T'} - \text{Log}\frac{A}{T} = F(\Delta) - F(\Delta') + K$$

where $K = C_s - C_s'$ at $\Delta = \Delta'$. If the function $F(\Delta)$ can be represented by a polynomial in Δ, the change in $F(\Delta)$ between the two stations can be written as,

$$F(\Delta) - F(\Delta') = a_1(\Delta - \Delta') + a_2(\Delta^2 - \Delta'^2) + \ldots\ldots\ldots + a_n(\Delta^n - \Delta'^n).$$

Hence,

$$\text{Log } \frac{AT'}{A'T} + e = a_1(\Delta - \Delta') + a_2(\Delta^2 - \Delta'^2) + \ldots\ldots\ldots + a_n(\Delta^n - \Delta'^n),$$

where e is the error.

The $F(\Delta)$ curve of Richter can be considered as two separate graphs, the two sections representing a change in the phase which has the maximum amplitude. When the measurements are restricted to the p-waves, a similar change may occur when the travel path changes. A simple polynomial in Δ will not preserve the knee in Richter's $F(\Delta)$ curve. As the data cannot be split into two parts to give two polynomials, a function was sought that would represent both sections of the curve. A function of the form,

$$F(\Delta) = (a_1 + a_2) \arctan(\Delta/a_3)$$

where a_1, a_2, a_3 are constants, can be used to represent the two curves and maintain the knee in the graph where the travel path changes character. Powell's method of minimization, (Powell, 1964, 1965), was used to minimize the errors in $F(\Delta) - F(\Delta')$ and to give values for a_1, a_2, and a_3. Powell's method of minimization requires estimates of the derivatives dF/da_1 and the choice of n conjugate directions which initially correspond to a_1, a_2, and a_3. The procedure starts from the best known approximation to the minimum and defines a correction to the approximation along each of the n directions. The direction with the largest correction is replaced by a new direction mutually conjugate to the existing directions and the process restarted. This procedure is carried on until the error on the function is less than a pre-defined value. The variation of the error on the function with change in a_1, a_2 and a_3, forms a steep parabaloid. The constants a_1, a_2 and

a_3 used to define the F(Δ) curve lie at the minima of the parabaloid and are sharply defined.

To test the method, Richter's curve was used to generate amplitudes for hypothetical earthquakes. These amplitudes were used as data for the prognam and Richter's curve regenerated. Fig (6:1) shows that the method is effective and has produced a fair representation of Richter's curve.

Using only events with well defined onsets at both stations and non-saturated records, the above method gave the following equation for F(Δ),

$$F(\Delta) = (0.7018 + (\Delta \times 0.0012)) \times \arctan(\Delta/382.2) + 2.65.$$

This equation was used to define the magnitude of earthquakes recorded by the Kaptagat array.

6:3 Corrections applied to the amplitude data.

For the standard events originating within the Uganda section of the Western Rift the difference between the $F(\Delta)|_{\Delta}$ values for Nairobi and Kaptagat is 0.38. This reflects a difference between the attenuation of the signal along the travel path to Kaptagat and the travel path to Nairobi. The path to Nairobi shows the greater absorption. A similar relationship exists for the events to the east of the Gregory Rift with the path to Kaptagat having the greater absorption. Therefore, at Nairobi, the anomalous amplitude of the standard events from Uganda is probably due to absorption within the Gregory Rift zone. Further evidence for anomalous absorption within the Gregory Rift comes from events located on the Siria fault. The epicentres for these earthquakes are equidistant from Kaptagat and Nairobi. As the epicentral distance is the same for each station, these earthquakes should have the same amplitude at Nairobi and Kaptagat. However a difference in F(Δ) of approximately 1.0 exists between the two

stations. This difference should not be due to the fault plane solution. The angle between the travel path to Nairobi and the fault plane is the same as the angle between the travel path to Kaptagat and the fault plane. This implies that both stations should see equivalent areas of the energy radiation pattern. Therefore the difference in $F(\Delta)$ at Nairobi and Kaptagat for the Siria fault events is probably due to anomalous absorption within the Gregory Rift.

To allow for the increased attenuation within the Gregory Rift zone the amplitude, at Nairobi, of earthquakes from Uganda has been multiplied by a factor of 2.37. A similar correction has been made to the amplitude of moho arrivals at Kaptagat for events to the east of the Gregory Rift.

A correction was not applied to the amplitude of moho arrivals from the south and south-east of the stations. Events from the south and southeast originate from the southern end of the Tanganyika Graben and the Eyasi Rift. Moho travel paths from these regions skirt the edge of the anomaly and do not suffer anomalous absorption.

Events from the Kavirondo Graben travel twice as far through the anomaly as events from the Ruwenzori area. To allow for this increase in distance travelled within the anomaly, the correction factor for Uganda events has been arbitrarily doubled and used to correct the amplitudes, at Nairobi, of events from the Kavirondo Rift.

Events from the Lake Naivasha area pose a problem in that neither station sees a signal completely unaffected by structures associated with the rift. The earthquakes in this region form a diffuse pattern across the rift. Events on the western flank have a travel path to Kaptagat predominantly through normal crust.

Those events on the eastern flank have a travel path to Nairobi predominantly within normal crust. To allow for the variation in distance travelled within the anomaly the correction factor was varied from event to event. The maximum correction was applied to the amplitude, at Nairobi, of events from the western flank of the rift.

6:4 Effect of the fault plane radiation pattern on Magnitudes.

Estimates of earthquake magnitudes made by one or two stations are susceptible to errors introduced by the radiation pattern from the source. For compressional body waves the radiation pattern is a function of the dip and slip angles of the fault plane, the azimuth of the event from the station and the angle of emergence of the signal from the focal sphere. Hence, if the radiation pattern is preserved, magnitude estimates will vary from station to station. The problem is not alleviated by using surface waves to determine magnitudes. The surface wave radiation pattern is dependent on the dip and slip angles of the fault plane, the azimuth of the event from the station and the focal depth of the earthquake. If the period of the measured surface waves is greater than fifty seconds the surface wave radiation pattern becomes dependent upon frequency. At short periods the length of the fault plane becomes important. As the length of the fault plane increases an interference pattern will develop. This interference pattern is superimposed upon the radiation pattern for both body waves and surface waves.

At local and regional distances the radiation pattern is distorted by the filtering effects of the crust. For this reason, the radiation pattern may not be preserved beyond the first half cycle of the compressive wave train (Von Seggern, 1970). The

amplitude of the first cycle of the wave train at Kaptagat is not normally the maximum of the first six cycles. This implies that the magnitudes at Kaptagat are not seriously distorted by the body wave radiation pattern. When the magnitude has been determined from the first cycle an estimate of the error on the magnitude can be determined by the method of Syed and Nuttli (1971). They developed the correction to adjust the body wave magnitude of events at teleseismic distances. At teleseismic distances the radiation pattern is better preserved because the filtering effects of the crust are not so pronounced. The correction of Syed and Nuttli has been applied to regional events.

The correction has the effect of distributing the ground displacement evenly over the focal sphere. The p-wave displacement, U, on the hypocentral sphere is given by,

$$U = \frac{2XYK(T - R/\alpha)}{4\pi\rho\alpha^3R^3} \qquad \text{where,}$$

X and Y depend on the force axis of the double couple mechanism,
R is the radius of the hypocentral sphere,
ρ is the density of the 'source rock',
K(T) is the double couple force,
α is the p-velocity of the source rock.

All the variables, except for X and Y, are constant for each event and the value of 2XY lies between 0 and 1 with an average value of 0.424. As the amplitudes seen at the station depend upon the displacement on the hypocentral sphere the magnitudes can be normalized using a factor of log(2XY/0.424). This is equivalent to spreading the displacement uniformly over the focal sphere and hence giving an average displacement. Using the fault plane solution given by Bangher and Sykes (1969), the magnitudes at Kaptagat of events located near the Ruwenzori mountains should be

increased by 0.23. This factor gives an indication as the possible inherent error in the magnitude estimates for this region. It was not possible to determine a similar correction for other regions because fault plane solutions were not available.

6:5 Earthquake frequency.

The frequency of occurrence of earthquakes with magnitudes greater than m_b can be represented by the equation,

$$\text{Log } N = a - bm_b \qquad (1)$$

where, N is the number of earthquakes with magnitudes greater than m_b, m_b is the central value of the magnitude interval, and a, b, are constants for each tectonic region. The magnitudes are grouped into discrete intervals defined by the range $m_b \pm \delta \frac{m_b}{2}$. Each magnitude interval is δm_b in width. The choice of δm_b depends on the density of the magnitude data. In previous studies, δm_b has been taken as small as 0.1 (Bath, 1973, and Francis, 1969) and as large as 0.5 (Wohlenberg, 1969). In this study, δm_b was taken as 0.25. Equation (1) assumes that the magnitude is an independent Poisson variable. Under this assumption the frequency of earthquakes with magnitude m_b is only a function of m_b. This implies that a series of large magnitude earthquakes can occur in a small time interval regardless of available deformational stress. Knopoff et al, (1972), have questioned the assumption that the magnitude-frequency relationship for the background seismicity is of Poissonian form. The background activity excludes those earthquakes which form an aftershock or foreshock sequence. Knopoff et al. have suggested that the background activity is better represented by a linear stochastic process. Suppose the maximum deformational energy that be stored within the rocks is E_{max} and the rate of addition of deformational energy is dE. Then in the

linear stochastic model two shocks with energy release of E_{max} must be separated by a time interval greater or equal to E_{max}/dE. From observations on models, Knopoff et al. found that the shocks were likely to be small rather than large and that the probability of a shock occurring in a small time interval is a function of the stored deformational energy. The linear stochastic model is difficult to apply to a real system because dE, E_{max} and the amount of deformational energy stored within the system at any one time are unknown.

Provided the constants, a and b, are known, equation (1) will give the frequency of occurrence within unit time of earthquakes with a magnitude m_b. Before a and b can be determined from existing data, the value of N has to be corrected for the observational cutoff. This correction consists of multiplying N by the ratio of the area sampled to the area within the observational cutoff. The area sampled is the area within which an earthquake with magnitude m_{bmax} will be seen at Kaptagat, m_{bmax} being the maximum magnitude seen from a tectonic area. Similarly, the area defined by the observational cutoff is the area within which an earthquake with magnitude m_b will be seen at Kaptagat. Two methods have been used to determine the constant b. In the first method, a straight line was fitted through the $\text{LogN}(m_b) - m_b$ data using the method of least squares. The least squares method assumes that there is no uncertainty in m_b and that the variance on $\text{LogN}(m_b)$ is uniform for all magnitude intervals (Page, 1968). The effect of the latter assumption is to emphasize the contribution of large magnitudes and decrease the importance of the small magnitudes. In the method of maximum likelihood, the second method used to determine b, no assumption is made about the variance on $\text{LogN}(m_b)$. However, it is assumed that there is no error in the measurement of m_b. This

condition is the same as applied in the least squares method. The constant b is given by the equation,

$$b = \text{Log}_{10}e \left[\bar{m} - m_{bmin} - \frac{m_{bmax} e^{-b'(m_{bmax} - m_{bmin})} - 1}{1 - e^{b'(m_{bmax} - m_{bmin})}} \right] \qquad (ii)$$

where,

m_{bmax} is the maximum magnitude within the sample,

m_{bmin} is the minimum magnitude within the sample,

$\bar{m}$ is the average magnitude of the sample and,

$b' = b/\text{Log}_{10}e$.

When $m_{bmax} - m_{bmin} > 2$, equation (ii) can be approximated to equation (iii), (Page, 1968):

$$b = \frac{0.4343}{\bar{m} - m_{bmin}} \qquad (iii)$$

The b values determined by the maximum likelihood method are consistently smaller than the b values determined by least squares. This discrepency is probably due to the inability to adequately sample the smaller magnitudes and the limited range of the data.

Using the data from Kaptagat, the b and a values were determined for four regions. Both methods were used to determine the b values which are as follows:-

Region	Least Squares	Maximum Likelihood
Albert Rift	$b = 0.81 \pm 0.18$, $a = 4.43 \pm 0.44$	$b = 0.84$
Gregory Rift	$b = 0.70 \pm 0.24$, $a = 3.77 \pm 0.50$	$b = 1.62$
Kavirondo Rift	$b = 0.84 \pm 0.33$, $a = 4.21 \pm 0.76$	$b = 0.95$
Siria Fault	$b = 0.77 \pm 0.67$, $a = 3.80 \pm 0.39$	

The high figures for b from the maximum likelihood method reflect the small range of magnitudes recorded from the Gregory Rift.

The Kaptagat data represents only a small sample of the seismic activity and consequently may not be typical of the long period activity. Using the I.S.C. data for the period 1965 - 1970, the b and a values were calculated for three regions, the Albert

Rift, the Tanganyika Rift, and the Eyasi Rift. Miyamura (1962), from seismic studies in Japan, has suggested that the age of the faulting may affect the b value in the equation, Log N = a - b_m. The age of the faulting in the Western Rift becomes progressively younger as the faults are traced north and so the Western Rift has been split into the two regions, the Albert Rift and the Tanganyika Rift. This division is apparently justified by the different values of b and a for the two regions. For the Albert Rift, the I.S.C. data gives b = 0.53±0.07 and a = 3.34±0.38, and for the southern section gives b = 0.91±0.12 and a = 4.54±0.54. The majority of the earthquakes, listed by the I.S.C., in the eastern arc of the rift system lie within the Eyasi Rift. For these earthquakes, b = 0.77±0.30 and a = 3.73±0.75. If the Eyasi Rift data is supplemented with data from Kaptagat, the values of b and a become 0.68±0.21 and 3.97±0.80 respectively. Within the 95% confidence limit these values are the same. If the maximum likelihood method is used to estimate the b value for each region, the values are:

Western Rift (North)	0.54±0.06
Western Rift (South)	0.43±0.07
Eyasi Rift	0.43±0.07

The low values of b, using the maximum likelihood method, for the last two regions are due to the inability to adequately sample the small magnitude earthquakes.

Wohlenberg (1968), using magnitudes determined by Lwiro seismic station calculated the constants as b = 0.65, a = 3.95 for the Western Rift and b = 0.79 and a= 4.85 for the Eyasi Rift. Providing that the upper magnitude limit of each area is the same, the above constants indicate that the Eyasi Rift shows a greater energy release than the Western Rift. The upper magnitude limit is

analogous to E_{max} in the linear stochastic model. The value of b for the Western Rift as determined by Wohlenberg is substantially different compared to the value determined by Lahr and Pomeroy (1970) for the aftershock and foreshock sequences associated with the 1966 Congo earthquake. Using 779 shocks, Lahr and Pomeroy calculated b as 1.05 ± 0.07 for the aftershock sequence and as 1.05 ± 0.35 for the foreshock sequence. Fairhead and Girdler (1971) using only 28 shocks calculated b as 0.83. If the b value of Lahr and Pomeroy is correct, the 1966 earthquakes cannot be considered as part of the background activity.

For the Kaptagat data the b value for the northern sector of the Western Rift is slightly higher than the same value derived from the I.S.C. data. The value of b = 0.81 is very close to the b value derived by Fairhead and Girdler for the aftershock sequence of the Congo earthquake of 1966. Comparison of the b and a values from the Kaptagat and I.S.C. data shows that the two distributions are equivalent for m greater than 4. The Kaptagat data predicts the larger number of small earthquakes. This is consistent with the data from Kaptagat being more representative at the smaller magnitudes. For the Gregory Rift, the b and a values, derived from the Kaptagat data, are similar to the constants for the Eyasi Rift. However, the two regions are different when the magnitude cutoff limits are compared. Both I.S.C. and the Kaptagat data for the Gregory Rift do not contain earthquakes greater than magnitude 4. In the Eyasi Rift, magnitude 4 earthquakes are quite common. This suggests that the two regions are, tectonically, the same at magnitudes less than 4. The seismicity in the Kavirondo Graben gives values for b and a of 0.84 and 4.21 respectively. These values are similar to those for the Western Rift as determined in this study. Both the Kavirondo Graben and the Albert Rift are

grabens bounded by single faults of large throw. The grabens are devoid of volcanic activity. It is therefore not surprising that the two regions have the same b and a value. However, the two regions do differ in the magnitude cutoff limit, the Albert Rift having the higher cutoff.

6:6 Energy release within each area.

The energy release in an earthquake is linked to the magnitude of the shock by the equation,

$$\text{Log } E = 5.8 + 2.4m \quad \text{(Richter, 1958)}$$

where E is the energy release. This equation can be used to give an estimate of the total seismic energy release per year per Km^2 if it is combined with the equation LogN = a - bm. If the equation for the energy is generalised to Log E = c+dm, the energy-frequency relationship is given by ,

$$N(E) = e^{2.3(a + bc/d)} E^{-b/d}$$

where N(E) is the number of events with energy E and above.

The estimated seismic energy release per year for each region is:-

Albert Rift	$0.3000\ 10^{19}$	Ergs yr^{-1}	$0.6000\ 10^{14}$	Erg Km^{-2} yr^{-1}
Tanganyika Rift	$0.1800\ 10^{19}$	" "	$0.1325\ 10^{14}$	" " "
Eyasi Rift	$0.4000\ 10^{19}$	" "	$0.2178\ 10^{14}$	" " "
Gregory Rift	$0.9156\ 10^{17}$	" "	$0.2888\ 10^{13}$	" " "
Kavirondo Graben	$0.6768\ 10^{17}$	" "	$0.1019\ 10^{14}$	" " "

The total energy release for each region has been normalized to the area of the region and this value is shown in the second column. From the above table it can be seen that the Albert Rift shows the highest energy release per unit area, EU, with an energy release of $0.6\ 10^{14}$ Ergs Km^{-2}. The Tanganyika graben shows approximately one quarter of the seismic energy release per unit area of the

Albert Rift. In the Albert Rift, the faulting is comparatively young and constrained at one end by the Aswa shear belt. If the Albertine faults are locked the stress will build up and be released in large shocks. Hence the high seismic energy release. The Kavirondo Graben has a value of EU similar to that for the Tanganyika graben. This suggest a similarity in the tectonics of the two areas.

Of the five areas considered the Eyasi Rift shows the second largest value for EU. However, it is a third smaller than the value for the Albertine Rift. Again the faults in the area are comparatively young. Further north, in the Gregory Rift, the value of EU drops to a tenth of that for the other regions. However, the calculated seismic energy release for this region is probably too low.

Earthquakes from the two outside groups of events in the Gregory Rift show an anomalously low signal frequency. This in itself does not lead to a lower magnitude if the displacement spectral density, at the source, is similar to Aki's model B (Aki, 1972). In this model the displacement spectra decays a $1/\omega$ for high frequencies. As the magnitude is determined from A/T the decay in the spectrum should not affect the magnitude. However, the anomalous low frequency does inidcate absorption, within the Gregory Rift, which may not be fully compensated for by the addition of a path correction in the magnitude determination.

The above values for the energy release in each area must be considered as approximate values. The equation used to derive the seismic wave energy from the magnitude is based upon investigations of large magnitude earthquakes. From the dislocation model of faulting the energy imparted to seismic waves during a shock is given by,

$$E = k\mu LD^2 f(\gamma)\eta \qquad (i)$$

where,

η is the efficiency of conversion of stress energy to seismic wave energy,

k is a numerical constant,

μ is the shear modulus,

$f(\gamma)$ is the fractional shear stress drop,

L is the fault length,

D is the depth of the fault.

If equation (i) is substituted into the equation for the energy-magnitude relationship the expression becomes,

$$a + bm = \text{Log}(k\mu LD^2 f(\gamma)\eta)$$

For large earthquakes, the accuracy of k, μ, η, and $f(\gamma)$ are not critical to the accuracy of the energy, E, in equation (i). However, for small earthquakes the accuracy of these values is extremely important (King and Knopoff, 1968). As imprecise values were used to determine the energy of large magnitude earthquakes the accuracy of a and b is limited.

6:7 Discussion.

The $F(\Delta)$ curve derived for East Africa forms a very shallow curve which approximates closely to a straight line. This is in agreement with the findings of Taner (1961) and Evernden (1967) who found that the body wave magnitudes of local earthquakes could be represented by the formula,

$$m_b = \text{Log}A/T + a\text{Log}(\Delta) + c \qquad \text{where,}$$

a and c are constants, and Δ is the epicentral distance.

Earthquakes which have crossed or originate inside the Gregory Rift show a reduced amplitude at one of the two stations. This attenuation of the signal is probably associated with the

same material that produces the calculated delay time at Nairobi. The attenuating material probably lies below the discontinuity postulated from the seismicity within the Gregory Rift. Using the formulae of Francis (1968), the apparent decrease in magnitude for events crossing the rift can be used to estimate a value for Q_p.

$$dm_b = \frac{\pi}{Q_p \text{Log}_e 10} \qquad \text{where,}$$

dm_b is the reduction in magnitude per wavelength within the anomaly, and Q_p is the attenuation factor for p-waves. For events from the Siria Fault this formula gives a Q_p of 55 and a Q_p of 130 for Uganda events. These values of Q_p are approximations as the estimates are based upon the number of wavelengths within the anomalous zone. Francis suggests that, beneath the oceanic ridges, the value of Q_p may be as low as 10. Therefore the above values do not seem unreasonable. Ward and Bjornsson (1971), from microearthquake studies in Iceland, have suggested that Q, in some regions, may be as low as 50. They suggest that these low values of Q may be due to magma chambers. The similar low values of Q for the Gregory Rift could also be due to magma chambers.

Miyamura (1962) has suggested that the value of b in the equation LogN = a - bm is a function of the mechanical properties of the tectonic area. If this is so, the data in this study indicates a similarity in the mechanical properties of the rock in the Kavirondo and Albert rifts. Similarly, the b values indicate a tectonic similarity between the Eyasi and Gregory rifts. In the former region the upper cutoff magnitude is higher than that in the latter region. This suggests that the two regions differ in the ability to store deformational energy with the latter region losing stress energy by creep. If a relationship exists between the stress drop and the radius of the fracture, assuming a circular

source, large values of b, for a set of magnitudes, indicates a small stress drop, (Wyss, 1973, and Scholz, 1968). This, if correct, suggests a smaller stress drop in the Tanganyika Rift than in the Albert Rift. Francis (1968) found that the b value for the seismicity of the fracture zone (b = 0.99) was different to that for the rift zone (b = 1.72). The b value for the fracture zones is similar to those for the various rifts in East Africa, suggesting a similarity in the tectonics of the two areas, In the Gulf of Aden, b= 2.13, and b = 1.92 for the Carlsberg Ridge (Francis, 1968), suggesting a lower stress release in these areas compared with the East African Rift system. The low stress release in the Gulf of Aden and Carlsberg Ridge is probably due to higher temperatures and weaker crust.

The discrepency between the b values, for the Albert Rift, derived from the I.S.C. and Kappagat data cannot be due to the different magnitude ranges. Allen et al. (1965) suggest that the linearity of the equation LogN = a - bm exists for a wide range of magnitudes. The low value for the I.S.C. data is probably due to a lack of the small magnitudes in the I.S.C. data.

The division of the Western Rift into two regions is justified by the two values of b. Miyamura (1962) has proposed that the variation of b represents the 'age' of the tectonic area. If this is true, the difference in b in the Western Rift reflects the various 'ages' of the tectonic areas.

CHAPTER 7

DISCUSSION AND CONCLUSION

7:1 Discussion.

Maps of the seismicity, within East Africa, drawn by Wohlenberg (1969, 1968) and DeBremaker (1959) show a conspicuous lack of activity in the Gregory Rift. The present study has shown that the suggested lack of activity in this region is false and that the Gregory Rift is occupied by an apparently discontinuous north-south band of seismicity. Tobin et al., (1969), have investigated the microseismic activity in the Gregory Rift and have located 'microseisms' in the 'shadow'zones. The magnitude of the microseisms is not known but is is probable that they are accompanied by larger shocks. This suggests that the apparent breaks, as seen at Kaptagat, in the band of seismic activity is an observational feature and not a feature of the activity. The line of epicentres correlate well with the centre of the negative gravity anomaly outlined by the various studies. A similar correlation has been found in the Rhinegraben (Mueller, 1970) and in the Baikal Rift (Riznichenko et al., 1969). In the latter region an even stronger correlation exists between the terrain and the seismicity.

In the Western Rift the events are associated with the boundary faults of the rift. This difference in the pattern of seismicity within the Gregory and Western Rifts lends support to the division, by Milanovsky (1969), of the World's rift systems into three types. In East Africa the Gregory Rift is an example of his arch-volcanic type and the Western Rift of the crevice type. Within the Western Rift the events also show a tendency to cluster near the Ruwenzori Mountains. This agrees with the pattern

ismic activity displayed by the I.S.C. data.
Outside of the two East African rift valleys the seismicity
four east-west trends, namely the Kavirondo Rift, the Sirha
, the Wamala region and the Speke Gulf. The inclusion of
ast area is based upon data listed in the I.S.C. bulletins.
(1974b) from ERTS-1 satellite imagery has suggested that
rending lineaments are a fundamental part of the tectonic
work of East Africa. Most of the lineaments of the area
ent to the Eastern Rift are found south and southeast of
Victoria; for example the Utimbara fault and the Speke Gulf.
lineaments do exist in the north including one on the
rn projection of the Kavirondo Graben and one in the vicinity
ali. On the western arc of the Rift System a lineament runs
the west of Lake Edward toward the Ruwenzori Mountains. This
ment is on the opposite side of the Western Rift to the
ity in the Wamala region. The apparent correlation between
west structures and the seismicity suggests that these
res are now being exploited to relieve stresses within the
. Activity along these trends may be due to a differential
of movement between the north and south of the Rift as
sted by Darracott et al., (1972), or the modification of the
s distribution by the Kenya Dome and the Ruwenzori block.
The two fault plane solutions determined for the northern
r of the Western Rift (Bangher and Sykes, 1969, and Sykes,
suggest that a tensional stress (least compressive stress)
ting perpendicular to the two main rifts. Maashar and
r, (1972), have shown that a stress system with a least
essive stress orientated east-west exists throughout the
rn side of the African continent. From the high scatter of
s in South Africa they suggest that the rifting has not yet

ended into this region. Fault plane solutions for South Africa
ll show an east-west least compressive stress. Roberts, (1969),
suggested that in the Ethiopian Rift the prominent vector of
ement is east-west with a small sinstral shear. From the
ve evidence it seems clear that the principle stresses in the
tern half of the African continent are tensional and acting
open the rifts. On to these regional stresses may be
erimposed local perturbations generated by features such as
Kenya Dome and the Ruwenzori Mountains. The action of these
al stress fields and the differential rates of opening between
north and south parts of the rift has lead to the development
east-west shears.

The pattern of seismic activity in the Gregory Rift is
ught to be the product of an anomalous crustal structure within
Gregory Rift. A model, for the structure of the crust within
Gregory Rift, has been developed to explain the observed
smicity and the apparent velocity, at Kaptagat, of the first
ival from events within the Rift. In the model the p-wave
ocity increases with depth until a discontinuity, which is
resented by a sharp drop in velocity. After the discontinuity
velocity once again increases steadily. The parameters which
ine this model are not accurately known but lie within the
ts imposed by the data. This model compared favourably with
model suggested by Francis and Porter, (1973), for the Mid-
antic Ridge near 45°N. They postulated an increase of velocity
depth truncated by magma chambers which give a reversal of
velocity gradient. The sharp discontinuity in the model for
crustal structure of the Gregory Rift may also be a reversal
the velocity gradient. However, the present data cannot be

l to distinguish between a reversal of the velocity gradient a sharp decrease in velocity.

The apparent velocity of the first arrivals from the Gregory t range between 6.6 and 8.0 Km sec^{-1}, with the majority of velocities laying in the middle of this range. Similar ocities are found further north in the Red Sea where the rift floored by material with a compressional velocity of 7.1 Km sec^{-1}, les, 1970). Under the Rhinegraben and Baikal Rift, there is ilar anomalous material which has a p-velocity 7.6 - 7.7 Km sec^{-1}, eller et al., 1967, 1969) in the former area and 7.1 - 7.5 sec^{-1} in the latter area (Artemjev and Artyushov, 1971). In United States anomalous material does not exist at high level hin the Basin and Range province. However, this area is erlain by mantle material with a p-velocity of 7.6 - 7.8 Km sec^{-1}, ok, 1962). This suggests that anomalous mantle and, or, crustal erial is common to the rift systems and is not a unique feature the Gregory Rift.

The anomalous crustal structure within the Gregory Rift gave e to a delay time at Nairobi for events that have crossed all, part of the Gregory Rift. These delay times at Nairobi have n interpreted using two models. A two layer model, similar to t of Griffith et al., (1971), for the crustal strucure will e the delay times providing that the anomaly is rotated west north and the anomalous crust exists from Lake Magadi to robi. This model will not give the shadow zones and the range apparent velocities seen at Kaptagat. The model used to explain seismicity will give the delay times at Nairobi and this is en as further support for this model.

Events which have crossed the Gregory Rift show attenuation

he signal amplitude. For p-waves this reduction in amplitude
ests a Q_α of between 55 and 135. The corresponding Q-factor
shear waves should be even lower as Q_α is approximately
- 2.6 times Q_β if all the energy loss is in shear and $V_p:V_s$
.74 (Anderson, 1967). Ward and Bjornsson, (1971), found
lar values of Q, in Iceland, for travel paths that had crossed
thermal areas. Further south Francis, (1968), has postulated
$_\alpha$ of approximately 10 for the mantle below the Atlantic ridge,
value of Q_α is much lower than $Q_\alpha = 440$ ($Q_\beta = 185$) for the
600 Km of normal mantle material (Anderson and Kovach, 1964).
the attenuation of the p-wave and the apparent lack of S
vals from the outside clusters within the Gregory Rift it
d seem that the crust is intruded by magma chambers. These
bers would also give rise to a velocity drop corresponding to
discontinuity in the velocity-depth model.

For the Gregory Rift the constants in the equation
N = a - bm indicate a low energy release, in the form of
thquakes, compared with the other areas. However, the high
flow and intensive fracturing within the Gregory Rift lends
lf to the release of stress by creep and ductal flow. It is
able that the stress release during seismic events represents
all part of the total stress release within the Gregory Rift.

From gravity studies Searle (1970), Baker and Wohlenberg (1971),
and Mansfield (1971) and Darracott et al. (1972) have
ulated a crustal intrusion derived from a low density mantle
aly. The shape and p-velocity of the anomaly has been refined
ong et al., (1972), using surface wave dispersion, delay times
slowness anomalies. The anomaly, which consists of material
a p-velocity of 7.0-7.5 Km sec^{-1}, must be in a plastic state

as S_n is severely attenuated in crossing the rift zone (Gumper and Pomeroy, 1970). Similar low velocity anomalies must underlie the Iceland ridge as indicated by the delays of 2.5 seconds found on teleseismic arrivals (Long and Mitchell, 1970).

From the above discussion a picture of the anomaly within, and below, the Gregory Rift emerges. The lower part of the crustal intrusion is an extension of the mantle anomaly both of which are in a plastic, if not fluid, state. Above the lower crustal intrusion the normal rock has been intruded by dykes, feeding the volcanoes and fissures, to give the crustal separation and the velocity gradient associated with the rock above the anomaly.

The difference between the Albert and Tanganyika sections of the Western Rift is displayed in the value of b in the equation $\text{Log}N = a - bm$. The higher value of b in the Tanganyika graben may be indicative of the age of the faulting and that it is fully developed. In the Albertine Rift the lower value of b could represent the comparitively young age of the faulting and the termination of the graben by the Aswa shear zone.

The faulting in the Western Rift correlates well with the Pre-Cambrian structures. In the Baikal Rift the faulting has developed independently of the Pre-Cambrian structures and is developing eastward through the Aldan shield (Florensov, 1969). If the Rift Systems of the World are interelated the independence of the Baikal Rift from Pre-Cambrian structures suggests the association between rifting and older structures in East Africa is not a key factor of the alignment of the rift.

7.2 Conclusions.

Within the Gregory Rift there is an axial zone of earthquakes. At each end of the Gregory Rift the axial alignment of the

quakes disappears and the epicentres of the shocks forma
se pattern across the whole width of the rift. In the
nyika shield the epicentres lie on east-west structures,
xample the Kavirondo Rift and the Siria Fault, or form a
se east-west pattern of activity in the Wamala region.
ntres of shocks from the Western Rift are associated with
ift boundary faults and in particular with the faults on
astern side of the Ruwenzori block.

The gradient, b, of the line describing the cummulative
ency-magnitude relationship suggests that the Western Rift
e split into two sections with the southern region showing
maller stress drop by earthquakes. Comparison between the
alues for the Albert and Kavirondo Rifts suggests that
nically the two regions are the same. Similarly the Gregory
yasi Rifts also appear to be tectonically comparable but
r in the maximum deformational stress that can be stored in
ock.

Within the Gregory Rift the crust is thought to be anomalous
a structure of the form indicated in chapter 4. Away from
onya Dome this anomalous structure grades into normal crust.
nomalous crust in the rift accounts for the pattern of
ic activity, seen at Kaptagat, within the Gregory Rift. The
lous material also has a low value of Q_p (C100) and the
part of the anomaly may be in a partially molten state.

No.													
						1970							
3038	1	6.73	229.88		17.2	-0.200	34.690	2.78	7	20	10	18	33.5
3035	1	7.29	140.21	17.4		-0.515	36.263	2.46	7	20	12	17	6.5
30902	1	6.03	235.47		17.5	-0.132	34.615	2.69	7	20	15	8	43.0
30177	1	8.04	284.38	65.2		1.845	30.020	4.46	7	21	2	56	22.6
30180	1	6.13	216.36	8.0		-0.009	35.122	2.94	7	21	5	15	46.5
30160	1	6.97	36.41		21.55	1.504	36.230	3.13	7	22	17	19	43.2
30162	1	7.59	116.26	57.2		-1.824	40.052	3.80	7	22	22	54	0.3
30171	1	6.06	223.19	6.25		0.127	35.156	3.78	7	23	0	33	4.2
3016	1	7.51	95.15	9.4		0.394	36.131	2.82	7	23	9	17	35.2
3009	1	7.63	247.10	8.9		0.205	34.875	3.53	7	24	4	45	48.9
3006	1	6.13	220.53	7.7		0.033	35.104	3.02	7	24	14	18	51.9
3024	1	7.49	232.26		27.2	-0.632	34.068	2.58	7	25	13	35	56.9
3031	1	7.04	280.64	9.8		0.585	34.772	2.12	7	26	10	56	56.2
30169	1	6.40	220.62	7.7		0.034	35.103	2.68	7	20	15	33	35.9
30191	1	6.04	222.67	7.3		0.068	35.108	3.86	7	31	17	17	45.8
						1971							
52751	2	6.83	180.22	42.6	67.4	-3.260	35.447	2.62	3	12	15	28	25.6
52756	2	7.34	210.49	50.3	75.8	-3.399	33.205	3.23	3	13	10	50	52.4

52767	1	7.54	226.28	17.2	20.9	-0.407	34.567	3.54	3	14	10	14	13.2
52769	1	7.66	226.15	17.3	20.0	-0.414	34.563	3.04	3	14	11	39	32.7
52770	1	7.33	231.11		17.5	-0.195	34.661	2.57	3	14	13	52	17.7
52772	2	6.11	301.09	44.8	64.0	2.482	32.115	3.67	3	15	9	37	17.4
52776	1	7.11	239.40		10.0	0.088	34.845	4.00	3	16	1	28	25.7
52798	1	7.61	83.54		8.8	0.508	35.933	3.24	3	18	14	36	31.9
52800	1	7.86	266.62	61.2		0.129	30.019	4.67	3	18	18	5	50.4
52804	1	7.87	265.03	60.7		-0.020	30.054	3.94	3	19	1	36	2.8
52805	1	8.19	269.58	60.4		0.413	30.048	3.98	3	19	3	8	2.8
52806	1	8.15	270.48	61.0		0.499	30.019	3.71	3	19	6	4	2.8
52819	1	6.83	22.20		26.5	2.041	36.105	3.58	3	20	4	3	0.2
52821	1	5.78	285.69	49.6		1.643	31.249	3.31	3	20	15	7	47.7
53858	1	10.24	297.02	2.6		0.537	35.300	3.19	3	27	12	13	28.9
53868	1	7.53	90.57	8.5	11.1	0.448	36.069	3.72	3	30	6	43	7.3
53870	1	10.00	62.61			0.471	35.493	3.20	3	30	20	48	23.4
53884	1	7.97	69.27		3.8	0.550	35.712	3.25	4	1	14	17	39.7
53894	1	6.49	201.29		30.3	-1.450	34.724	3.18	4	2	17	59	39.1
53896	1	6.45	201.93		30.5	-1.458	34.696	3.46	4	3	3	12	16.5
54900	1	6.82	21.08		26.8	2.073	36.081	2.72	4	3	19	9	57.5

54901	1	6.92	22.78		27.0	2.074	36.137	3.59	4	3	20	14	49.5
54902	1	7.80	17.45		26.8	2.114	35.980	3.46	4	4	1	35	29.8
54905	1	7.68	73.48	8.4		0.625	36.038	2.13	4	4	9	52	57.3
54906	1	6.85	20.60		27.0	2.099	36.075	3.29	4	4	12	26	25.7
54929	1	7.23	115.41	11.1	15.7	0.111	36.179	3.56	4	9	10	22	10.1
54940	1	6.58	196.62	26.4	29.0	-1.392	34.914	3.81	4	11	1	9	50.1
54941	1	6.39	204.83		30.4	-1.409	34.605	3.15	4	11	1	35	28.2
54946	1	6.36	198.09		29.8	-1.447	34.844	3.16	4	11	23	44	23.2
55965	1	6.92	71.75	7.8		0.629	35.987	2.55	4	16	19	18	49.3
55966	1	7.56	75.84	7.8		0.501	35.998	2.27	4	16	20	55	57.1
55968	2	5.94	271.26		81.8	0.560	30.615	3.10	4	17	11	9	4.4
55972	1	8.36	270.94		68.8	0.518	31.603	2.29	4	17	21	44	36.7
55978	1	8.49	267.19	60.0		0.186	30.077	3.82	4	18	0	35	53.7
55979	1	7.72	273.10	62.6		0.754	29.918	4.24	4	18	5	51	7.6
55980	1	7.95	268.38		68.4	0.341	31.520	4.18	4	18	6	5	50.6
55987	1	8.08	273.81		76.4	0.755	30.963	2.79	4	18	17	27	57.6
55993	2	5.85	271.07	61.8	79.9	0.556	29.981	2.97	4	18	21	39	27.3
55200	2	6.59	268.21		75.2	0.315	31.066	2.94	4	19	12	0	27.2
55210	1	6.56	214.34	6.1	7.3	0.093	35.216	3.35	4	20	20	28	43.6

55215	1	6.13	240.13		12.3	0.315	34.856	3.45	4	21	15	3	10.3
55216	1	7.30	274.80	53.1	83.9	0.850	30.761	4.15	4	21	16	20	38.7
55216	2	7.90	275.39	53.1		0.898	30.765	4.15	4	21	16	20	38.7
55217	2	5.76	271.91		78.2	0.608	30.861	3.54	4	21	17	10	34.7
55220	2	6.50	268.59	53.9	83.4	0.334	30.668	3.66	4	21	17	38	49.7
55221	1	7.87	271.57	61.2		0.603	30.011	4.00	4	21	18	52	18.7
55222	2	6.11	272.10	52.0	83.6	0.623	30.855	3.57	4	21	18	55	18.7
55223	2	5.92	276.49	58.3	83.3	1.046	30.269	3.57	4	21	18	58	15.7
55232	2	6.56	269.47	58.6		0.403	30.209	3.68	4	21	21	6	12.7
55233	2	6.26	269.89	57.2	83.2	0.443	30.344	4.23	4	21	21	9	37.7
55253	2	5.90	270.20		79.0	0.469	30.804	3.75	4	22	6	22	51.5
55254	2	5.71	269.63		84.2	0.420	30.451	2.69	4	22	7	39	48.5
55259	2	6.10	318.10	56.7	89.2	4.249	32.070	3.17	4	22	20	38	6.5
55275	1	7.76	302.87	64.0	94.0	3.557	30.677	4.31	4	23	22	57	18.3
55276	2	6.20	264.18	56.8	84.2	-0.050	30.477	3.56	4	23	22	53	15.3
55277	1	6.40	203.64		30.5	-1.434	34.640	2.93	4	24	0	29	8.1
55278	1	6.57	194.16	24.5		-1.418	34.992	3.77	4	24	0	35	57.1
55284	2	6.17	22.87		32.0	2.475	36.308	3.60	4	24	16	17	46.1
55285	2	6.86	4.58		29.5	2.433	35.616	3.88	4	24	16	21	31.1

56087	2	5.66	271.67		83.7	0.599	30.486	3.77	4	24	21	3	57.1
56090	1	7.57	254.92	81.0		-1.471	28.358	4.41	4	25	0	10	12.8
56096	1	7.77	195.04		28.6	-1.377	34.972	3.08	4	26	3	47	16.8
56097	1	6.47	186.94	10.5		-0.297	35.370	3.44	4	26	3	58	55.1
56098	1	6.64	197.43		29.3	-1.413	34.879	2.95	4	26	7	26	2.7
56099	1	8.08	272.81	61.0		0.721	30.025	3.57	4	26	13	25	22.6
56109	1	6.38	179.05			0.136	35.466	2.33	4	29	0	3	51.9
56110	1	6.45	176.79			0.138	35.479	2.86	4	29	0	4	31.0
56111	1	6.45	179.14			0.151	35.466	2.33	4	29	0	10	7.0
56114	1	6.60	177.17			0.168	35.475	2.39	4	29	1	26	47.9
56118	1	6.18	176.44		29.6	-1.525	35.584	3.42	4	29	19	58	28.7
56120	1	7.91	258.64	45.5		-0.332	31.576	3.68	4	29	21	39	16.9
56123	1	6.18	184.90			0.157	35.436	1.57	5	1	6	4	41.6
56124	1	6.51	181.31			0.168	35.455	1.58	5	1	6	5	16.5
56125	1	6.45	179.40			0.157	35.464	1.92	5	1	6	17	6.5
56132	1	6.42	200.14		31.1	-1.530	34.738	3.22	5	2	7	38	11.6
56133	1	7.83	260.13	54.8		-0.389	30.651	3.22	5	2	8	10	8.3
56138	1	6.44	195.27		30.7	-1.551	34.917	3.12	5	3	14	34	11.3
56140	1	6.43	197.30		28.4	-1.339	34.906	2.87	5	3	17	13	43.1

56141	2	6.52	269.16	54.8		0.381	30.579	2.08	5	3	17	44	41.2
56142	1	8.21	267.54	44.8		0.285	31.561	2.42	5	3	17	54	47.2
56146	1	7.97	262.94		55.1	0.030	32.064	2.77	5	4	3	33	32.8
56149	1	6.59	197.86		29.2	-1.400	34.808	3.48	5	4	15	51	36.0
56150	1	6.31	199.77		30.1	-1.453	34.780	3.01	5	4	19	49	37.6
56151	1	7.52	262.51	47.0		-0.087	31.377	2.87	5	4	20	22	7.1
56152	1	5.93	233.58		9.2	0.061	34.932	2.84	5	4	23	49	18.0
58163	1	8.73	266.37	59.8	87.3	0.110	30.101	4.38	5	17	8	13	46.9
58169	1	8.11	263.62	64.6		-0.190	29.745	3.46	5	17	16	10	24.0
58175	1	8.27	263.72		65.1	0.035	31.676	2.92	5	17	22	10	18.3
58179	1	7.11	228.49		20.3	-0.351	34.557		5	18	21	10	56.6
58183	1	7.52	230.65		18.4	-0.236	34.625	2.83	5	19	5	27	13.3
58184	1	8.54	235.40	74.6		-3.389	29.916	3.58	5	19	7	51	15.4
58185	1	8.26	266.36	47.5		0.187	31.302	3.09	5	19	15	52	3.3
58188	2	7.30	177.07	40.2	56.3	-3.019	35.638	3.31	5	25	1	4	34.0
58214	1	6.41	212.28	10.9		-0.210	35.045	3.14	5	26	20	19	58.2
5918	1	7.83	193.18	78.8	118.8	-6.544	33.826	4.71	5	28	21	3	29.5
5931	2	6.37	319.85	60.1		4.605	31.972	3.88	5	29	14	47	36.3
5935	2	7.12	92.09	23.5		0.387	37.2 0	2.90	5	29	18	13	38.3

5941	1	6.87	87.21		9.7	-0.570	35.951	3.79	5	31	4	15	20.5
5953	1	6.82	157.24		28.7	-1.302	36.193	3.43	6	2	18	28	4.5
5954	1	6.90	149.86		32.0	-1.442	36.555	3.18	6	2	18	32	18.5
5955	1	6.60	157.14		28.5	-1.285	36.190	2.99	6	2	19	12	19.7
5956	1	6.50	154.40		29.6	-1.334	36.313	3.65	6	2	21	24	28.5
5957	1	6.83	158.70		28.5	-1.304	36.142	3.05	6	2	21	29	44.5
60280	1	6.54	206.87	8.8		-0.111	35.177	3.09	6	8	1	14	3.3
60282	1	7.50	154.21		29.2	-1.300	36.303	2.97	6	8	3	57	11.2
60284	1	6.64	13.34		35.6	2.892	36.036	3.10	6	8	20	55	16.8
60289	1	7.49	158.75	23.4		-1.244	36.117	3.12	6	9	4	16	36.2
60301	1	6.51	228.39	[illegible]	16.8	-0.203	34.726	3.03	6	11	0	14	4.3
60307	1	6.62	102.98		10.5	0.323	36.030	3.28	6	11	15	59	20.5
60319	1	6.63	87.38	7.3		0.478	35.979	3.24	6	12	22	55	24.4
60324	2	6.81	186.62		57.9	-3.077	35.054	2.97	6	13	15	51	5.7
60325	1	6.83	9.47	29.2	36.4	2.990	35.882	2.86	6	14	0	48	10.9
60327	1	6.45	236.95		19.8	-0.190	34.478	3.48	6	14	23	51	9.1
60329	1	8.15	268.49	60.0	84.8	0.310	30.072	3.39	6	15	4	16	11.3
60337	1	6.74	22.81		25.7	1.970	36.094	2.79	6	16	0	18	51.0
60340	1	6.88	200.56			0.115	35.335	1.58	6	16	17	4	23.4

6151	1	7.73	330.91	3?0?		0.330	35.359	1.88	6	16	19	27	30.C
6143	1	6.50	4.83		29.8	2.448	35.629	2.47	6	17	19	56	40.5
6152	1	7.21	122.63	11.3		0.016	36.142	3.88	6	19	8	30	39.9
6153	1	6.39	118.44		12.3	0.120	36.075	2.47	6	19	9	15	53.8
6163	1	7.12	160.98		47.4	-2.521	36.481	2.42	6	22	6	52	38.6
6164	1	7.13	159.35	38.0	45.9	-2.436	36.544	2.49	6	22	7	24	16.8
6165	1	7.04	227.30	17.0		-0.380	34.563	3.39	6	22	14	37	47.5
6166	1	6.34	179.14			0.167	35.466	1.85	6	22	18	39	10.3
6167	1	6.90	183.73			0.180	35.443	1.83	6	22	18	44	31.0
6168	1	7.23	227.66	17.0		-0.374	34.558	2.99	6	22	19	6	19.4
6169	1	6.43	179.35			0.160	35.465	1.95	6	22	19	39	40.2
6170	1	6.41	175.86			0.166	35.482	2.42	6	22	19	40	40.2
6171	1	6.52	178.20			0.152	35.471	2.61	6	22	20	22	53.7
6172	1	6.44	177.17			0.188	35.476	1.89	6	22	20	23	42.5
6173	1	6.56	230.60		16.5	-0.162	34.716	3.30	6	23	0	55	25.3
6202	1	6.18	230.53	16.7		-.0313	34.536	3.39	6	28	17	48	58.5
6206	1	6.26	232.06		17.8	0.194	34.636	3.26	6	29	0	2	49.3
6210	1	6.24	141.05	5.5		0.148	35.707	3.12	6	29	9	8	31.1
6214	2	6.56	116.42	36.4	47.3	-0.939	38.260	3.70	6	29	12	39	40.2

6219	1	8.24	231.13	77.2		-3.954	30.016	3.97	6	30	3	14	14.3
6221	1	6.78	217.00	8.1		-0.011	35.113	2.41	6	30	5	52	49.0
6233	1	7.68	255.90	73.2		-1.162	29.067	4.56	7	1	8	39	41.9
6243	1	8.19	182.36	76.1	122.3	-6.463	35.177	4.50	7	2	0	8	17.2
6249	2	7.48	174.18		107.8	-6.082	36.125	3.68	7	2	7	14	6.6
6253	1	6.76	221.33	8.0		0.022	35.084	3.58	7	2	8	15	9.6
6257	1	6.69	28.51		25.8	1.906	36.245	2.87	7	2	21	14	25.6
6259	1	8.42	188.40	81.7		-6.939	34.371	3.84	7	3	22	36	22.6
6263	1	7.45	222.77	37.0	45.8	-1.867	33.328	3.78	7	4	7	58	39.7
6267	1	6.59	175.23	34.8		0.141	35.487	2.62	7	4	12	44	15.2
6268	1	7.90	229.04	90.7		-5.018	29.175	4.31	7	4	22	59	38.8
6270	1	7.99	151.51	30.6	35.0	-1.771	36.661	3.36	7	5	1	27	23.1
6271	1	6.34	179.61		108.5	-6.164	35.506	3.56	7	5	6	27	8.8
6277	1	6.81	144.26		36.5	-1.643	36.961	2.67	7	6	1	6	4.9
6278	1	8.05	267.68	50.5		0.271	31.003	3.71	7	6	4	3	22.3
6280	1	8.23	265.00	61.4	88.8	-0.028	29.995	3.79	7	6	11	28	14.7
6288	1	6.61	186.74		9.0	-0.033	35.404	3.27	7	7	11	49	7.5
6289	1	6.80	190.04		9.8	-0.080	35.367	3.41	7	7	11	54	7.5
6290	1	7.08	188.30		9.4	-0.051	35.387	2.20	7	7	11	57	59.5

6291	1	6.52	204.09	8.4		-0.098	35.216	3.55	7	7	12	50	37.5
6292	1	6.01	207.20	9.4		-0.148	35.154	3.25	7	7	13	8	51.5
6297	1	6.76	202.24		8.3	-0.027	35.288	3.12	7	7	17	43	23.5
6298	1	6.74	196.69		8.3	0.027	35.334	2.55	7	7	18	59	4.6
6299	1	6.36	204.44		9.8	-0.040	35.238	2.65	7	7	21	53	56.6
62100	1	6.47	204.29		9.5	-0.023	35.247	3.02	7	7	22	15	55.6
62101	1	6.60	188.68	[illegible]	8.9	-0.025	35.389	3.01	7	8	1	57	54.6
62104	1	6.80	202.20	6.4		0.040	35.393	3.54	7	8	13	27	5.6
62106	1	7.38	203.05		9.8	-0.045	35.250	3.04	7	8	13	59	27.3
62107	1	6.98	205.27		8.3	0.050	35.271	3.59	7	8	14	10	57.6
62108	1	7.00	202.96		8.0	0.066	35.298	3.63	7	8	14	30	24.1
62110	1	6.49	208.13	5.7		0.094	35.370	3.69	7	8	16	34	24.3
62111	1	6.47	203.76		8.4	0.040	35.280	3.15	7	8	17	0	3.5
62114	1	6.60	206.14	5.9		0.075	35.276	3.67	7	8	18	38	40.4
62117	1	6.78	205.73	7.9		-0.058	35.216	3.54	7	8	20	51	40.4
62119	1	6.12	207.24		9.6	-0.017	35.220	2.65	7	8	22	7	31.1
62120	1	5.93	212.88	8.8		0.078	35.119	2.28	7	8	22	14	42.7
62124	1	6.38	209.80		7.9	0.090	35.254	2.88	7	9	2	46	34.4
62125	1	6.30	207.61		9.6	-0.015	35.217	1.92	7	9	2	56	51.3

62128	1	6.42	205.85	9.3		-0.145	35.173	3.18	7	9	3	9	49.8
62130	1	6.60	201.90		9.5	-0.031	35.267	2.87	7	9	3	26	48.5
62132	1	6.32	198.68	9.4		-0.035	35.297	3.02	7	9	4	23	11.5
62133	1	6.48	202.52		8.5	0.030	35.287	2.82	7	9	4	30	3.4
62135	1	6.46	205.86	8.4		-0.092	35.198	3.26	7	9	7	28	9.6
62137	1	6.35	204.26		8.8	0.018	35.266	2.67	7	9	8	45	38.7
62138	1	6.78	204.44			0.233	35.361	2.65	7	9	9	38	42.7
6814	1	7.00	96.69	7.2		0.394	35.972	2.15	9	1	4	50	37.3
6815	1	7.80	159.06		30.4	-1.463	36.190	3.12	9	1	5	40	45.1
6819	1	6.83	84.13	8.1		0.514	36.038	3.58	9	1	12	44	17.7
6820	1	7.77	107.24	8.5		0.273	36.042	2.30	9	1	19	31	41.8
6829	1	8.29	263.66	58.0		-0.123	30.302	2.80	9	4	2	25	3.1
6831	1	6.18	220.01		19.8	-0.450	34.707	2.39	9	4	11	11	52.1
6835	1	6.63	173.34		28.5	-1.420	35.679	2.69	9	7	9	30	35.8
6907	1	8.23	156.82		31.4	-1.513	36.298	3.00	9	9	1	27	38.1
6908	1	7.37	274.98	58.0		0.906	30.285	3.34	9	9	7	7	31.0
6911	1	7.19	151.63		28.7	-1.222	36.360	2.90	9	9	15	10	3.1

6913	1	7.07	156.44		32.4	-1.587	36.456	2.92	9	9	15	41	13.7
6914	1	7.94	152.22		31.6	-1.455	36.461	2.84	9	9	16	4	27.9
6915	1	8.06	165.14		30.2	-1.513	35.980	3.09	9	9	16	32	31.9
6918	1	7.85	152.31		28.7	-1.232	36.341	3.62	9	10	0	54	52.2
6935	1	8.07	294.96	53.6		2.476	31.138	3.77	9	13	18	11	39.3
6939	1	7.29	158.15		31.0	-1.500	36.260	2.79	9	14	8	56	53.3
6940	1	6.91	25.17		24.8	1.867	36.121	3.40	9	14	12	31	38.2
6941	1	6.38	22.32		25.4	1.951	36.072	3.14	9	14	13	31	54.5
6943	1	8.40	178.34		29.7	-1.537	35.519	2.87	9	14	16	25	24.6
6945	1	7.76	98.78	8.9		0.357	36.091	3.97	9	15	14	34	36.0
7402	1	7.41	32.39		26.0	1.864	36.350	3.14	11	5	20	10	19.4
7410	1	7.33	93.39	8.6	10.3	0.418	36.075	3.30	11	7	22	6	38.1
7414	1	7.26	28.36		28.8	2.138	36.365	3.57	11	8	6	1	25.0
7425	1	5.68	237.62		12.6	0.070	34.859	3.10	11	9	19	16	53.6
7426	1	6.13	159.68	26.9	30.3	-1.462	36.166	3.63	11	9	20	16	20.3
7429	2	6.66	304.99	43.5	66.9	2.633	32.364	3.78	11	10	18	15	10.6
7433	1	6.12	354.92	23.6	26.9	2.196	35.307	3.01	11	11	18	19	43.1

7441	1	6.18	166.21	4.0		0.083	35.528	2.88	11	13	11	44	42.0
7446	1	6.28	232.52		24.1	-0.459	34.279	3.06	11	15	21	24	2.7
7448	2	7.16	206.18	52.8	74.6	-3.780	33.391	3.73	11	14	8	32	55.8
7450	1	6.32	215.86	17.3	22.8	-0.674	34.651	2.78	11	14	14	3	51.2

Note : Figure 1 in column 2 denotes a first arrival.

Figure 2 in column 2 denotes a second arrival.

Velocity in Km sec^{-1}.

Epicentral coordinates in degrees.

REFERENCES

. (1972). Scaling Law of Earthquake Source Time Function. eophys. J.R. astr. Soc. 31, 3-25.

C.R., St Amand, P., Richter, C.F., and Nordquist, J.M. (1965). elationship Between Seismicity and Geologic Structure in the outhern California Region. Bull. seism. Soc. Am. 55, 753-797.

on, D.L. (1965). Recent Evidence Concerning Structure and omposition of the Earth's Mantle. Phys. Chem. of Earth 6, -131.

on, D.L. (1967). Latest Information from Seismic Observations. n: The Earth's Mantle. Ed. Gaskell T.F.

ev, M.E., and Artynshkov, E.V. (1971). Structure and Isostasy f the Baikal Rift and the Mechanism of Rifting. J. geophys. es. 76, 1197-1211.

use, R.W. (1972). Upper Mantle Structure using P-wave Data rom an East African Array Station. Ph.D. Thesis, University f Durham.

, D.K. (1964). Crustal Warping - a Possible Tectonic Control f Alkaline Magmatism. J. geophys. Res. 69, 1103-1111.

B.H., Williams, L.A.J., Miller, J.A., and Fitch, F.J. (1971). equence and Geochronology of the Kenya Rift Volcanoes. ectonophysics 11, 191-215.

B.H., and Wohlenberg, J. (1971). Structure and Evolution of he Kenya Rift Valley. Nature, Lond., 229, 538-542.

B.H., Mohr, P.A., and Williams, L.A.J. (1972). Geology of he Eastern Rift System of East Africa. Geol. Soc. Am. Spec. ap., 136.

r, A.R., and Sykes, L.R. (1969). Focal Mechanisms of Earthquakes n the Indian Ocean and Adjacent Regions. J. geophys. Res. 74, 23-649.

M. (1966). Earthquake Energy and Magnitude. Phys. Chem. of arth 7, 115-166.

M. (1973). Introduction to Seismology. Halsted.

, W.W. and Trendall, A.F. (1966). Erosion Surfaces, Tectonics nd Volcanic Activity in Uganda. Q. Jl. geol. Soc. Lon. 122, 85-420.

S., Hales, A.L., and Landisman, M. (1969). Velocities in the rust and Upper Mantle of Southern Africa from Multimode Surface ave Dispersion. Phil. Trans. R. Soc. Lon. Series A 258, 421-443.

...r., Fuchs, K, and Kohlenberg, J. (1970). Crustal Structure the East African Rift System from Spectral Response Ratios ong-Period Body Waves. Geophys. 36, 287-297.

.N., Dorman, J. (1963). Seismic Waves and the Earth Structure the Canadian Shield. Bull. seism. Soc. Am. 53, 167-210.

E.C. (1936). Gravity Measurements in East Africa. Phil. ns. R. Soc. 235, 435-531.

r, E.W. (1966). Onset Time Analysis. AWRE Blacknest Note /AG, 66.

L. (1962). The Problem of the Mantle-Crust Mix: Lateral omogeneity in the Uppermost Part of the Earth's Mantle. an. Geophys. 9, 295-360.

L., Smith, R.B. (1967). Seismicity in Utah 1850 Through June 5. Bull. seism. Soc. Am. 57, 689-718.

ey, D.J. (1969). Measurements of the Derivatives of the P Wave vel Time Curve by Means of an Array Network. Ph.D. Thesis, versity of Durham.

. (1939). Hebnng-Spattung-Vulkanismus. Geologische Rundschan, 405-527.

t, B.W., Fairhead, J.D., and Girdler, R.W. (1972). Gravity Magnetic Surveys in Northern Tanzania and Southern Kenya. tonophysics 15, 131-141.

t, B.W. (1974). The Structure of Speke Gulf, Tanzania, and Relation to the East African Rift System. Tectonophysics 23, -175.

K.A. (1951). The Uganda Section of the Western Rift. Geol. ., 102, 377-386.

J.B., Powell, D.G. and Reid, A.M. (1970). Ultrabasic Xenoliths Lava from the Lashaine Volcano, Northern Tanzania. J. Petrol. 519-548.

cher, J.C. (1959). Seismicity of the West African Rift Valley. geophys. Res., 64, 1961-1966.

E.T., Von Herzen, R.P., and Wong, H-K, (1971). Lake Tanganyika: er, Chemistry, Sediments, Geological Structure. urwissenschaflen, 58, 220-241.

. (1946). Erosion and Tectonics in the East African Rift System. Jl. geol. Soc. Lon., 102, 339-888.

R. (1963). Geology of the South Horr Area. Kenya Geol. Survey t. No. 60.

(1964). Preliminary Note on the Refracted P-phase in the tern Rift Valley of Africa. J. geophys. Res. 69, 3027-3081.

.J., Nuttli, O.W. (1974). Earthquake Magnitude Scales.
ophys. Surv. 1, 429-458.

J.W. (1966). Penetrative Convection: Its Role in Volcanism.
ll. Volcan., 29, 327-343.

n, J.F. (1967). Magnitude Determination at Regional and Near-
gional Distances in the United States. Bull. seism. Soc. Am,
, 591-639.

n, J.F. and Filson, J. (1971). Regional Dependence of Surface-
ve versus Body-Wave Magnitudes. J. geophys. Res., 76, 3303-3308.

d, J.D., Girdler, R.W. (1969). How Far Does the Rift System
tend Through Africa. Nature, Lond. 221, 1018-1020.

d, J.D., Girdler, R.W. (1971). The Seismicity of Africa.
ophys. J. R. astr. Soc., 24, 271-301.

ov, N.A. (1969). Rifts of the Baikal Mountain Region.
ctonophysics, 8, 443-456.

, T.J.G. (1968). The Detailed Seismicity of Mid-Oceanic Ridges.
rth and Planetary Sci. Letters, 4, 39-46.

, T.J.G., Porter, I.T. (1973). Median Valley Seismology: The
d-Atlantic near 45°N. Geophys. J. R. astr. Soc. 34, 279-311.

R. (1966). Rift Valleys in the World Rift System - UMC Symposium.
nada Geol. Survey paper, 66-14, 330-344.

R. (1970). Plate Tectonics of the Red Sea and Africa.
ture Phys. Sci., 228, 453.

.G., Atkins, A.R., Sellschop, J.P., Seligman, P. (1956).
ustal Structure in the Transvaal. Bull. seism. Soc. Am., 46,
3-316.

.G., Gibson, I.L. (1969). Structural Evolution of the Rift Zones
the Middle East. Nature, Lond., 221, 925-930.

.G. (1970). Tectonic and Magmatic Evolution of the Afro-Arabian
me. In 'African Magmatism and Tectonics', p285-297, Oliver and
yd.

, R.W. (1964). Geophysical Studies of Rift Valleys. Phys. Chem.
Earth, 5, 121-156.

, R.W., Fairhead, J.D., Searle, R.C. and Sowerbutts, W.T.C. (1969).
olution of Rifting in Africa. Nature Lond., 224, 1178-1182.

, R.W., Sowerbutts, W.T.C. (1970). Some Recent Geophysical
udies of the Rift System in East Africa. J. Geomag. Geolect.,22,
3-163.

D.H., Ringwood, A.E. (1967). The Genesis of Basaltic Magmas.
ntrib. Mineral Petrol., 15, 103-190.

, J.W. (1921). The Rift Valleys and Geology of East Africa.
eley and Service Co. Ltd.

s, D.H., King, R.F., Khan, M.A., Blundell, D.J. (1971).
ismic Refraction Lines in the Gregory Rift. Nature Phys. Sci.,
), 66-71.

ns, D.H. (1972). Some Comments on the Results of a Seismic
fraction Experiment in the Kenya Rift. Tectonophysics, 15, 151-156.

F., Pomeroy, P.W. (1970). Seismic Wave Velocities and Earth
ructure on the African Continent. Bull. seism. Soc. Am., 60,
1-668.

rg, B. (1945a). Amplitudes of Surface Waves and Magnitudes of
allow Earthquakes. Bull. seism. Soc. Am., 35, 3-12.

rg, B. (1945b). Amplitudes of P, PP and S and Magnitudes of
allow Earthquakes. Bull. seism. Soc. Am., 35, 57-69.

rg, B. (1945c). Magnitude Determination for Deep Focus Earthquakes.
ll. seism. Soc. Am., 35, 117-130.

rg, B., Richter, C.F. (1956a). Earthquake Magnitude Intensity,
ergy and Acceleration. Bull. seism. Soc. Am., 46, 105-143.

rg, B., Richter, C.F. (1956b). Magnitude and Energy of
rthquakes. Ann. Geof., 9, 1-15.

n.L., Sacks, I.S. (1959). Evidence for an Intermediate Layer
om Crustal Structure Studies in the Eastern Transvaal.
ophys. J. R. astr. Soc., 2, 15-35.

P.G. (1969). Basalt Type and African Rift Valley Tectonism.
ctonophysics, 8, 427-436.

h, J.V. and MacDonald, R., (1966). Organic Belts of Northern
anda Basement. Nature 210, 726-727.

E., Taggart, J. (1968). Regional Variations in P Travel Times.
ll. seism. Soc.,Am., 58, 1325.

A. (1965). Principles of Physical Geology. Nelson.

J.H. (1970). Graben Tectonics as Related to Crust-Mantle
teraction. International Upper Mantle Project, Graben Problems.
p. 27, 4-27.

, H.S. (1968). Body Wave Magnitude and Source Mechanism.
I.T. Seismic Data Laboratory Rep. No. 225.

s, D.J. (1964). Geology of the Kaptagat Plateau Area.
ol. Survey Kenya. Rep. 63.

, R.J., Williams, C.E.F. (1961). Explanation of Sheet 59 (Kiboga).
ol. Survey Uganda.

, R.J. (1969). Explanation of Sheet 69 (Lake Wamala).
ol. Survey Uganda.

L.J. (1964). Limited Network Processing of Seismic Signals.
I.T. Lincoln Lab. Group Report 44.

M.A., Mansfield, J. (1971). Gravity Measurements in the Gregory ift. Nature, Lond., 229, 72.

B.C. (1970). Vulcanicity and Rift Tectonics in East Africa. n: African Magmatism and Tectonics, p285-300. Oliver and Boyd.

C.Y., Knopoff, L. (1968). Stress Drop in Earthquakes. ull. seism. Soc. Am. 58, 249-257.

R.B. (1970). Evolution of Rifting in Africa. Nature, Lond., 26, 538.

f, L., Mitchel, R., Jackson, D.D. (1972). A Stochastic Analysis f a Model Earthquake Sequence. Geophys. J. R. astr. Soc., 29, 55-261.

f, L., Schlue, J.W. (1972). Rayleigh Wave Phase Velocities for he Path Addis Ababa-Nairobi. Tectonophysics, 15, 157-163.

o, I. (1965). The Liquidus Relation in the Systems Forsterite - aAl_2SiO_6 - Silica and Forsterite-Nepheline-Silica at High ressures. Carnegie Inst. Wash., Yearbook, 64, 101-108.

R., Pomeroy, P.W. (1970). The Foreshock-Aftershock Sequence of he March 20, 1966 Earthquake in the Republic of the Congo. ull. seism. Soc. Am., 60, 1245-1258.

on, A.S. (1966). The Gulf of Aden. In: A Discussion Concerning he Floor of the Northwest Indian Ocean. Royal Soc. London hilos. Trans., Ser. A, 259, 150-171.

, M.J. (1971). Per-Alkaline Volcanism, Crustal Swelling, and ifting. Nature Phys. Sci., 230, 85-87.

on, X., Heirtzler, J.R. (1968). Magnetic Anomalies in the Indian cean and Sea Floor Spreading. J. geophys. Res. 73, 2101-2117.

l, R.C., Douglas, A. (1970). Estimation of P-wave Travel Times sing the Joint Epicentre Method. Geophys. J. R. astr. Soc., 19, 21-334.

hev, N.A., Beloussov, V.V., Milanovsky, E.E. (1972). East frican Rift Development. Tectonophysics, 15, 71-81.

R.E. (1968). Temporary Seismic Array Stations. Geophys. J. R. str. Soc., 16, 37-45.

R.E., Mitchell, N.G. (1970). Teleseismic P-wave Delay Times in celand. Geophys. J. R. astr. Soc., 20, 41-48.

R.E., Backhouse, R.W., Maguire, P.K.H., Sundarlingham, K. (1972). he Structure of East Africa using Surface Wave Dispersion and urham Seismic Array Data. Tectonophysics, 15, 165-178.

R.E., Maguire, P.K.H. (1976). The Structure on the Western lank of the Gregory Rift. In Press.

ine, I.S. (1968). Seismology in East Africa. In: Report on he geology and geophysics of the East African Rift System; Nairobi), East African Comm. Cooperation Geophysics, p20-32, 1965.

, P., Molnar, P. (1972). Earthquake Fault Parameters and ectonics in Africa. J. geophys. Res., 77, 5731-5740.

skiy, Kalashnikova (1970). Problem of Phase Transitions in the pper Mantle and its Connection with the Earth's Crustal Structure. . geophys. Res., 75, 877-885.

e, F.K.H. (1974). The Crustal Structure of East Africa through rthquake Seismology. Ph.D. Thesis, University of Durham.

, G.J.H. (1967). Geology of the Nakuru-Thomson's Falls-Lake nnington Area. Geol. Survey Kenya, Rep. 78.

, G.J.H., Hornung, G. (1972). A Geochemical Study of Siali olcano, Kenya, with Special Reference to the Origin of the ntermediate-Acid Eruptives of the Central Rift Valley. ectonophysics, 15, 97-113.

ell, R.B. (1967). The East African Rift System. Nature, Lond., 15, 578-581.

ell, R.B. (1972). Geological Development of the Rift System f East Africa. Geol. Soc. Am. Bull., 83, 2549.

ie, D.P., Davies, D., Molnar, P. (1970). Plate Tectonics of the ed Sea and East Africa. Nature, Lond., 226, 243-248.

vsky, E.E. (1972). Continental Rift Zones: their Arrangement nd Development. Tectonophysics, 15, 65-70.

ra, S. (1962). Magnitude-Frequency Relation of Earthquakes and ts Bearing on Geotectonics. Proc. Japan Acad., 88, 27-30.

P.A. (1970). Plate Tectonics of the Red Sea and East Africa. ature, Lond., 228, 547-548.

P.A. (1974a). Structural Geology of the African Rift System: ummary of New Data from ERTS-1 Imagery. Third ERTS. ymposium, Washington, D.C. Centre for Astrophysics.

P.A. (1974b). ENE-trending Lineaments of the African Rift ystem. First International Conference on the new basement ectonics, Salt Lake City, Utah. Centre for Astrophysics.

, P. and Aggarwal, Y.P. (1971). A Microearthquake Survey in enya. Bull. seism. Soc. Am., 61, 195-201.

r, St., Peterschmitt, E., Fuchs, K., Ansorge, J. (1967). he Rift Structure of the Crust and the Upper Mantle Beneath the hinegraben. Abh. Geol. Landesamt Baden-Wurtemberg, 6, 108-113.

r, St., Peterschmitt, E., Fuchs, K., Ansorge, J. (1969). rustal Structure Beneath the Rhinegraben from Seismic Refraction nd Reflection Measurements. Tectonophysics, 8, 529-542.

r, St. (1970). Geophysical Aspects of Graben Formation in ontinental Rift Systems. International Upper Mantle Project. raben Problems. Rep. 27, 27-36.

, M.J. (1965). Primary Magmas and the Origin of Basalts. cot. Jour. Geol., 1, 19-40.

:on, M.F. (1971). Genesis of Ocean Ridge Median Valleys and Continental Rift Valleys. Tectonophysics, 11, 387-405.

:h, W.R., Turcotte, D.L. (1968). Mid-Ocean Ridges and Geotherm Distribution During Mantle Convection. J. geophys. Res. 73, 2643-2661.

:h, E.R., Turcotte, D.L. (1974). Membrane Tectonics and the East African Rift. Earth and Planetary Sci. Letters, 22, 133-140.

R. (1968). Aftershock and Microearthquakes of the Great Alaska Earthquake of 1964. Bull. seism. Soc. Am., 58, 1131-1168.

, M.J.D. (1964). An Efficient Method for Finding the Minimum of a Function of Several Variables without Calculating Derivatives. Comput. J., 7, 155-162.

, M.J.D. (1965). A Method for Minimising Squares of Non-Linear Functions with Calculating Derivatives. Comput. J., 8, 303-307.

ikov, K.V. (1970). Analysis of the Epicentral Field of Earthquakes in the Baikal Rift Zone during 1961-65. Moscow Akad. Nank. SSSR. Izv. Fizika. Zemli., 187-190.

ell, A.M. (1956). Summary of the Geology of Tanganyika. Part 1: Introduction and Stratigraphy. (Ed. Quennell, A.M., McKinley, A.C.M., Aitken, W.G.). Geol. Sur. Tanganyika.

A., Harris, P.G. (1964). The Partial Fusion of Peridotite. Bull. Volcan., 27, 115-127.

A.W. (1961). Explanation of the Geology of Sheet 76 (Buhwezu). Uganda Geol. Surv., Rep. 4, 73p.

er, C.F. (1935). An Instrumental Earthquake Magnitude Scale. Bull. seism. Soc. Am., 25, 1-32.

er, C.F. (1958). Elementary Seismology. Freeman.

ke, T. (1972). Earthquake Prediction Studies in Japan. Geophys. Surv., 1, 4-26.

henko, Yu.V., Pshennikov, K.V., Zorin, Yu.A. (1969). Seismic ctivity in the Baikal Area in Comparison with the Relief and ravity Anomalies. Akad. Nank. SSSR. Izv. Fizika. Zemli., 10, 1-27.

s, D.G. (1969). Structural Evolution of the Rift Zones in the Middle East. Nature, Lond., 223, 55-57.

ov, L.N., Sedov, V.V., Savrina, L.A., Bourmin, V.J.U. (1972). tudy of Microearthquakes in the Rift Zones of East Africa. ectonophysics, 15, 123-130.

s, L.D. (1963). Geology of the Eldoret Area. Geol. Survey enya., Rep. 64.

, C.H. (1968). The Frequency-Magnitude Relation of Microfracturing n Rock and its Relation to Earthquakes. Bull. seism. Soc. Am. 58, 99-416.

e, R.C. (1970). Evidence for Thinning of the Lithosphere Beneath the Rift Valley in Kenya. Geophys. J. R. astr. Soc., 21, 13-31.

, R.B. (1968). Earthquake Interpretations. Colarado School of Mines.

on, S.C. (1972). Seismic Wave Attenuation and Partial Melting in the Upper Mantle of North America. J. geophys. Res., 77, 1483-1502.

rlingham, K. (1971). Seismic Investigation of the Crust and Upper Mantle of East Africa. Ph.D. Thesis, University of Durham.

n, G.H., Berg, E. (1958). Seismological Studies of the Western Rift Valley of Africa. Trans. Am. Geophys. Un., 39, 474-481.

n, J., Watson, J. (1959). Metamorphism in Deep-Seated Zones of Transcurrent Movement at Kungwe Bay, Tanganyika Territory. J. Geol., 67, 1-13.

A.A., Nuttli, O. (1971). A Method of Correcting P-wave Magnitudes for the Effect of Earthquake Focal Mechanism. Bull. seism. Soc. Am., 61, 1811-1826.

, L.R., Landisman, M. (1964). The Seismicity of East Africa, the Gulf of Aden, and the Arabian and Red Seas. Bull. seism. Soc. Am., 54, 1927-1940.

, L.R. (1967). Mechanisms of Earthquakes and Nature of Faulting on the Mid-Ocean Ridges. J. geophys. Res.,72, 2131-2153.

ni, M., LePichon, X., and Ewing, M. (1965). Crustal Structure of the Mid-Ocean Ridges. J. geophys. Res., 70, 341-352.

, D. (1961). Equation de magnitude pour la station seismologique d'Istanbul - Kandilli concernant les seismes proches, non profonds (h 60 Km). Milli. Egtim Bakanligi 6, 1-8.

tson, E. (1937a). African Rift Valley Earthquake of 1928 January 6. M. N. Royal Astroc. Soc. Geophysics Sup.4, 72-93.

tson, E. (1937b). Further Note to the African Rift Valley Earthquake of 1928 January 6. M. N. Royal Astroc. Soc. Geophysics Sup. 4, 315.

, D.G., Ward, P.L., and Drake, C.L. (1969). Microearthquakes in the Rift Valley of Kenya. Geol. Soc. Am. Bull. 80, 2043-2046.

nti, C.B., Davies, O. (1969). A Seismic Refraction Survey in the Red Sea. Geophys. J.R. astr. Soc., 17, 225-241.

J.R. (1967). Fourth Symp. on African Geology, Sheffield. Unpublished.

erzen, R.P., Vacquier, V. (1967). Terrestial Heat Flow in Lake Malawi, Africa. J. geophys. Res., 72, 4221-4226.

eggen, D. (1970). The Effects of Radiation Patterns on Magnitude Estimates. Bull. seism. Soc. Am., 60, 503-516.

, J.B. (1969). New Analysis of Attenuation in Partially Melted Rock. J. geophys. Res., 74, 4333-4337.

Walsh, J., and Dodson, R.G. (1969). Geology of Northern Turkana. Kenya Geol. Survey, Rep. 82.

Ward, P.L., Bjornsson, S. (1971). Microearthquakes, Swarms and Geothermal Areas of Iceland. J. geophys. Res., 76, 3953-3982.

Williams, L.A.J. (1964). Geology of the Mara River - Sianna Area. Geol. Survey Kenya., Rep. 66.

Williams, L.A.J. (1972). The Kenya Rift Volcanics: a Note on Volumes and Chemical Composition. Tectonophysics, 15, 85-96.

Willis, B. (1936). East African Plateau and Rift Valleys. Carnegie.

Willmore, P.L., Hales, A.L., Gane, P.G. (1952). A Seismic Investigation of Crustal Structure in the Western Transvaal. Bull. seism. Soc. Am., 42, 53-80.

Wohlenberg, J. (1966). Remarks on the Uganda Earthquake of March 20, 1966. Chronique de L'IRSAC, 1(2), 7-12.

Wohlenberg, J. (1968). Seismizitat der Ostafrikanischen Grabenzonen zwischen 4°N und 12°S sowie 23°E und 40°E. Ph.D. Thesis, Munchen 1968.

Wohlenberg, J. (1969). Remarks on the Seismicity of East Africa between 4°N - 12°S and 23°E - 40°E. Tectonophysics, 8, 567-577.

Wohlenberg, J., Bhatt, N.V. (1972). Report on Airmagnetic Surveys of Two Areas in the Kenya Rift Valley. Tectonophysics, 15, 143-149.

Wong, H.K., Von Herzen, R.P. (1966). A Geophysical Study of Lake Kivu, East Africa. Geophys. J. R. astr. Soc., 37, 371-389.

Wyss, M. (1973). Towards a Physical Understanding of the Earthquake Frequency Distribution. Geophys. J. R. astr. Soc., 31, 341-359.

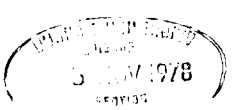

Lake Rudolf

Kir
Fault E

Lake Albert (Mobutu Sese Seko)

Silali

Pakka

Uasin
Gishu
Plateau

Ruwenzori Mts.

Lake Wamala

Nandi

Elgeyo

Lake George

Nyando

Menegai

Kavirondo
Gulf

Lake Edward (Idi Amin Dada)

Lambwe

Lake Naivasha

Lake Victoria

Suswa

Siria

Lake Kivu

Speke Gulf

Lake Natron

Oldoinyo Lengai

Kerimasi

Essimingor

Eyasi

Lake Eyasi

Lake Manyara

Lake Tanganyika

Lake Rukwa

2 N

0

2S

4

6

8